

# 19. Amorphous Selenium and Nanostructures

Keiji Tanaka

The chapter reviews studies of amorphous, glassy, and nano-structural Se, focusing on their atomic structures, physical properties, light-induced phenomena, and recent photoconductive applications. Among the group VIb (16) elements, Se forms a *monatomic glass* having two-folded covalent and van der Waals bonds that possesses a bandgap of  $\approx 2$  eV, in contrast to SiO<sub>2</sub> having three-dimensional networks consisting of fairly ionic Si–O bonds and a wide bandgap ( $\approx 10$  eV). The dualistic bonding structure of Se causes a low glass-transition temperature ( $\approx 310$  K), the narrow gap provides photoconductive responses covering visible wavelengths, and also the heavy atomic mass of 79 can afford high x-ray sensitivity. In addition, the one-dimensional atomic structure becomes a framework of needle-like and single-chain nano-structures.

19.1	<b>Samples</b>	7
19.1.1	Preparation Methods	7
19.1.2	Impurities and Dopants	8
19.2	<b>Non-crystalline Structure</b>	9
19.2.1	Heterogeneity	9
19.2.2	Normal Bonding Structure	9
19.2.3		11
19.3	<b>Structural Properties</b>	12

19.3.1	Static and Dynamic	12
19.3.2	Glass Transition and Crystallization	12
19.4	<b>Electronic Spectra</b>	14
19.4.1	Band Structure	14
19.4.2	Band Edge	16
19.4.3	Gap States and Defects	17
19.5	<b>Electrical Properties</b>	20
19.5.1	Electrical Conduction	20
19.5.2	Avalanche Breakdown	20
19.5.3		21
19.5.4	Electrode, Junction, and Multilayer	22
19.6	<b>Light-induced Phenomena</b>	22
19.6.1	Transitory Effects	23
19.6.2	Photodarkening and Deformations	24
19.6.3	Photo-crystallization	25
19.6.4	Vector Effects	26
19.6.5	Simulations	26
19.7	<b>Applications</b>	27
19.7.1	Vidicon	27
19.7.2	X-ray Imager	27
19.7.3	Other Devices	29
19.8	<b>Nano-Structures and Single Molecules</b>	29
19.8.1	Nano-Selenium	29
19.8.2	Isolated Molecules	29
19.9	<b>Summary</b>	30
	<b>References</b>	31

Studies on the material science of Se have continued for more than a century mainly with two motivations [19.1–6]. One stems from its simplicity and diversity. It is an element bridging the group VIb (16) materials O, S, Se, Te and Po, which form varied atomic structures; O<sub>2</sub> dimer, S<sub>8</sub> ring, Se chain/ring, and cubic Po crystal [19.7]. Here, in comparison with S and Te, Se has more crystalline and non-crystalline allotropes [19.8, 9], all of which are composed normally with two-fold coordinated Se atoms, reflecting the s<sup>2</sup>p<sup>4</sup> electron configuration (Fig. 19.11). The atom can gather to *cis*-configured ring molecules of different members, which are stacked in respective ways; Se<sub>6</sub> in rhombohedral,

Se<sub>7</sub> in orthorhombic, Se<sub>8</sub> in  $\alpha$ -,  $\beta$ - and  $\gamma$ -monoclinic (m-)forms, among which  $\alpha$ -m-Se illustrated in Fig. 19.1 has been studied from early days. In trigonal (t-)Se, also shown in Fig. 19.1, which is the most stable form at standard conditions, the atom can possess right- and left-handed helical chains, being held together with intermolecular forces. It should also be noted that Se exists as only-one element which retains glassy structures at atmospheric conditions [19.10], the glass-transition temperature being  $\approx 35^\circ\text{C}$  ( $\approx 310$  K) [19.1–6]. The structure seems to be dominated by entangled helical chains (Sect. 19.2), which contrast with the three-dimensional network in oxide glasses [19.11], and

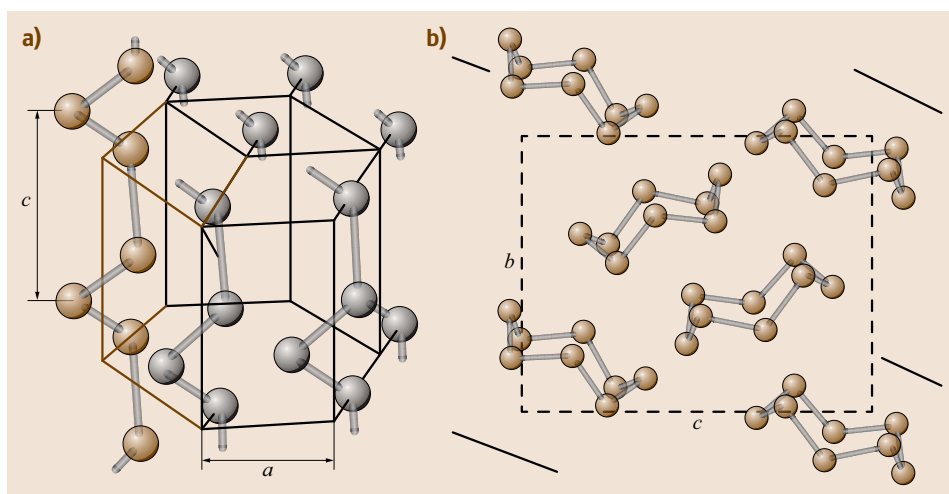


**Fig. 19.1a,b**  
Crystalline  
structures of  
trigonal (a) and  
 $\alpha$ -monoclinic (b)  
Se (after [19.2])

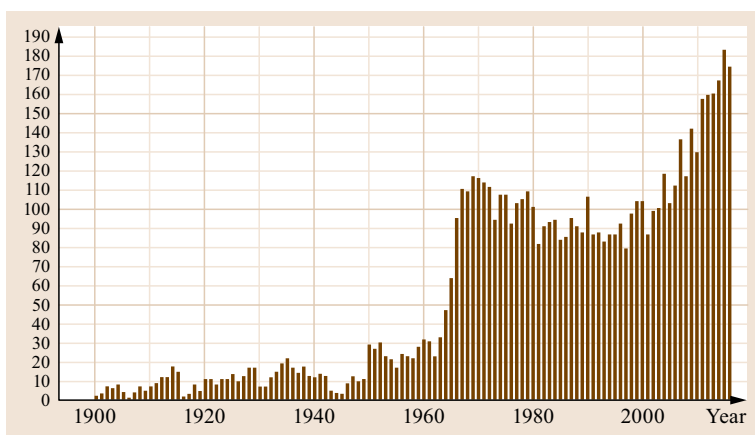


**Fig. 19.2** Number of papers on  
*physics and chemistry of Se* (according  
to Web of Science in March 2017) [\[TS.1\]](#)

accordingly, glassy (g-)Se can be regarded as an *inorganic polymer*, probably the simplest substance among ubiquitous polymeric materials [19.12]. Amorphous (a-) Se also behaves, in covalent chalcogenide materials such as the As-Ge-S(Se,Te) systems, as an intrinsic lone-pair electron semiconductor [19.13]. (Following the terminology by *Mott* and *Davis* [19.4], we define *amorphous* as non-crystalline solid, and restrict *glassy* to the melt-quenched one through super-cooled liquid states.) Besides, the melting temperature  $217^\circ\text{C}$  ( $= 490\text{ K}$ ) [19.1, 2, 5] of t-Se is not so high that the (super-cooled) liquid state can be investigated relatively easily. These multifaceted aspects of Se make its fundamental properties worthy of exploration.

The other reason for interest is that solid Se, specifically a-Se films, exhibit useful semiconductor properties such as high photoconductivity. Actually, *Smith* [19.14] discovered the *photoconduction* of Se in the 19th century, and the phenomenon had been utilized for photo-cells and xerographic photorecep-

tors [19.1–6, 15]. Although these two applications were replaced with crystalline Si sensors and organic films, respectively, new a-Se devices including avalanche vidicons and x-ray imagers have now been developed (Sect. 19.7). We may also note intriguing features such as unique phase transitions [19.16–18], superconductivity [19.19], and light-induced phenomena (Sect. 19.6). Besides, zero- and one-dimensional Se nano- and molecular structures have attracted considerable interest recently (Sect. 19.8).

Such longstanding scientific and technological studies of a-Se have unveiled many features, e.g., short-range atomic structures and photoconductive properties, though a lot of unresolved problems still remain. For instance, why can the avalanche breakdown (Sect. 19.5.2) occur in the disordered semiconductor? Nevertheless, after comprehensive reviews published during the xerography era [19.1–4], few articles referring to recent Se researches seem to be available [19.5, 6]. The aim of this chapter is therefore to summa-

size updated understandings and developments of Se, specifically, a- and g-Se. We will also cast a look at nano-structures. Nevertheless, the present review cannot touch details of doping effects of As, Ge, Te, etc. to Se, due to numerous references.

At the outset, it may be valuable to take a bird's-eye view of the Se research. Figure 19.2 shows the number of publications per year till 2016, analyzed using Web of Science, having a title word *selenium* in material sciences. (As known, there are a huge numbers of Se-related biological and medical papers, which

are excluded as possible.) The total number is more than 6000, in which we can mark two features, a peak around 1970 and an increase after  $\approx 2000$ . The peak appears to be related with *xerography* [19.15], and the recent increase may be related with nano-science. It is also mentioned that a lot of work have recently been published from Canadian groups, which greatly contribute to the progress in photoconductive applications (Sect. 19.7). Incidentally, a Wikipedia column states that major countries producing Se ingots are Japan, Canada, and the US.

## 19.1 Samples

### 19.1.1 Preparation Methods

As shown in Fig. 19.3 [19.2,20,21], a-Se can be prepared from gas, liquid, and crystalline phases. Since the amorphous material is in a quasi-equilibrium state, it is plausible that the atomic structure depends upon preparation procedures and aging processes, which is a reason giving rise to varied properties and less-reproducible results, despite of the elemental composition.

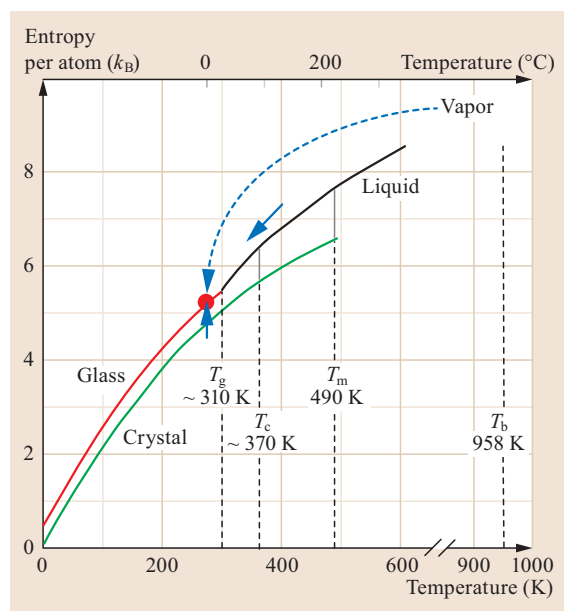


**Fig. 19.3** Entropy as a function of temperature, with three preparation routes of a- and g-Se from vapor, liquid, and crystalline phases: glass-transition temperature  $T_g \approx 35^\circ\text{C}$ , crystallization temperature  $T_c \approx 100^\circ\text{C}$ , melting temperature  $T_m = 217^\circ\text{C}$ , and boiling temperature  $T_b = 685^\circ\text{C}$  (after [19.2, 20, 21])

G-Se is prepared through quenching of the melt. As the source material we may employ commercially available Se beads with nominal purity of 5N–6N or chemically-purified flakes through various techniques [19.2, 22]. Those materials are vacuum-sealed in quartz ampoules, melted at some temperature, and quenched with a selected cooling rate to room or lower temperatures. Bulk ingots can be shaped into slabs by lapping and polishing [19.2] or flattened by squeezing [19.23–25] around the glass-transition temperature.

A-Se films have been prepared in several ways. Among those, the most conventional is the thermal evaporation in vacuum, which can straightforwardly produce large-area films with thicknesses up to  $\approx 0.5$  mm [19.26] through condensation of gaseous molecules such as  $\text{Se}_6$  [19.2, 27–29]. However, the method yields films with varied properties depending upon substrate materials [19.30, 31], substrate temperatures  $T_s$  ( $20\text{ K} - 70^\circ\text{C}$ ) during evaporation [19.4, 27, 32–45], substrate vibration [19.46], boat temperatures ( $\leq 800^\circ\text{C}$ ) or deposition rates ( $\leq 4\text{ }\mu\text{m/min}$ ) [19.2, 22, 27, 28, 40, 41], film thicknesses [19.26, 27, 47–50], deposition angle [19.38], light irradiation from boats, and so forth. Reflecting these diverse conditions, as listed in Table 19.1, the density [19.2, 9] of films for instance appreciably scatters [19.27, 48], in contrast to relatively fixed values in g-Se [19.24, 48, 51, 52], t-Se [19.27, 48], and  $\alpha$ -m-Se [19.27]. It has also been demonstrated that even preparation procedures of Se beads employed for evaporation sources affect structures and photoelectrical properties of deposited films [19.28, 53, 54].

In addition, less-common methods have been reported. Those include sputtering [19.55], chemical vapor deposition [19.56], laser-pulse deposition [19.57], and electron-beam evaporation [19.58]. Electrodeposition techniques have been employed for preparing porous films [19.59]. Peled's group continues to explore photo-chemical depositions of thin films from

**Table 19.1** Bond lengths and physical properties in the three Se solids at room temperature with references in [19.449–452]. For other references, see the texts. Optical gaps in the crystals depend upon the definitions, while for the amorphous the Tauc gap is cited

Property	Trigonal	$\alpha$ -monoclinic	Amorphous
Bond length (Å)	2.31–2.37	2.31–2.33	2.30–2.37
Density (g/cm <sup>3</sup> )	4.807 [19.8] 4.819, 4.76 [19.2]	4.400 [19.8] 4.389 [19.2]	4.285, 4.26 for g-Se [19.2] 3.7 ± 0.2 [19.48] ( <i>T</i> <sub>s</sub> = room temperature) 4.1 ± 0.3 [19.27] ( <i>T</i> <sub>s</sub> = 100–290 K)
Optical energy gap (eV)	1.87 [19.2]	2.25, 2.5, 2.85 [19.452, 453]	2.05 [19.4]
Refractive index ( $\lambda \approx 1 \mu\text{m}$ )	2.79 ( <i>n</i> <sub>o</sub> ), 3.61 ( <i>n</i> <sub>ex</sub> ) [19.2] 2.6 ( <i>n</i> <sub>o</sub> ), 3.25 ( <i>n</i> <sub>ex</sub> ) [19.451]	$\approx 2.5$ [19.451]	2.50 [19.2]
Dielectric constant	$\approx 7.5$ ( $\perp c$ ), $\approx 12$ ( $\parallel c$ ) [19.449]	7.4 [19.449]	6.0 [19.450], 6.2–6.4 [19.73]
$\mu_e$ (cm <sup>2</sup> /V s)	$\mu_e/\mu_h \approx 1/4$ [19.250]	2 [19.251]	$\approx 0.005$
$\mu_h$ (cm <sup>2</sup> /V s)	0.13, 28, 40 ( $\parallel c$ ) [19.2, 250] 6, 17 ( $\perp c$ ) [19.2, 250]	10 [19.251]	$\approx 0.15$

Se solutions [19.60, 61]. The so-called red a-Se, which can be prepared through several ways, has attracted some interest, while its atomic structure and properties remain speculative, partly due to its un-stability at room temperature [19.2, 9, 62–64].

Lastly, we mention solid-state a-Se preparation through ball millings [19.65–68]. In this method, mechanical energy with frictional heat continuously transforms t-Se samples to non-crystalline powders, the conversion process having been monitored using x-ray and neutron beams. The preparation method is unique and scientifically interesting, while the sample shape may limit applications.

19.1.2 Impurities and Dopants

It is assumed that, in general, amorphous semiconductors or chalcogenide glasses are less susceptible to impurities and dopants. Actually, a-Si:H films possess much lower doping efficiencies than that in crystalline Si, which may imply that different valencies of foreign atoms tend to be compensated by disordered, flexible bonding structures.

However, we should pay special attention to some impurities in Se, particularly, oxygen [19.2]. As shown in Fig. 19.4 [19.69], an exceptionally conspicuous O effect on the electrical resistivity in g-Se is known: Only  $\approx 10$  ppm O atoms cause a drastic decrease in the resistivity by six orders of magnitude, which can be ascribed to creation of acceptors by chain-terminating O-atom pairs,  $-\text{Se}=\text{O}_2$  [19.69, 70]. Interestingly, however, if Si or As is co-doped with O, the resistivity does not decrease (Fig. 19.4), the compensation mechanism being ascribed to formation of more stable Si(As)–O bonds [19.69]. It is also known that O contaminations in g-Se provide marked effects upon

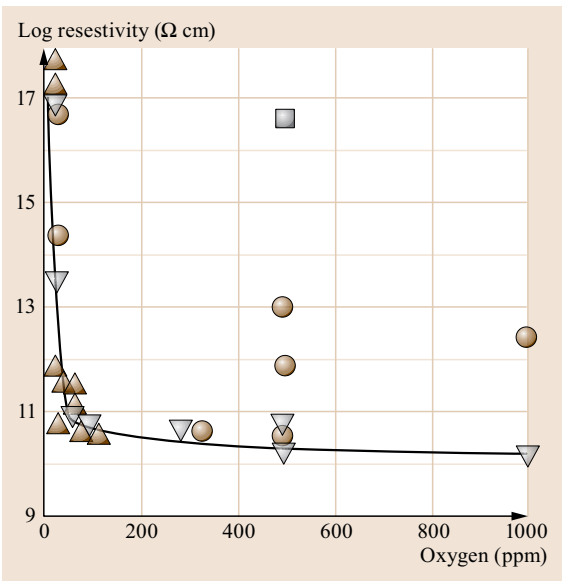


**Fig. 19.4** Resistivity of g-Se as a function of doped oxygen content, reported from MacKenzie’s group ( $\nabla$  with a solid line,  $\bullet$ , and  $\triangle$ ). The square ( $\blacksquare$ ) at upper middle shows a result of g-Se co-doped with 500 ppm  $\text{SeO}_2$  and 500 ppm Si (after [19.69] [\[CE.2\]](#))

photoluminescence behaviors [19.71, 72] and the dielectric constant [19.73]. On the other hand, for a-Se films, which have exhibited resistivities scattering over  $10^{10} - 10^{16} \Omega \text{ cm}$  [19.2, 47, 74, 75], we may also envisage similar O-effects, while no systematic studies have been presented, except for transport properties [19.53, 54, 76]. We should also take structural relaxations into account: O-related aging effects have been demonstrated in infrared spectra of g-Se [19.69] and transport properties of a-Se [19.54].

[\[CE.2\]](#) Please check reference [19.69], do you mean [19.70] instead?



Pure a-Se films have some unsatisfactory properties, and accordingly, doping effects have been explored over decades. So far, a variety of atoms with densities up to a few atomic percent, which clearly surmount the conventional doping level ( $\approx$  ppm) in crystalline semiconductors, have been incorporated. Regarding examined dopants, in addition to intensively studied Cl [19.25, 30, 43, 54, 77–83], As [19.45, 55, 71, 82–87], and Te [19.32, 45, 51, 77, 86, 88–93], we may list Li [19.94], K [19.95], Ag [19.96], Ge [19.97], O [19.30, 54, 72, 76], S [19.51, 77, 98, 99], and so forth [19.25, 71, 100]. Also, several doping procedures have been employed, the conventional being direct alloying to Se ingots [19.51, 85], which may be used as (flash) evaporation sources [19.77–84, 87]. Otherwise, Se and dopants are co-evaporated [19.86], or dopants are ion-implanted [19.94] or molecularly-incorporated [19.100]. Besides, the dopant profile may be spatially uniform [19.83] or modulated [19.81], the ultimate being multi-layers [19.86, 92] (Sect. 19.5.4).

What are the outcomes of doping in a-Se films? We may expect improved thermal stability by incorporation of cross-linkers such as As [19.77, 84] or different-size atoms as Te [19.78], enhanced red-sensitivity by

bandgap reduction [19.32, 51, 86], and efficient carrier transports [19.4, 79–83]. Such doping effects seem to depend not only on the atomic species and quantities but upon various conditions including the substrate temperature [19.44]. However, in most cases, the doping tends to degrade transport properties [19.4, 77, 100], which is a plausible consequence arising from trapping centers produced by compositional disorders. A notable exception is the case of *stabilized a-Se films*, evaporated onto substrates held at  $T_s \approx 60^\circ\text{C}$  ( $\approx 330\text{ K}$ ) using ingots containing 0.2–0.5 % As and 10 ppm-level Cl, which exhibit ameliorated photoconducting characteristics [19.44, 45, 82, 84, 101–103]; the co-doping mechanism being theoretically explored recently [19.104]. Here, it may be interesting to point out that this  $T_s$  satisfies a universal rule,  $T_s/T_b \approx 0.34$  [19.105], where  $T_b$  ( $= 958\text{ K}$ ) is the boiling temperature, while its origin remains unclear. We also note that, in many cases, a dopant (and impurities) modifies a property continuously with the concentration, though the modification being not necessarily proportional to the concentration, as we have seen in Fig. 19.4. Besides, in a vector photo-deformation in a-Se:As films, a dramatic, *qualitative* change (Fig. 19.21) appears at  $\approx 1\text{ at.}\%$  As [19.106].

## 19.2 Non-crystalline Structure

### 19.2.1 Heterogeneity

When studying non-crystalline structures, the first issue to be known is if the atomic structure is homogeneous, or spatially uniform. For pure Se, we can naturally disregard the compositional disorder. However, even in the elemental material, some structural heterogeneity could exist. For instance, it is known that the liquid has thermo-dynamical density fluctuations, given by the Einstein-Smolukovskii equation, which are likely to affect quenched glassy structures [19.11, 107, 108]. Actually, light-scattering correlation spectroscopy of liquid (l-)Se detected clusters with sizes of  $\approx 150\text{ nm}$  just above the melting temperature [19.109]. Or, microscopy inspections of a-Se films counted numerous crystalline inclusions, the structure varying with substrate temperatures [19.32, 34]. Small-angle scattering measurements of Se glasses [19.24, 110] and films [19.40, 111] suggested some inhomogeneity such as ellipsoidal voids and fractal structures. Positron annihilations detected voids and free volumes [19.112, 113], which may be responsible for the density deficit of  $\approx 10\%$  of g-Se with respect to that in t-Se (Table 19.1). Provided that a heterogeneous scale is wider than the wavelength of excitations, analyses of a related property

taking the heterogeneity into account will be needed. However, as described hereafter, in standard analyses using radial-distribution-functions (RDFs) and (vibrational and electronic) densities-of-states (DOSs), such structures are inevitably neglected.

Suppose the atomic structure being homogeneous, it could consist of *normal bonding structures* and *defects* [19.6]. The former is the atomic connection which exists in the corresponding ideal crystal, i.e.,  $-\text{Se}-\text{Se}-$  bonds in the present case. The latter includes point-defect-like structures such as dangling bonds, three-fold coordinated Se, and so forth. The densities are  $\approx 1\text{ at.}\%$  at most, which is fewer than detection limits of structural analyses methods, while the defects may play significant roles as electronic gap states (Sect. 19.4.3).

### 19.2.2 Normal Bonding Structure

#### Short-range Structure

After a comprehensive study by Kaplow et al. [19.33], a lot of structural analyses have been performed for g-Se [19.2, 24, 64, 114–118], with fewer for a-Se films and powders [19.40, 66, 67, 119]. Since there exists only the Se–Se homopolar bond, diffraction and EXAFS profiles can straightforwardly be converted to

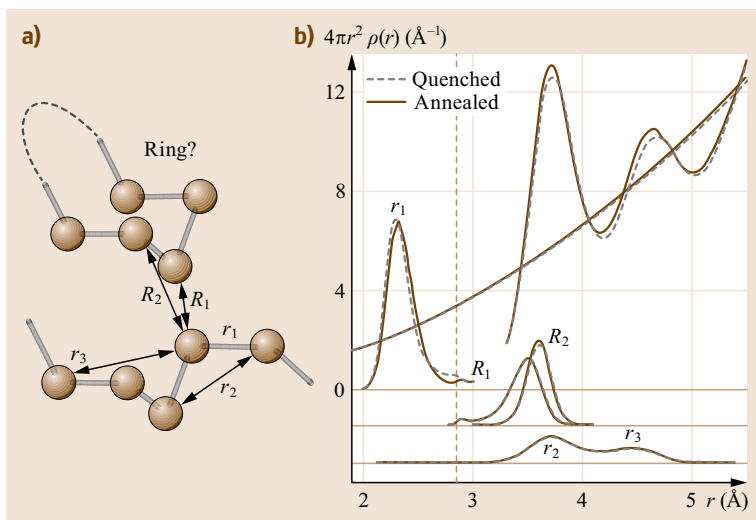


**Fig. 19.5** (a) Schematic a-Se structure with definitions of the intra- ( $r_1$ ,  $r_2$ ,  $r_3$ ) and inter-chain ( $R_1$  and  $R_2$ ) distances, and (b) RDFs of quenched and annealed (room temperature, 1 day) g-Se, in which the three peaks at  $\approx 2.4$ ,  $\approx 3.7$ , and  $\approx 4.6 \text{ \AA}$  are resolved into pair distances through a reverse Monte Carlo procedure (after [19.52])

RDFs, a result being shown in Fig. 19.5. The short-range structure determined by the three parameters, i.e., the nearest-neighbor coordination number  $Z = 2 \pm 0.1$ , the covalent bond length  $r = 2.30 \approx 2.37 \text{ \AA}$ , and angle  $\theta \approx 105^\circ$  [19.24, 33, 52, 67, 114–120] in g-Se are nearly the same with those in t- [19.2, 33, 64, 67, 119, 121] and m-Se [19.2, 24] (Table 19.1). Here, we underline that, even in t-Se, reported  $r$  values substantially scatter, which may be caused by defective and/or contaminated crystals. Accordingly, the resonant-bond (between the covalent and the van der Waals) concept applied to t-Se [19.122], after taking a relatively long  $r$  ( $= 2.37 \text{ \AA}$ ) for t-Se, might be re-examined. We also note that, as shown in Fig. 19.5b, since the second RDF peak at  $\approx 3.7 \text{ \AA}$  is made up with the three ( $r_2$ ,  $R_1$ ,  $R_2$ ) correlations [19.24, 52, 120], it is difficult to accurately estimate the  $\theta$  value.

### Medium-range Structure

The medium-range structural parameters include the intermolecular distance  $R$ , the dihedral angle  $\varphi$  (*trans/cis* configurations), ring/chain ratio, and so forth. For  $R$ , since both  $r_2$  and  $R$  are distributed at  $\approx 3.7 \text{ \AA}$  (Fig. 19.5), precise values have hardly been estimated [19.24, 52, 115]. For  $\varphi$ , a problem is if it varies freely or takes nearly-fixed values characteristic to *trans* (t-Se like) and/or *cis* (m-Se like) configurations. If the value varies, entangled chains may exist (Fig. 19.6a). Or, if it is fixed over several Se bonds, chain segments (Fig. 19.6b) may exist. However, as shown in Fig. 19.5, the third RDF peak spreads at 4–5  $\text{\AA}$ , and accordingly, no convincing conclusions have been obtained, despite of repeated studies [19.24, 33, 52, 66, 114, 115, 118, 120].

The ring/chain ratio in g-Se has been a longstanding problem. In retrospect, solubility of g-Se samples into liquid  $\text{CS}_2$  was assumed to be proportional to the content of  $\text{Se}_8$  rings [19.2], and this idea had been employed for estimating the ring content. In addition, a relationship between the densities  $\rho(\text{t-Se}) > \rho(\text{m-Se}) \approx \rho(\text{g-Se})$  (Table 19.1) and some RDF analyses [19.33, 123] supported the view that g-Se and l-Se contain large fractions of ring molecules. However, Lucovsky [19.124] casts doubt upon the solubility, taking the observation that the solubility is enhanced by light illumination and it became negligible in the dark. It is also doubtful if the solubility can distinguish (closed) ring molecules from ring-like (curled) chains. Besides, diffraction studies seem to be powerless in this problem: J  v  ri et al. [19.66] concludes through comparing diffraction profiles and reverse Monte-Carlo models that diffraction data alone cannot evaluate the ring/chain ratio. On the other hand, viscosity [19.2], magnetic [19.16], and structural [19.125, 126] studies strongly suggest that l-Se is composed by chain molecules, with chain lengths of  $\approx 10^5$  atom at just above  $T_m$  ( $= 217^\circ\text{C}$ ). Under these circumstances, it seems reasonable to envisage entangled chain structures, such as Fig. 19.6(a), for g-Se.

Vibrational studies may add some insights into this problem. Since t-Se and m-Se undergo clearly different vibrations at stretching frequencies ( $\approx 250 \text{ cm}^{-1}$ ,  $\approx 30 \text{ meV}$ ) [19.4], vibrational spectra had been employed for analyzing the ring/chain ratio in g- and l-Se [19.2]. (IR measurements at wavenumbers below  $\approx 200 \text{ cm}^{-1}$  are experimentally more-or-less limited, which makes Raman spectroscopy more useful.) However, Lucovsky [19.124] also suggested that  $\Omega$ -shaped (open ring) curling chains can cause ring-like (*cis*-

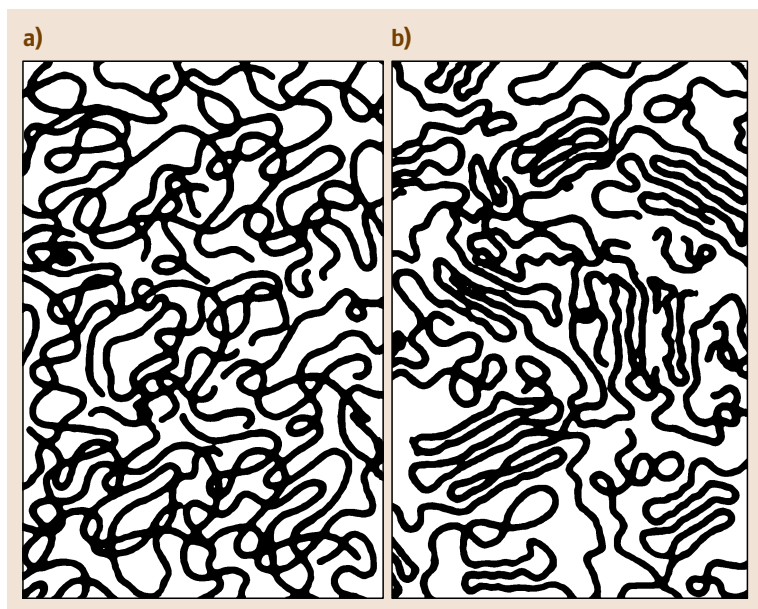


**Fig. 19.6a,b** Schematic models of amorphous polyethylene  $-(CH_2)-$ . (a) interpenetrating coils and (b) folded-chain fringed micellar grain model (after [19.107])

type) vibrations (at  $113$  and  $256\text{ cm}^{-1}$ ), making the ratio-evaluation procedure useless. Though his assertion was argued [19.127], the ring-chain problem has as a whole appeared to shift to estimation of ringlike-chainlike (*cis/trans*) configurations. Following the idea, Nakamura and Ikawa [19.128] theoretically predicted that vibrational spectra at the bond-bending regime ( $50\text{--}130\text{ cm}^{-1}$ ) can give insights into the chain configurations. Yannopoulos and Andrikopoulos [19.129] have focused on Raman-scattering spectroscopy at  $5\text{--}450\text{ cm}^{-1}$ , evaluating the contents of ring- and chain-like fragments at  $143\text{--}353\text{ K}$ . These studies reinforce the model that not  $Se_8$  molecules but long chains, which are probably mixed up with entangled ring- (*cis*) and chain-like (*trans*) segments, are major constituents of g-Se. Nevertheless, the chain conformation in wider scales is largely speculative; it may form random coils [19.120], segments connected with kinks [19.36], and so forth, the notions paralleling those proposed for polyethylene (Fig. 19.6) [19.107, 130], in which intra- and inter-chain conformations ( $r_1 \approx 1.5\text{ \AA}$ ,  $R \approx 5\text{ \AA}$ ) are more distinguishable than those in Se. We also note that the medium-range structures are possibly modified by the aging.

Lastly, we refer to four topics. The first relates to the *first-sharp diffraction peak* appearing at  $\approx 1\text{ \AA}^{-1}$  in chalcogenide glasses such as  $As_2S(Se)_3$  [19.6, 11]. Compositional studies of the peak in the As-Se system have demonstrated that the peak reduces to a shoulder at  $\approx 1.5\text{ \AA}^{-1}$  in g-Se [19.66, 131]. Averbach's group examined the shoulder through a correlation analysis, suggesting the existence of clusters with a ra-

dius of  $\approx 10\text{ \AA}$  [19.115, 120], in harmony with similar scales repeatedly pointed out [19.33, 132]. On the other hand, Caprion and Schober [19.133] proposed through molecular dynamics analyses that the prepeak is explainable in terms of void correlation, with reasoning that it disappears in densified samples. The two ideas appear different, while those may merely emphasize different aspects of the same structure; i.e., voids possibly exist between atomic clusters. Second, the origins of the *Boson peak* at  $\approx 20\text{ cm}^{-1}$  and quasi-elastic component peaking at  $\approx 0\text{ cm}^{-1}$  in Raman-scattering spectra are still matters of controversy [19.11, 129, 134]. Third, despite of wide applications of (stabilized) a-Se films with varied preparation conditions (Sect. 19.1.2), the structural studies are surprisingly a few [19.33, 34, 37, 40]. Lastly, Scopigno et al. [19.57] have demonstrated that the vibrational DOS of a-Se surfaces is markedly smooth at  $5\text{--}15\text{ meV}$  regions, suggesting the existence of hypervalent defects.

### 19.2.3 Molecular Dynamics Simulation of Atomic Structures

Molecular dynamics simulation has continuously been employed for structural studies. Principally, the simulation proceeds from equilibrating a molten Se cluster and to quenching it into disordered solids [19.128, 135–145]. In some cases, structural disorder is introduced artificially [19.145], or the equilibration is set at *under-melt* conditions, or temperatures below the melting temperature of the corresponding crystal [19.144]. Otherwise, Kugler's group [19.140–143] has obtained

a-Se films from gaseous states, through pitching Se atoms with fixed kinetic energies and incident angles at cold substrates, which produces amorphous structures with comparable densities, 3.2–4.5 g/cm<sup>3</sup>, to the observed ones (Table 19.1). Atomic potentials employed for calculations are either semi-empirical [19.128, 136, 138–143, 145] or ab-initio [19.135, 137, 144], in which the total numbers of studied atoms have been limited by computer capacities to  $\approx 2000$  and  $\approx 200$ , respectively.

Such studies have shed light upon atomic structures of a-Se and also what kinds of defects could exist therein. Simulated short-range structures well repro-

duce the experimental RDF. However, since the (effective) quenching rate is anomalously fast  $10^{10}$ – $10^{14}$  K/s due to limited computation times, produced structures tend to be far more disordered and contain too many defects, with densities of  $\approx 10$  at.%, which disagree with experimental observations. Actually, the structural and vibrational measurements, possessing typical sensitivities of  $\approx 1$  at.%, have never detected any defects such as dangling and three-folded bonds in *bulk* a-Se. In addition, the maximal number of studied atoms of  $\approx 2000$  is still insufficient for drawing medium-range (and heterogeneous) structures. For other computation studies, readers may refer to Sect. 19.6.5.

## 19.3 Structural Properties

### 19.3.1 Static and Dynamic

Substantial data have been obtained for g-Se on mechanical [19.2, 85, 89] and thermal [19.2, 21, 63] properties, including the low-temperature ( $\leq 5$  K) anomalies [19.146, 147], and remaining subjects will be to relate these macroscopic properties with microscopic atomic structures. For instance, how can we connect the specific heat with disordered atomic structures, without using the periodic boundary condition? If an amorphous structure were homogeneous and could be explicitly delineated, we would follow the conventional procedure which is established for understanding structural properties in ideal crystals; atomic structure  $\rightarrow$  vibrational dispersion relation and DOS  $\rightarrow$  macroscopic properties. However, the disordered structure does not sustain the dispersion relation in principle, and accordingly, considerable efforts have been devoted to experimental determinations of the vibrational DOS.

In such studies, IR and Raman spectroscopies have been employed [19.2, 37, 127, 129], and recently, inelastic x-ray [19.57, 148] and neutron [19.20, 63, 149] scatterings provide more complete vibrational spectra  $D(E, q)$  resolved in energy  $E$  and wavenumber  $q$ . Those results appear to be fairly consistent, and a typical DOS is reproduced in Fig. 19.7, which consists of three bands. The spectrum can explain temperature variations of the specific heats, shown in Fig. 19.8, which are nearly the same in t-, g- and red a-Se at 10–300 K [19.63]. By contrast, it seems still difficult to identify a structural entity causing the universal low-temperature ( $\leq 10$  K) anomaly in glasses, which has conceptually been explained using *some* two-level systems with spectral densities of  $10^{20}$ – $10^{21}$  eV<sup>-1</sup> cm<sup>-3</sup> [19.11, 146, 147].

### 19.3.2 Glass Transition and Crystallization

Among many macroscopic properties in condensed matters, the glass transition poses undoubtedly one of the biggest challenges [19.11, 150]. And, since the glass-transition temperature  $T_g$  ( $\approx 310$  K) in g-Se is just above room temperature, it is more-or-less straightforward to evaluate glassy and super-cooled liquid properties, including atomic volumes [19.113], heat capacities [19.151–154], elasticity [19.155–157], viscosity (fluidity) [19.158–162], hardness [19.163, 164], and relaxation (aging) behaviors [19.52, 152, 165–167]. For instance, Košťál and Málek [19.162] have demonstrated that the viscosity  $\eta$ , plotted in Fig. 19.8, follows

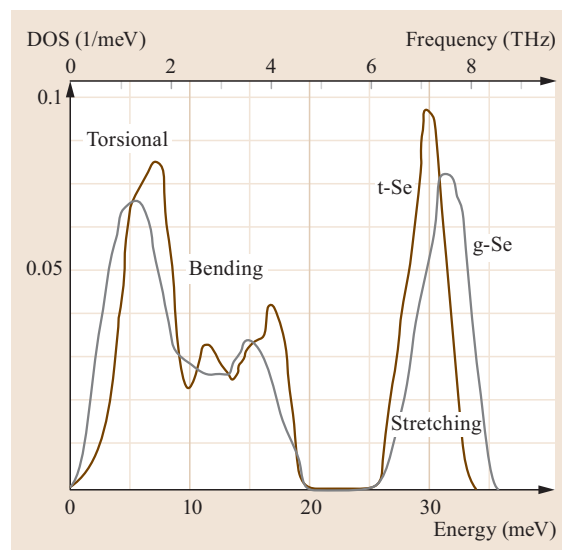
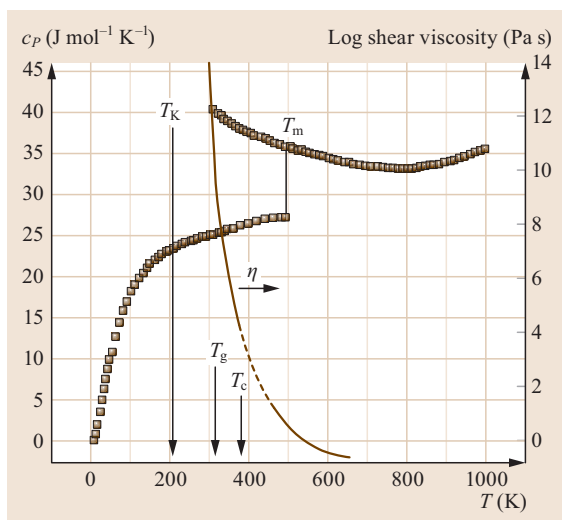


Fig. 19.7 Vibrational DOSs in t- and g-Se (after [19.63])



**Fig. 19.8** Temperature variations of the heat capacity  $c_p$  (after [19.63, 162]) and viscosity  $\eta$  (after [19.160, 162]) in l- and t-Se.  $T_K$  ( $\approx 226$  K) is the Kauzmann temperature,  $T_g$  the glass-transition temperature,  $T_c$  the crystallization temperature,  $T_m$  the melting temperature

the empirical Vogel-Fulcher-Tammann equation

$$\ln \eta = \frac{A + B}{T - T_K}, \quad (19.1)$$

where  $A \approx -9.3$ ,  $B \approx 2800$  K, and the Kauzmann temperature  $T_K \approx 226$  K. The curve gives the fragility index ( $= d(\ln \eta)/[d(T_g/T)]$  at  $T = T_g$ ) of 50–100 [19.160, 167]. Note that  $T_K$  is assumed to be a material parameter (as  $T_m$ ), while  $T_g$  and  $\eta(T)$  vary with melt-quenching rates. In addition, some differences of transition behaviors between bulk samples and films have been pointed out [19.68, 153]. It has also been demonstrated that the glass-transition, crystallization, and melting temperatures become higher under hydrostatic compression [19.168–170].

How can we understand such glass-transition behaviors? As known, the glass transition has formally been interpreted using the free-volume concept, the mode-coupling theory, and so forth [19.11], while can

we connect the transition to real atomic structures? Since no compositional disorder exists in g-Se, theoretical treatments could be less demanding. However, the non-isotropic chain-like structures make the analysis complicated. Several ideas have been proposed, such as a polymeric-polymorphoid structural transformation [19.9] and a kinematic treatment [19.159], both appearing to be challenging. Molecular dynamics simulations are hardly practical, due to the limitation of computation times [19.108, 133, 171]. Otherwise, a formulation based on an enthalpy landscape approach and non-equilibrium statistical mechanics, presented by Mauro et al. [19.161], despite the numbers of dealt Se atoms being limited to 60, attains a fair success in predicting, e.g., temperature variations of atomic volume and viscosity.

Crystallization of a-Se also attracts continuing interest. At 1 atm the amorphous-to-trigonal crystallization sets in at temperature of  $T_c \approx 100^\circ\text{C}$  [19.49, 68, 151, 172, 173], and at room temperature it occurs at pressure of  $p_c \approx 11$  GPa ( $= 110$  kbar) [19.19, 168, 174, 175]. What govern these threshold values?

We see implicative trends in Fig. 19.9 for the period-four solids, Ge, As, and Se:  $T_c$  (and also  $T_g$  [19.176, 177]) increases roughly linearly with the coordination number  $Z$ , and  $p_c$  increases with the bond energy  $E_B$ . By contrast, no simple correlations seem to exist between  $p_c$  and  $Z$  and between  $T_c$  and  $E_B$ . The monotonous  $T_c \propto Z$  relation may imply that the thermal crystallization in a-Se is governed by rearrangements of two-fold coordinated bonds [19.178], as reptational motions in polyethylene to spherulitic forms [19.179]. It proceeds with activation energies of 50–100 kJ/mol ( $\approx 0.5$ –1 eV/atom) [19.93, 172, 180], being smaller than the bond energy of  $\approx 2$  eV/atom. On the other hand, the  $p_c \propto E_B$  relation fuels a speculation that the pressure crystallization proceeds from breakage of covalent bonds. We envisage that, in a-Se under compression, the intermolecular separation is substantially compressed [19.168], which reduces the difference between covalent and van-der-Waals bonds, and at some critical pressure –Se–Se– bonds will be intermingled and ordered, leading to the phase transformation.



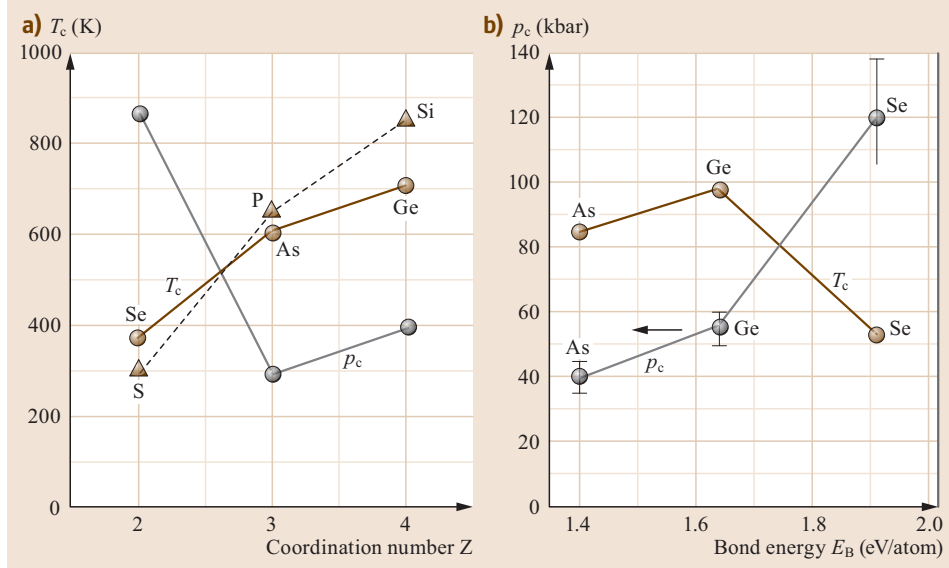


**Fig. 19.9a,b** Crystallization temperature  $T_c$  and pressure  $p_c$  as functions of the covalent coordination number  $Z$  (a) and the bond energy  $E_B$  (b) for series of atoms in the same lines of the periodic table Se, As and Ge (after [19.178]). Note that S, P, and Si also shows the  $T_c \propto Z$  correlation, while  $p_c$  of a-S is not known

## 19.4 Electronic Spectra

### 19.4.1 Band Structure

The electronic structures of t-,  $\alpha$ -m- and a-Se, evaluated using ultraviolet and x-ray photoemission spectroscopies (UPS, XPS) [19.4, 36, 181–184], have confirmed the concept of *lone-pair semiconductors* [19.13]. As shown in Figs. 19.10 and 19.11, the two-fold coordinated  $p^4$  wavefunctions produce the valence and the

conduction band peaking at around  $-2.5$  and  $+3.0$  eV, which are composed with lone-pair electron and anti-bonding states, respectively. In addition, there exists a band consisting mostly of bonding p-states at around  $-6$  eV, the detailed shape attracting some interest: The band has double peaks at  $-5$  and  $-6$  eV, with the intensity ratios in a- and m-Se being contrastive to that in t-Se, which may originate from alternative (or dis-

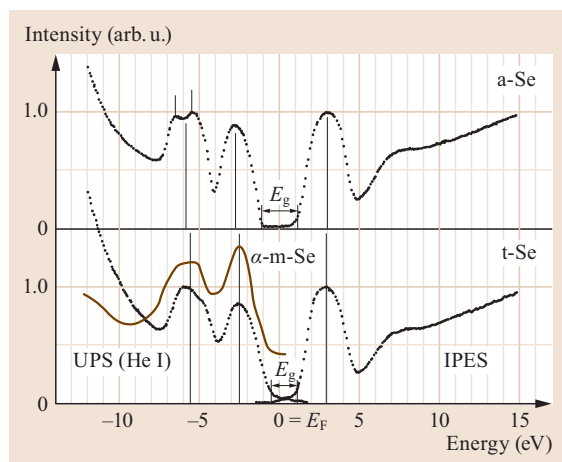


**Fig. 19.10** Photoemission spectra (UPS and inverse UPS) of a-Se, deposited onto Au substrates at room temperature, and t-Se (after [19.184]), compared with that (XPS) of  $\alpha$ -m-Se (after [19.183])

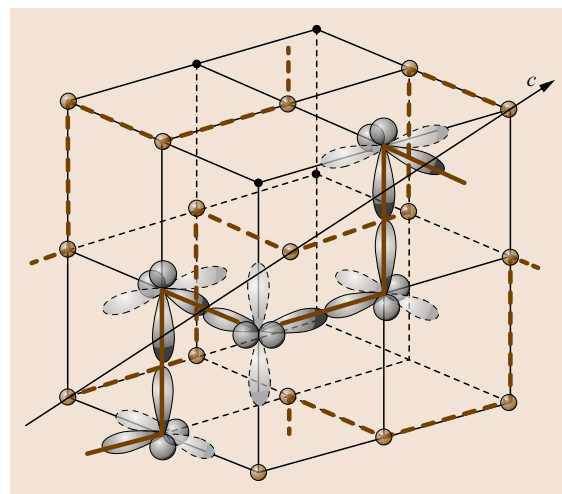


**Fig. 19.11** A simplified t-Se structure with the bond and the dihedral angle of  $90^\circ$ . Dashed ellipsoids represent the lone-pair wavefunctions



ordered) and fixed dihedral angles [19.4, 36, 183, 185]. It should be mentioned here that limited sensitivity of photoemission spectroscopy cannot yet afford information on gap states.

The lone-pair semiconductor concept is consistent also with electron dispersion curves of t-Se, which have been calculated by several methods [19.2, 4, 186–192]. The simplest is a tight-binding approximation under the simplification of  $\theta = \varphi = 90^\circ$  [19.186], sketched in Fig. 19.11. More sophisticated calculations have manifested, as shown in Fig. 19.12a, an indirect-transition type dispersion, in agreement with experimental results [19.2], with the conduction-band bottom at H and the valence-band top at L in the  $k$ -space, both the points slightly deviating from the chain axis A [19.188–192]. Nevertheless, we see in the figure that the valence-band top is broader so that the dispersion can roughly be regarded as a direct-transition type with the bandgap at H, as previously been assumed [19.2, 4].

As known, once the dispersion relation having been fixed, the DOS can directly be calculated. Fig. 19.12b shows the electronic DOS in t-Se [19.189, 190], the overall feature being in harmony with the photoemission spectrum in Fig. 19.10. We also mark that the shape of the conduction-band bottom is typical to that ( $D \propto E^{-1/2}$ ) of the one-dimensional crystal. In contrast, such

a characteristic does not exist at the top of the valence band, which may be ascribed to spatially extended lone-pair wavefunctions (Fig. 19.11). On the other hand, the red line in Fig. 19.12b shows a DOS calculated for a modeled a-Se structure, consisting of disordered 50 Se atoms which are placed under a periodic boundary condition [19.189]. We see that the disorder makes the DOS smoother. We also see in Fig. 19.12b,c, that these DOSs possess some similarities to the energy levels of related molecules [19.69]. Incidentally, the work function of Se is experimentally estimated at  $6.0 \pm 0.25$  eV [19.193, 194].

We can get insight into the band structure also using the absorption spectrum  $\alpha(\hbar\omega)$ , calculated from reflectance spectra, at super-gap regions [19.4, 195]. Neglecting the wavenumber-conservation rule, we write down  $\alpha(\hbar\omega)$  as

$$\alpha(\hbar\omega) \approx |M(\hbar\omega)|^2 \int D(E)D(E + \hbar\omega)dE, \quad (19.2)$$

where  $M(\hbar\omega)$  is the transition matrix,  $D(E)$  is the DOS, and the integration is performed over  $E_F - \hbar\omega$  to the Fermi energy  $E_F$ . Thus, if  $M(\hbar\omega)$  were constant,  $\alpha(\hbar\omega)$  would represent convoluted  $D(E)$ , though the presumption being questionable [19.4].

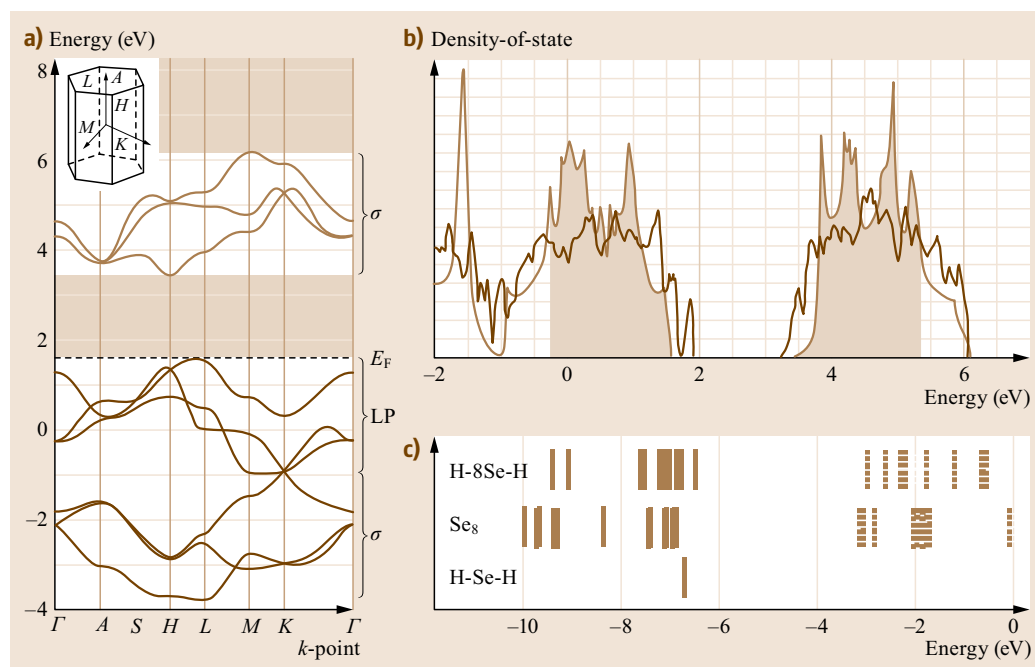


**Fig. 19.12** (a) Dispersion curves for t-Se and (b) DOSs for t-Se (shaded) and a-Se (brown line) with the left-hand side energy-scale (after [19.189, 190]), and (c) the energy levels of helical H-8Se-H, Se<sub>8</sub> ring, and H-Se-H clusters (calculated by an ab-initio method (after [19.69])) with the right-hand side scale, the zero being set at the vacuum level

### 19.4.2 Band Edge

#### Optical Absorption

Fig. 19.13 shows the optical absorption edge of a-Se, which consists of, at least, two curves [19.1, 4, 196]. At  $\alpha \geq 10^3 \text{ cm}^{-1}$ , the spectrum is approximated by the Tauc curve

$$\alpha \hbar\omega \approx (\hbar\omega - E_g^T)^n, \quad (19.3)$$

where  $n = 1$  and  $E_g^T$  ( $\approx 2.0 \text{ eV}$  at room temperature) is the Tauc optical gap [19.1], which becomes smaller at higher temperatures [19.40, 56, 196]. The fitting parameter  $n = 1$  is peculiar to a-Se, which has been ascribed to the one-dimensional atomic structure [19.4]. However, the one-dimensional  $D(E)$  is not evident in a-Se, Fig. 19.12(b), and accordingly, the more general  $n = 2$  may be preferred [19.56, 196, 197]. Below the curve, we see the Urbach edge

$$\alpha(\hbar\omega) = \alpha_0 \exp \left\{ \frac{\hbar\omega - E_U^0}{E_U} \right\}, \quad (19.4)$$

where  $\alpha_0$  ( $\approx 10^7 \text{ cm}^{-1}$ ) and  $E_U^0$  ( $\approx 2.4 \text{ eV}$ ) gives the Urbach focus, in which  $E_U^0$  is assumed to be a measure of the mobility gap [19.4, 198], and  $E_U$  ( $\approx 60 \text{ meV}$  at room temperature) is the Urbach energy, which

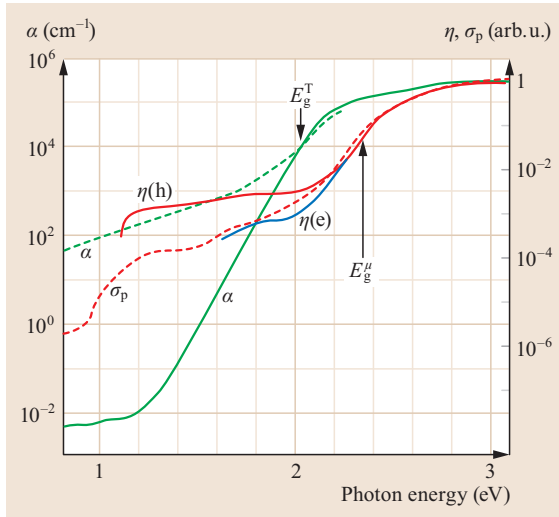


**Fig. 19.13** Spectral variations of the absorption coefficients  $\alpha$  in g-Se (solid line) and a-Se (dashed line) (after [19.201]), photoconduction  $\sigma_p$  (after [19.202]), and photogeneration quantum efficiencies for electron  $\eta(e)$  and hole  $\eta(h)$  (after [19.203]) in a-Se films ( $T_s \approx 60^\circ\text{C}$ ) at room temperature. Tauc optical gap  $E_g^T$  (after [19.196]) and the mobility gap  $E_g^\mu$  (after [19.204]) are indicated

tends to increase with temperature ( $\leq 900^\circ\text{C}$ ) [19.4, 16, 196]. Note that  $E_U \geq 50 \text{ meV}$  is universally observed in amorphous semiconductors and insulators, which may arise from thermodynamical density fluctuation [19.199]. Also note that the spectral shape and position of the absorption edge in evaporated films hardly change with ppm-level Cl doping and substrate temperatures (Sect. 19.1.1), though some aging modifications have been pointed out [19.27, 43].

Features below the Urbach edge in a-Se remain vague, in contrast to exponential weak-absorption tails in g-As<sub>2</sub>S(Se)<sub>3</sub> [19.1, 4, 6]. As shown in Fig. 19.13, the absorption level at  $\hbar\omega \approx 1 \text{ eV}$  in nominally-pure a-Se varies at  $10^{-2}$ – $10^2 \text{ cm}^{-1}$  from sample-to-sample and the intrinsic spectrum has not been revealed [19.69], the reason being ascribable to employed samples and experimental artifacts. For instance, in many experiments [19.1, 2, 196], the optical spectrum at higher and lower absorption regions than  $\approx 10^3 \text{ cm}^{-1}$  has been evaluated, respectively, using a-Se films and polished g-Se ingots, and accordingly, the purity of the ingot (Sect. 19.1.2) is crucially important when inspecting low absorption characteristics at  $\alpha \leq 1 \text{ cm}^{-1}$ . In addition, small attenuation (high transmission) is susceptible to light scattering caused by heterogeneous structures, even in photo-thermal spectroscopies [19.200, 201]. Further studies using well-characterized samples with scattering-calibrated measurements are required for elucidating the residual absorption spectrum, which is indispensable for obtaining reliable insights into gap states.

#### Photoconduction Spectra

Photoconductivity remains the most useful property of Se (Sect. 19.7). Hence, many studies have been performed on a-Se films [19.1–6], while few data are available for g-Se [19.25, 96] and l-Se [19.205]. Photocurrents appear through two processes; carrier generation and transport [19.4, 6], the former being affected by geminate recombination [19.203, 206] as described below and the latter by multiple trapping transport (Sect. 19.4.3) [19.207].

Photoconduction spectra, which are governed by the photogeneration process, of a-Se have been studied in details. Fig. 19.13 compares photogeneration quantum-efficiencies  $\eta(\hbar\omega)$  [19.203] and photoconductivity  $\sigma_p(\hbar\omega)$  obtained by a constant-photocurrent method [19.202] for a-Se films with  $T_s \approx 60^\circ\text{C}$ . We see that, despite of different samples and the measuring methods, the two spectra resemble in shape, which consist of three curves; with increasing  $\hbar\omega$ , a steep rise at  $\hbar\omega \leq 1.2 \text{ eV}$ , a gradual increase at  $1.2$ – $2.2 \text{ eV}$ , which overlaps with the optical Urbach-edge, and a steep rise again above  $\approx 2.2 \text{ eV}$ . It is mentioned that a-Se

films with  $T_s \approx 25^\circ\text{C}$  exhibit somewhat different spectra with a shoulder at  $\approx 1.4\text{ eV}$  [19.203].

Here, comparing the absorption and photoconduction spectra in Fig. 19.13, we can point out two features. One is the fading photoconductive response at  $\hbar\omega \leq 1.2\text{ eV}$ , in contrast to the fairly stable level of the optical absorption. This fact may suggest that the absorption at  $\hbar\omega \approx 1\text{ eV}$  is ascribed to electron (less mobile than hole) excitations from mid-gap states to the conduction band (Fig. 19.16). The other is the existence of a non-photoconducting gap, a spectral blue-shift of the photoconduction edge by  $0.3\text{--}0.5\text{ eV}$  from the optical absorption edge [19.47, 203, 208], which was first reported by *Weimer* [19.209]. The gap is understood to be a manifestation of recombination of photogenerated geminate electron-hole pairs, the idea being comprehensively analyzed by *Pai and Enck* [19.206] using an Onsager model. (It should be mentioned that, different from the exciton, the geminate pair is treated as classical charged particles.) The geminate-pair recombination model predicts that  $\eta(\hbar\omega)$  can be approximated by two curves [19.204]

$$\eta(\hbar\omega) \approx \exp\left\{\frac{\hbar\omega - E_g}{k_B T}\right\} \quad \text{and} \quad \exp\left\{-(\hbar\omega - E_g)^{-1/2}\right\}, \quad (19.5)$$

respectively, below and above  $\eta \approx 10^{-2}$ , in harmony with the observation, where  $E_g \approx 2.4\text{ eV}$  can be regarded as the mobility gap. The former equation manifests a *photoconducting Urbach edge*, though it is substantially masked by the residual response at  $\hbar\omega \leq 1.2\text{ eV}$ . The photoconduction spectrum red-shifts under high electric fields, which can be interpreted using an extended Onsager model [19.210, 211]. Finally, it seems worth mentioning that similar non-photoconducting gaps exist in g-Se [19.25], l-Se [19.205], and in all the Se crystals, *except* t-Se [19.2, 212], the reason being speculative.

### 19.4.3 Gap States and Defects

Studies of the gap state in a-Se are indispensable to two purposes. One is fundamental, i.e., the identification of defects, and the other concerns with device applications. Experimentally, related insights can be obtained through measurements of electron-spin resonance (ESR), optical and photoconductive spectroscopy, photoluminescence, thermally-stimulated currents, photoinduced changes, and so forth. However, since the gap-state density is typically of ppm levels, which are naturally sensitive to disordered structures and impurities (Fig. 19.4), reproducibility of gap-state data is more-or-less problematic. In the following, we

briefly touch the known charged defect model [19.4–6], and then, will summarize experimental results on the gap state, in which transient photocurrents at room temperature are specifically interested in accordance with growing applications.

#### Charged Defect Model

The gap state in pure materials originates from some kinds of defects. And, for the defect in chalcogenide glasses including a-Se, the most frequently employed concept is undoubtedly the charged dangling bonds,  $\text{D}^+(\cdots\text{Se}-\text{Se})$  and  $\text{D}^-(\cdots\text{Se}-\text{Se})$ , proposed by *Street and Mott* [19.213], or a modified one, the valence alternation pairs ( $\text{C}_{3+}$ ,  $\text{C}_{1-}$ ) by *Kastner et al.* [19.214]. They assumed that the positively- and negatively-charged defects, with a density of  $10^{16}\text{ cm}^{-3}$  in a-Se [19.215], produce gap states below the conduction band and above the valence band, respectively. The ideas have been analyzed theoretically and employed in interpreting many observations [19.4–6, 216].

However, the concept still remains unconvincing. Actually, there is no direct experimental evidence revealing the existence of the charged defects. Or, we have no experimental tools which can detect ESR-inactive, point-defect like, atomic structures with ppm densities in amorphous materials. Besides, theoretical calculations of defective states, specifically the formation energy and electronic level, in flexible disordered structures encounter very subtle situations [19.69, 135, 137, 218–227]. For instance, through an ab initio calculation of the total energy, *Vanderbilt and Joannopoulos* [19.218] argued that the charged defects have *positive* correlation energy in a-Se, suggesting few densities. On the other hand, several calculations support the existence of intimate valence-alternation pairs  $=\text{C}_{3+}-\text{C}_{1-}$  with modified charges [19.69, 137, 220, 224], an example being shown in Fig. 19.14. In addition, different ideas have been proposed for defective structures, which include four-fold coordinated Se atoms [19.135, 223, 224], polarons [19.69, 220, 222], and also disorders in the dihedral angle [19.225–227], segmental lengths [19.69], and interactions between lone-pair electrons [19.228, 229]. Gap states probably arise also

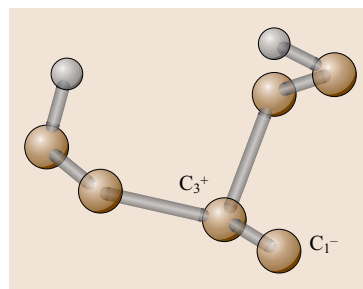


**Fig. 19.14** An atomic structure of  $(\text{H}-2\text{Se})=\text{Se}-\text{Se}$ , calculated using an ab initio chemical method (after [19.69]), in which  $\text{C}_{3+}$  and  $\text{C}_{1-}$  have the total Mulliken charges of  $\pm 0.17$

from heterogeneous structures such as embedded crystalline grains [19.31,34]. In short, it seems fair to assert that, although the charged-defect concept has been a good working hypothesis, it still faces a matter of debate.

### Low-Temperature Observations

ESR characteristics of Se have been explored since the 1960s [19.2]. In pioneering studies, spin signals appearing in Se solids were ascribed to O impurities [19.2, 69]. Afterwards, *Agarwal* [19.230] demonstrated that in pure g-Se the spin density was less than  $10^{15} \text{ cm}^{-3}$ , which was nearly an ESR detection limit. However, Bishop et al. [19.215] discovered that light exposures to g-Se at 4.2 K produce spin signals with a density of  $10^{16} \text{ cm}^{-3}$ , and later, Kolobov et al. [19.231] notified that the density increases up to  $10^{20} \text{ cm}^{-3}$  in a-Se films upon exposures to intense illumination at 20 K, which disappears with annealing at  $\approx 100 \text{ K}$  ( $\approx T_g/3$ ). These spin signals evince the photo-creation of neutral dangling bonds  $D^0$  ( $\cdots\text{Se}-\text{Se}\cdot$ ), which may be produced through conversion from the charged defects, i.e.,  $D^\pm \pm e \rightarrow D^0$  ( $e$  depicts an electron) [19.4]. However, since  $D^0$  can be produced also by breakage of normal  $-\text{Se}-\text{Se}-$  bonds, the spin signal cannot prove the existence of the charged defects,  $D^+$  and  $D^-$ .

Photoluminescence in a-Se exhibits both similar and dissimilar behaviors from those in other chalcogenide materials [19.4, 216, 217, 232]. As illustrated in Fig. 19.15, similarities lie in the two points; the peak

position  $E_{\text{PLE}}$  of photoluminescence excitation spectrum at the Urbach-edge region and the spectral location of a luminescence peak at  $E_{\text{PL}} \approx E_{\text{PLE}}/2$ , referred to as the *half-gap rule*. It applies to t-Se as well [19.233]. a-Se also exhibits the so-called photoluminescence fatigue under continuous excitation at 4 K [19.234], as those in As(Ge)-S(Se) glasses [19.217]. However, in more details, Se presents some peculiar facets. For the peak positions, we see that  $E_{\text{PL}}/E_{\text{PLE}} \approx 0.8/2.1(\text{eV}) = 0.38 < 0.5$  [19.217, 232], clearly deviating from the half-gap rule. For emitted light intensity, photoluminescence efficiency in g-Se has been demonstrated to be smaller by  $\approx 10^{-2}$  and  $\approx 10^{-3}$  than those in g-As<sub>2</sub>Se<sub>3</sub> and g-GeSe<sub>2</sub> [19.97, 217]. Also, it is known that the efficiency in g-Se is strongly quenched by O impurities [19.71, 72, 95].

How can we understand these observations? In terms of the charged defect model, the mid-gap luminescence has been related with  $D^0$  levels [19.4, 216]. Otherwise, some researchers have applied excitonic models [19.233, 234]. Nevertheless, no convincing interpretations have been given for the spectral deviation and weak intensity.

The last topic concerns the photoinduced mid-gap absorption [19.4, 6]. It is known that, in g-As<sub>2</sub>S(Se)<sub>3</sub> under illumination at low temperatures, an absorption band with  $\alpha \approx 10 \text{ cm}^{-1}$  appears at  $\hbar\omega \approx E_g/2 - E_g$ , the origin being ascribed to  $D^0$  defects [19.4, 6, 214–216]. For a-Se, however, such an absorption band has not been reported, to the author's knowledge, though photoinduced below-gap absorptions are known to emerge in t-Se [19.235], l-Se at 590 °C [19.236], a-Se nano-particles [19.237], and single Se chains in zeolite [19.238, 239]. Nevertheless, it has been demonstrated, as shown in Fig. 19.15, that a-Se films at 13 K undergo photoinduced photocurrent enhancement extending to  $\hbar\omega \geq 1.0 \text{ eV}$ , which recovers with annealing at 200 K [19.74]. This enhancement may be related with the photoinduced mid-gap absorption.

In short, these photoinduced phenomena at low temperatures evince the creation of mid-gap defects. However, the idea that the  $D^0$  level is located at mid-gap regions cannot be justified in the lone-pair semiconductor [19.4–6, 13], in which the level is assumed to lie in the vicinity of the valence band [19.69, 229]. Several candidates, including impurities, can also be envisaged for the mid-gap state [19.69, 220], and accordingly, the atomic structure still remains vague.

### Transient Photo-Responses and Thermally-stimulated Currents

Transient photocurrents  $I_p$  in samples with stacked/planar electrodes and decaying surface potentials  $V_x$  in xerographic configurations give insights into the gap-

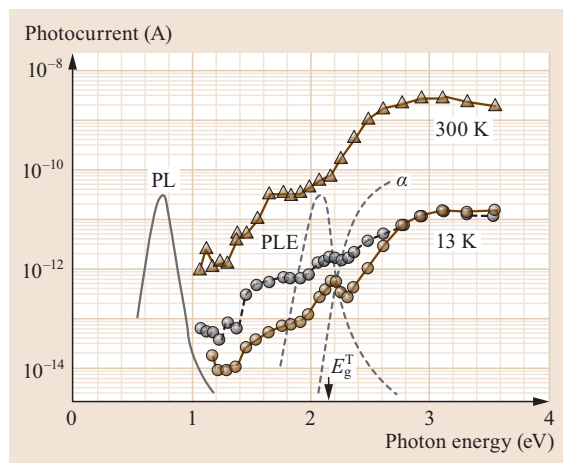


**Fig. 19.15** Comparison of photocurrent, photoluminescence (PL and PLE) (after [19.217]), and absorption spectrum  $\alpha$  with the Tauc optical gap  $E_g^T$  at  $\approx 10 \text{ K}$ . Symbols show photocurrent spectra in a-Se before (*open circles*) and after (*solid circles*) illumination of 2.5 eV light, and at room temperature (*triangles*), where illumination exerted no changes (after [19.74])

state DOSs [19.45, 91, 101, 240–242]. In details, there are several experimental and analytical procedures, in which a common principle is to convert the time variations  $I_p(t)$  or  $V_x(t)$ , where  $t \approx 1 \text{ ns} - 10^2 \text{ s}$ , to  $D(E_t)$ , where  $E_t$  is the trap depth. The derivation follows a multiple-trapping model, in which trapped charges are assumed to be thermally activated from gap states lying at varied  $E_t$  after a delay  $t$ , which satisfies  $t \approx \exp(E_t/k_B T)$ , where in many experiments  $T \approx 300 \text{ K}$ . Such procedures have provided considerable results so far, while the gap-state DOSs are not necessarily reproducible [19.4, 6], which may be due to different samples and experimental problems. For instance, in optical time-of-flight measurements of  $I_p(t)$ , photo-generated and/or deep-trapped charges may modify applied electric fields. In the conventional transient photocurrent method using thin samples with planar electrodes,  $I_p(t)$  is likely to be affected by surfaces. Xerographic measurements probe slow  $V_x(t)$  responses with  $t \geq 0.1 \text{ s}$ , governed by deep states, which are plausibly sensitive to impurities, prehistory, and so forth.

Recently, Kasap et al. [19.242] have reported comprehensive results for a-Se films with  $T_s \approx 60^\circ \text{C}$ . Their DOS, in conjunction with an assumption of  $E_g^\mu \approx 2.35 \text{ eV}$  [19.198], is plotted in Fig. 19.16. We see that the valence-band edge at 0–0.5 eV is exponential,  $\approx \exp(-E/E_v)$  with the steepness parameter  $E_v \approx 25 \text{ meV}$ . On the other hand, the conduction-band edge consists of a similar exponential curve with an additional peak at a depth of  $\approx 0.3 \text{ eV}$  and a small hump at  $\approx 0.45 \text{ eV}$ . They ascribe these peaks to  $C_{3+}$  defects, which may be incompatible with their presumption of neutral defects. Alternatively, these edge states may arise from heterogeneous structures, e.g., crystalline in-

clusions [19.32, 34]. They also suggest that the total density of deep gap states at 0.7–1.5 eV, occupied and unoccupied, is less than  $10^{14} \text{ cm}^{-3}$ .

Is the Kasaps' DOS compatible with previous observations? The DOSs at the conduction- and valence-band edges are connected with the Urbach energy  $E_U$  (Fig. 19.13) through the convolution integral (19.2), and accordingly, the steepness parameters of  $\approx 25 \text{ meV}$  in both edges are consistent roughly with the  $E_U$  value of  $\approx 60 \text{ meV}$ . However, taking the different origins (lone-pair and anti-bonding states) of the two bands, we may be puzzled about the same values. Actually, Lanyon [19.47] obtained  $E_v \approx 67 \text{ meV}$  from voltage variations of space-charge limited currents, and also theoretical results [19.69, 243] predict more gradual valence-band edges than conduction-band edges. Another remark is that, in contrast to the simple exponential valence-band edge, many researchers assert the existence of a DOS peak at  $\approx 0.3 \text{ eV}$  [19.87, 102, 240, 241]. Reasons of this discrepancy are speculative; the peak may be so small and broad that it could merge into the exponential edge [19.244]. Regarding the conduction-band edge, the 0.3 eV peak is consistent with previous results [19.4, 77], which are obtained from thermal activation energies of the drift mobility. It is plausible that the DOS peak produces an optical absorption peak at  $\hbar\omega \approx 2.0 \text{ eV}$  ( $= 2.35 - 0.3 \text{ eV}$ ), while it may merge into the Urbach edge (Fig. 19.13). Also, the 0.45 eV hump may cause a spectral peak at  $\approx 1.9 \text{ eV}$ , which could be related with a small electron response of  $\eta$  at the energy (Fig. 19.13). Finally, the result that the total deep-state density is less than  $10^{14} \text{ cm}^{-1}$  is in harmony with previous results [19.91, 200].

Thermally-stimulated depolarization currents (TSCs) also give insights into trap parameters [19.80, 94, 245–249]. In this experiment, traps are first filled with photogenerated carriers at low temperatures, e.g. 80 K, and the carriers are detected as thermally-stimulated currents upon rising sample temperature with a fixed rate of 0.1–1.0 K/s. We may assume that, under the thermal activation process which occurs in proportion to  $\approx \exp(-E_t/k_B T)$ , the temperature scan takes a determinative role, instead of the time delay in the transient photoconductivity. Using this method, Kang et al. [19.94] and Mikla and Mikla [19.245] reproducibly identified hole traps at depths of  $\approx 0.22 \text{ eV}$ , which should be re-examined in conjunction with the simple exponential edge in Fig. 19.16 [19.242]. They also inferred other deeper traps at 0.6–1.1 eV from current peaks appearing above  $\approx 300 \text{ K}$  [19.94, 245–249], while those could be affected by the glass transition and crystallization.

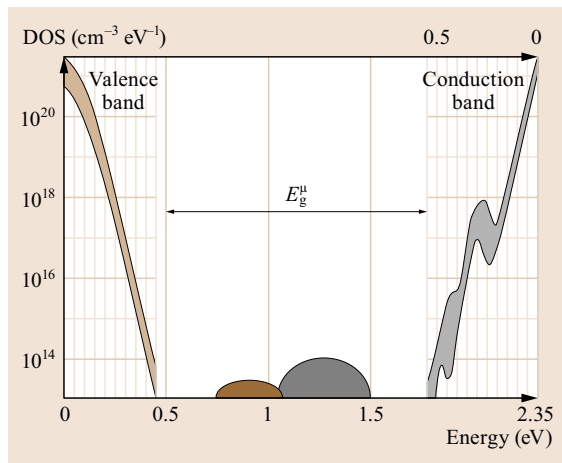


**Fig. 19.16** DOS of band-edge and gap states reported (after [19.242])



## 19.5 Electrical Properties

### 19.5.1 Electrical Conduction

Substantial studies have been performed on electrical conduction in crystalline Se. As known, the conductivity is written as  $\sigma = en\mu$  ( $n$  is the carrier density and  $\mu$  is the mobility), and intrinsic conduction in Se with  $E_g \approx 2$  eV suggests few thermal carriers ( $n \leq 10^4$  cm $^{-3}$ ) at room temperature, which makes the mobility  $\mu$  a matter of concern. It is formally written as  $\mu = e\tau^s/m^*$  in Drude model, where  $\tau^s$  is the scattering time and  $m^*$  ( $=\hbar^2/(\partial^2 E/\partial k^2)$ ) is the effective mass, for which the dispersion curve (Fig. 19.12) suggests  $m_c^* < m_h^*$  in t-Se. On the other hand, experimental  $\mu$  values in t-Se appreciably scatter, probably owing to defective and/or contaminated samples, with typical  $\mu_h$  of  $\approx 30$  and  $\approx 10$  cm $^2$ /Vs for parallel and normal to the chain axis and  $\mu_h/\mu_e \approx 4$  (Table 19.1) [19.2, 250]. We may then assume  $\tau_e^s < \tau_h^s$ , which implies stronger electron–lattice interaction. Or, the electron may form a small polaron. The hole is known to be more mobile also in  $\alpha$ -m-Se [19.251].

In pure g-Se the electrical conduction is totally electronic, with no ionic contribution being reported. The dc electrical conductivity is evaluated as low as  $10^{-17}$  S/cm (Fig. 19.4) at room temperature with the activation energies of 0.7–1.0 eV [19.2, 4, 75, 88]. Holes dominate the conduction (Table 19.1) [19.2, 4], which also applies to l-Se [19.252]. n-Type conduction, e.g., by Cl doping, seem to be more-or-less difficult to attain [19.25, 42, 78, 83, 252].

For a-Se, important quantities which govern the motion of photogenerated carriers are two. One is the drift (trap-controlled) mobility  $\mu_d$ , defined as  $\mu_d \approx \mu(n/n_t)$  [19.4], where  $\mu$  is the band (conventional) mobility, and  $n$  and  $n_t$  are the carrier densities in a band and band-tail traps. The other is the carrier lifetime  $\tau$ , which may be governed by deep traps. And, the product  $\mu_d\tau$ , the so-called *range*, becomes a measure which characterizes the transport of photogenerated carriers. These values have been evaluated using transient experiments such as optical time-of-flight measurements (Fig. 19.17), in which photo-generated carriers in a-Se output conventional rectangular-shaped (non-dispersive)  $I_p(t)$  signals at room temperature [19.23, 241, 242]. Specifically, for the evaporated films, these transport parameters have been evaluated as functions of substrate temperatures [19.44], film thicknesses [19.26], relaxation (aging) [19.82, 84], bias illumination [19.253], and doping [19.76–83, 103].

These studies have demonstrated the followings: In good-quality a-Se films [19.1, 4, 54, 76, 84, 254] and g-Se layers [19.23],  $\mu_d$  is fairly reproducible;  $\mu_{dh} \approx 0.15$

and  $\mu_{de} \approx 0.005$  cm $^2$ /V s (Table 19.1), while  $\tau$  considerably scatters;  $\tau_h \approx 10$ –50  $\mu$ s and  $\tau_e \approx 10$ –500  $\mu$ s, the combined results giving  $\mu_{dh}\tau_h > \mu_{de}\tau_e$ , which may be termed *p-like* conduction [19.255]. Since  $\mu_d$  and  $\tau$  are governed by shallow and deep traps, respectively, the latter appears to largely depend upon samples and/or experimental artifacts. In stabilized a-Se films, the carrier ranges tend to become higher than those in pure films [19.79, 103], the reason having been theoretically considered [19.104]. To the author's knowledge, no transport data have been available for l-Se.

### 19.5.2 Avalanche Breakdown

Juška and Arlauskas discovered that a-Se films in an optical time-of-flight configuration (Fig. 19.17) exhibit photoconductive avalanche breakdown [19.256, 257]. We see in Fig. 19.17 that, at electric fields above  $\approx 1$  MV/cm, hole and electron photocurrents abruptly increase. On the other hand, during investi-

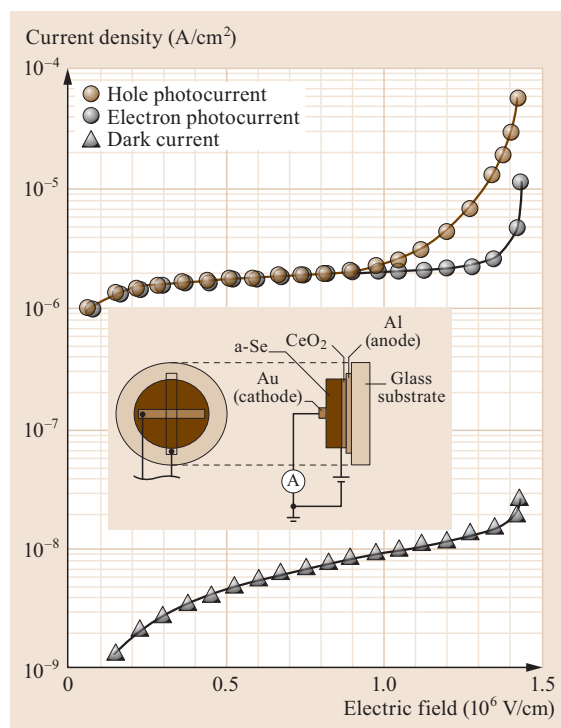


**Fig. 19.17** Electric field dependence of photo- and dark-current density at room temperature for a 1  $\mu$ m thick a-Se film under illumination of 400 nm light. The inset illustrates the sample structure, in which the facing electrode area is 1 mm  $\times$  1 mm and excitation light is incident on the glass substrate (after [19.259])



gations of a-Se vidicon targets, Tanioka et al. noticed dramatic sensitivity enhancements [19.258], arising from carrier multiplications, which have been developed to HARP (high-gain avalanche rushing amorphous photoconductor) vidicons (Sect. 19.7). These two discoveries have then initiated many fundamental studies, which delineate avalanche behaviors as functions of electric field ( $\leq 1.6$  MV/cm) [19.259], temperature (100–300 K) [19.256, 257, 259], a-Se film thickness (0.5–200  $\mu\text{m}$ ) [19.257, 259], and light wavelength (400–600 nm) [19.259, 260], and also in several sample-electrode arrangements [19.261–263].

However, scientifically, the avalanche breakdown in a-Se still remains puzzling. The avalanche breakdown in crystalline semiconductors such as Si and InSb has been known, which appears through successive impact ionizations by field-accelerated hot carriers. But, why can the avalanche breakdown occur in an amorphous semiconductor, probably having short carrier mean-free paths? In addition, the breakdown in a-Se becomes more conspicuous at higher temperatures [19.256, 257, 259], which is opposite to the behavior of conventional and impurity-related [19.264] carrier multiplications in crystalline semiconductors. And, why does the phenomenon appear clearly only in a-Se, but not in other amorphous semiconductors as g-As<sub>2</sub>Se<sub>3</sub> and a-Si:H and in crystalline Se [19.265, 266]? We just know that single crystalline t-Se undergoes piezo-electric oscillations at high fields [19.2], and poly-crystalline Se rectifiers exhibit injection-related current increases [19.267, 268].

For such fundamental problems, Canadian groups continue active studies [19.188–190, 269–273]. They have applied a lucky-drift model [19.274] to the amorphous film [19.270–272], under an assumption that carriers undergo *elastic collisions with disorder potentials*, thereby its energy can successively increase, giving rise to the impact ionization. Nevertheless, estimated lengths of the mean-free path between elastic collisions are only  $\approx 0.5$  nm [19.270, 272], and we may cast doubt upon the particle picture [19.275]. Following the model, they have interpreted the temperature dependence with a thermally-activated increase in the hole mobility [19.273], which is governed by tail states. Besides, the uniqueness to a-Se has been related with its low vibrational energy ( $\approx 30$  meV, Fig. 19.7) [19.271], arising from the heavy atomic mass, 79, which is effective to suppressing energy dissipation of accelerated carriers. If this were the case, can we envisage the avalanche multiplication in a-Te (or a-Se-Te alloy) films?

Finally, other approaches to the breakdown phenomenon should also be mentioned: Masuzawa et al. [19.262] have demonstrated carrier multiplication in Se/As-Se multilayers sandwiched between indium-

tin-oxide (ITO) and Al films (no blocking electrodes inserted) at  $\approx 1$  MV/cm, and proposed a different idea for the multiplication mechanism. Park and Tanioka [19.263] analyze HARP characteristics in a phenomenological way. Tanaka suggests a role of tail states above the valence band for impact ionization of holes [19.275].

### 19.5.3 Electrical Switching and Crystallization

Since the crystallization temperature of a-Se is relatively low  $\approx 100^\circ\text{C}$  (Fig. 19.3), Joule-heated crystallizations are likely to occur. It may behave as an electrical Ovonic memory effect [19.276, 277], which is an ongoing topic of phase-change materials such as Ge<sub>2</sub>Sb<sub>2</sub>Te<sub>5</sub>. Actually, the electrical switching and/or memory phenomena of a-Se had been explored in the 1970s and 1980s [19.278–285], while those results seem to be mostly forgotten. However, further studies of the behavior in the elemental material, which may have some relation with the photocrystallization (Sect. 19.6.3), will shed light upon the electrical phase-change. Hence, we briefly take a look upon previous studies below.

Several pioneering experiments uncovered switching (breakdown) behaviors in g- [19.278] and a-Se [19.279–285] samples having symmetric [19.278] or asymmetric [19.279, 280, 285] electrodes. For instance, Matsushita et al. [19.279] investigated a memory effect in Fe point-contacted a-Se/SnO<sub>2</sub> structures. Petretis et al. [19.281] observed electrical breakdowns in a-Se films subjected to corona charging. In these phenomena, transformations from a- to t-Se are likely to take place. The threshold fields of these switching were 0.1–1 MV/cm [19.278–285], which are similar to that in the avalanche breakdown (Sect. 19.5.2). However, in contrast to the *bulky* avalanche breakdown, the electrical switching seems to occur with carrier injections from electrodes or surfaces.

Mechanisms of the electrical crystallization remain confusing. Taking the photocrystallization phenomenon (Sect. 19.6.3) into account, we may envisage pure electronic mechanisms [19.280, 285]. Or, Bolotov and Komarova [19.282] demonstrate electric field effects on thermal crystal growth in a-Se. Otherwise, Joule heating could be responsible. In some memory effects, diffusion of electrode metals such as Pt and Ag has been detected [19.278, 284, 285]. It is hence plausible that several switching and/or memory processes play roles in each observation. Finally, we mention that optical effects upon electrical memory phenomena have been demonstrated using a-Se/SeO<sub>2</sub> hetero-junctions [19.286] and corona-charged

a-Se films [19.287], which also seem to involve the crystallization.

### 19.5.4 Electrode, Junction, and Multilayer

The choice of metal electrodes is a key issue when examining (photo-)electrical properties of semiconductors. For pure a-Se films ( $T_s = 50^\circ\text{C}$ ), *Mort* and *Lakatos* [19.193] demonstrated using internal photoemission spectroscopy that the barrier height  $\phi_h$  for holes, defined in Fig. 19.18, becomes smaller in the order of Al ( $\phi_h \approx 1.40\text{ eV}$  and  $\phi_M \approx 4.3\text{ eV}$ ), Cu ( $\approx 1.10\text{ eV}$ ,  $\approx 4.7\text{ eV}$ ), and Au ( $\approx 0.85\text{ eV}$ ,  $\approx 5.1\text{ eV}$ ), which suggests that Au makes a good hole-injecting contact. Au is also known to be less reactive with a-Se than Al [19.288]. Nevertheless, for stabilized a-Se films contacting with metal electrodes of various kinds, *Kasap* and *Rowlands* [19.102] found no correlation between dark currents and the metal work-functions. Reasons of these seemingly different observations are unknown.

Blocking electrodes have also been explored, mainly for photoconductive experiments and applications. In the usage in xerographic photoreceptors, a-Se films deposited upon oxidized Al layers are exposed to positive corona discharges, in which the oxide is expected to work for suppressing electron injection [19.15, 79]. For similar purposes,  $\text{Sb}_2\text{S}_3$  [19.86, 261], poly-vinylcarbazole [19.249, 289], and cellulose acetate [19.261] films have also been employed. In other cases, we may need blocking electrodes for both polarities. Specifically, since the hole is more mobile, good blocking anodes – even under high voltages – would be required. For such purposes, several layers have been inspected, e.g.,  $n^+$ -type  $\text{SnO}_2$  ( $E_g \approx 3.5\text{ eV}$  and  $\phi_M \approx 4.8\text{ eV}$ ) [19.86, 286],  $\text{CeO}_2$  ( $E_g \approx 3.4\text{ eV}$ ) [19.86, 261, 263, 290],  $\text{GeO}_2$  ( $E_g \approx 5\text{ eV}$ ) [19.263],  $\text{ZnO}$  ( $E_g \approx 3.2\text{ eV}$ ) [19.291], and polyimide ( $E_g \approx 7\text{ eV}$ ) [19.290, 292, 293].

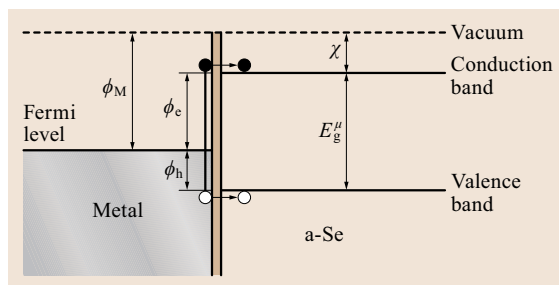


**Fig. 19.18** Band diagram of a metal/a-Se junction (after [19.193]). The work function  $E_g^\mu + \chi \approx 6\text{ eV}$  and the mobility gap  $E_g^\mu \approx 2.3\text{ eV}$

Junctions including a-Se films have been prepared mainly for investigating and/or improving photoconductive characteristics. For instance, a-Se/polyvinylcarbazole and a-Se/a- $\text{Se}_{1-x}\text{Te}_x$  were devised as xerographic photo-receptors [19.193, 294, 295]. More recently, *Campbell* [19.296] has demonstrated that the hetero-junction using a-Se and an organic film, octabutoxy tin naphthalocyanine dichloride, can extend photoconductive responses to wavelengths of  $\approx 1\text{ }\mu\text{m}$  under reverse-bias conditions. Here, it is mentioned that few studies have been performed for a-Se/t-Se junctions [19.247], while the inspections will be valuable for understanding electronic properties of partially-crystallized a-Se films.

Multi-layer structures are expected to extend spectral performance and enhance thermal stability. *Maruyama* [19.86] examined  $\text{Se}/\text{As}_2\text{Se}_3$  films, demonstrating that the  $1\text{ nm}$ -periodicity structures can be regarded as an almost uniform material. *Masuzawa* et al. [19.262] and *Yu* et al. [19.297] also studied similar systems for improving photoconductive responses. *Nesheva* et al. uncovered interfacial effects on thermal stability in  $\text{Se}/\text{CdSe}$  [19.298] and  $\text{Se}/\text{Se-Te}$  [19.92] films. In  $\text{Se}/\text{As}_2\text{S}_3$ , however, photoinduced diffusion is likely to take place [19.299, 300].

## 19.6 Light-induced Phenomena

Discovery of light-induced structural changes in chalcogenide glasses can be traced back to a short note reporting “the fluidity in g-Se under illumination” by *Vonwiller* about a century ago [19.301]. Nevertheless, his note might attract little interest. Afterwards, the pioneering work of optical (and also electrical) phase changes by *Ovshinsky*’s group [19.276] triggered worldwide studies on light-induced structural changes. And, we now know several kinds of phenomena in chalcogenide glasses such as a-Se and  $\text{As}_2\text{S}_3$ ,

which have repeatedly been reviewed [19.5, 6, 216, 302].

What are the outcomes obtained through studying the light-induced phenomena in a-Se? It may be fair to admit that since the glass-transition temperature ( $\approx 310\text{ K}$ ) of a-Se is just above room temperature, applications of the phenomena will be limited. Or, in some cases, those may cause serious problems in photoconductive applications, e.g., photocrystallization in HARP films [19.303], and accordingly, suppres-

sion is strongly required, for which the understanding of induction processes is a prerequisite. On the other hand, the existence of only the homopolar bond  $\text{—Se—Se—}$  makes the underlying mechanisms more specific. In other words, it is important to examine whether a phenomenon is unique to the elemental material or universal to compound chalcogenide glasses. In such contexts, studies using S and Te are also tempting, while the glass-transition temperature in a-S is below room temperature ( $\approx 260$  K [19.304]) and a-Te films appear to crystallize at room temperature ( $\approx 285$  K) without undergoing a glass transition [19.305]. Incidentally, *Sakaguchi and Tamura* [19.302] have investigated light-induced phenomena in thin ( $\approx 1\ \mu\text{m}$ ) l-Se and l-S samples (above the melting temperatures), the results being very valuable to examine roles of the equilibrium states.

Light-induced phenomena in a-Se are of several kinds, and then a classification may be instructive. At the outset, the phenomena can be divided into two. One is the thermal change – heat mode –, in which temperature rises induced by light absorption are assumed to govern the structural changes; a known example being the optical phase change [19.276], which has widely been commercialized using  $\text{Ge}_2\text{Sb}_2\text{Te}_5$  films [19.277], while studies for a-Se remain. The other is the photoinduced change – photon mode –, in which not the temperature rise but electronic excitations directly cause successive atomic transformations. The photon mode can further be divided into two; those appearing only during illumination (as photoconductivity) and those existing after illumination, the two being referred to as *transitory* and *memory* effects. Besides, the memory effect may be *irreversible* (permanent) or *reversible* (meta-stable), in the sense whether annealing treatments cannot or can restore the state before illumination. We may regard the irreversible change as a kind of photoinduced stabilization processes, the known examples being photocrystallization (Sect. 19.6.3) and ring-to-chain transformations [19.62, 306]. The reversible can further be divided into two by needed annealing temperatures, which may be  $\approx T_g/2$  (defective) or  $\approx T_g$ , the former being already touched in Sect. 19.4.3. Here, it is plausible that a transitory change at room temperature and a low-temperature defective phenomenon have some common origins, which remains to be studied. Finally, all the photo-induced changes can be divided into *scalar* or *vector*, in the sense if the polarization of excitation light provides isotropic or anisotropic changes. It should also be mentioned here that, not only visible light, but electron [19.5, 307, 308] and high-energy [19.5, 181, 309] beams can exert some structural changes.

### 19.6.1 Transitory Effects

As mentioned above, g-Se undergoes *softening* when exposed to light [19.301], and later studies have emphasized respective features; photoinduced “relaxation” [19.310, 311], “aging” [19.310, 312], “melting” [19.313], “fluidity” [19.314], “viscosity” [19.315], and so forth [19.316–318]. It is plausible that these transitory changes cause modifications of thermal properties [19.310, 319]. Transitory volume expansion and oscillation have also been discovered [19.320, 321]. Besides, transitory absorption, which has been known for As-S films [19.6], was demonstrated also for a-Se at room temperature [19.322, 323]. The origin may be related with the defective absorption (Sect. 19.4.3) and/or the photodarkening (Sect. 19.6.2). Mechanisms of photoinduced changes could be inferred from the excitation spectra. Fig. 19.19 [19.324] compares three kinds of spectra with the absorption spectrum  $\alpha$ . (1) shows the photoluminescence excitation spectrum (Fig. 19.15), (2) represents the photodarkening magnitude (Sect. 19.6.2), which peaks at the non-photoconducting spectral region (Fig. 19.13), and (3) includes the photoconduction (Fig. 19.15). Larmagnac’s result implies that the photoinduced relaxation

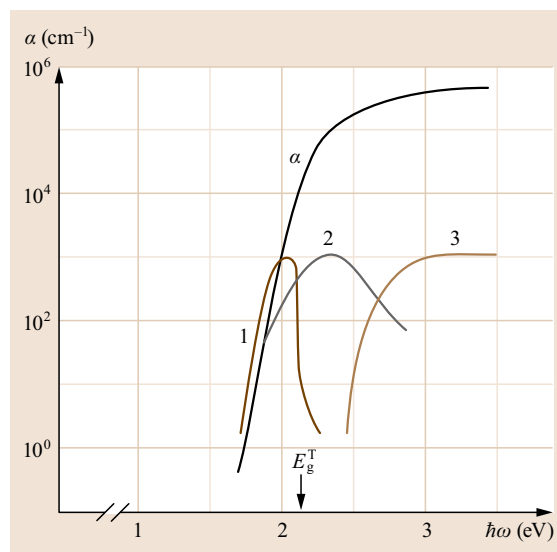


**Fig. 19.19** Comparison of the absorption-edge spectrum  $\alpha$  and the Tauc optical gap  $E_g^T$  with three spectral types of photoinduced phenomena at  $\approx 80$  K (after [19.324]); (1) includes photoluminescence-excitation spectrum (after [19.217]), (2) saturated edge-shift in the photodarkening (after [19.324]), and (3) photoconductivity (after [19.202]), a quantum efficiency of photo-etching (after [19.124]), and probably the photocrystallization (after [19.247, 325])

efficiency has the type (2) [19.310]. We then straightforwardly assume geminate-pair excitations as the first step of the transitory change.

The next problem is whether the excitation induces some atomic changes directly through electron–lattice interaction or indirectly through temperature rises. Inasmuch as the glass-transition temperature of a-Se is just above room temperature, low-temperature experiments are preferred for the distinction. And, such studies [19.311] seem to support major roles of the direct mechanism, e.g., excited geminate pairs cut –Se–Se– bonds through some processes, the consequence appearing as the fluidity increase etc. Intra- and inter-bond mixing may occur in the process, which is consistent with an EXAFS result, demonstrating an increase in the atomic coordination number by  $\approx 4\%$  in a-Se films at 30 K *during* illumination (Xe lamp,  $\approx 100 \text{ mW/cm}^2$ ) [19.326]. With terminations of the exposure, relaxational bond restorations take place. Quantitative formulation connecting induced fluidity with light intensity will be a challenging subject.

### 19.6.2 Photodarkening and Deformations

There may be some confusion about the usage of *photodarkening*. In the broadest sense, the word can represent all the photochromic effects, i.e., decreases in optical transmittance induced by illumination, which make the material darker. In the research area of chalcogenide glasses, however, it has restrictively been utilized to denote “photoinduced nearly-parallel red-shifts of the optical absorption edge which can be recovered with annealing at around the glass-transition temperature” [19.6, 216, 302] [TS.3]. The word does not include transitory and irreversible photochromic effects.

The photodarkening in chalcogenide glasses such as  $\text{As}_2\text{S}(\text{Se})_3$  has been comprehensively studied [19.6, 216, 302]. And, we may trace its discovery in a-Se back to *Chang* [19.327], though he seemed to examine optically-thick samples. (For quantitative evaluation of photodarkening characteristics, specifically the time variation, inspected samples are preferred to be optically-thin,  $\alpha L \leq 1$ , where  $L$  is the sample thickness and  $\alpha$  ( $\approx 10^4 \text{ cm}^{-1}$ ) is the absorption coefficient to excitation light. Accordingly, most of experiments have employed deposited films of  $L \leq 10 \mu\text{m}$ . Such experiments demonstrate *exponential* growths, which can be connected with the first-order reaction kinetics [19.328].) Later studies have confirmed its existence, e.g., a red-shift of  $\approx 50 \text{ meV}$  at  $\hbar\omega \approx 2.3 \text{ eV}$  in a- and g-Se at  $\approx 80 \text{ K}$  [19.56, 324, 329, 330], and also under high pressures [19.331–333]. In addition, although no spectral shifts having been presented, photoinduced transmission decreases reported in [19.334–337] seem to arise

from the photodarkening. Taking the Kramers–Kronig relation into account, we straightforwardly envisage that the photodarkening accompanies an increase in refractive index [19.6, 328].

Despite of its simple appearances, the mechanism of the photodarkening in chalcogenide glasses has been controversial. For instance, some researchers asserted that the hetero- to homo-polar bond-change causes the photodarkening [19.302]. Actually, Raman-scattering spectroscopy manifests that in  $\text{As}_2\text{S}_3$  (super-)bandgap illumination produces As–As bonds, which may be oxidized to  $\text{As}_2\text{O}_3$  crystals in some conditions, and also give rise to the photodarkening. Practically, it is very plausible that super-bandgap photons induce several structural changes. However, why is the production of As–As bonds able to cause a red-shift of the optical absorption edge? It should also be noted that sub-gap illumination can induce the photodarkening in  $\text{As}_2\text{S}_3$  [19.324, 337], with producing few As–As bonds. In addition, the fact that the photodarkening occurs unambiguously in a-Se, and also in a-S [19.332], evinces that such bond alternations cannot be a universal origin.

For the photodarkening mechanism, it is valuable to recall the excitation spectra. In a-Se, the red-shift is the highest ( $\approx 50 \text{ meV}$  at 80 K) upon illumination of light with the photon energy of  $\approx 2.4 \text{ eV}$  [19.324, 329, 332], which is located at the non-photoconducting gap region, i.e., the type (2) in Fig. 19.19. This fact manifests that the photodarkening is triggered by geminate (excitonic) carriers, which may cause local ( $\approx 5 \text{ \AA}$ ) twisted bonds and overall *structural disordering* [19.216, 228, 302, 326, 332], giving rise to broadening of the lone-pair band, and consequently, the red-shift of the optical absorption edge. As an example, Fig. 19.20 illustrates a bond-twisting model [19.332] in a trimer structure consisting of two H–Se–H and a H–3Se–H, in which the central Se can take electronically transferable bi-stable positions. An ab initio chemical calculation [19.104] demonstrate that, reflecting stronger inter-cluster interaction between lone-pair states, the twisted (lower) structure has a higher HOMO level by  $\approx 0.3 \text{ eV}$  with little change in LUMO levels (not shown), which is assumed to cause the photodarkening. Incidentally, the number of atoms contributing to the photodarkening is estimated at  $\approx 1 \text{ at.}\%$ , the density being consistent with the reversible behavior [19.328].

The structural disordering, with the transitory photoinduced fluidity described in Sect. 19.6.1, may cause quasi-stable volume expansions. Actually, expansions of  $\approx 0.3\%$  are detected in a-Se after illumination at room temperature [19.338], despite that the photodarkening is short-lived at the temperature, which is just below  $T_g$  [19.335, 336]. How can these observations be mediated? We assume that both the phenomena are

[TS.3] Is this a direct quote?



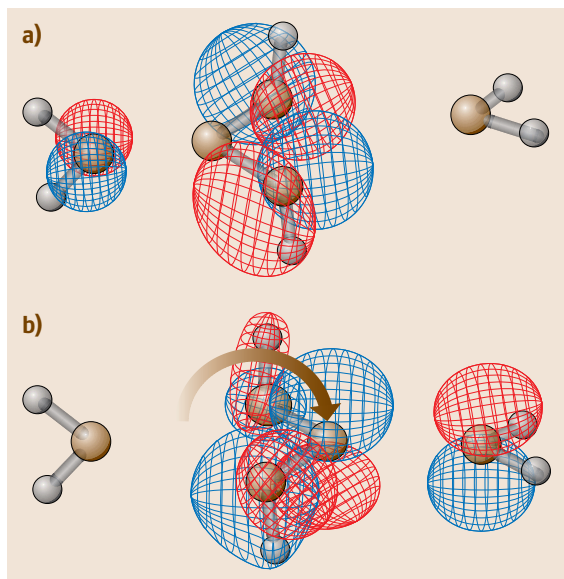


**Fig. 19.20a,b** Bond-twisting motion in a Se trimer, with HOMO wavefunctions, which models three Se chains in a-Se structures: **(a)** stable configuration, in which the central atom rotates to the right-hand side under electronic excitation, and relaxes to **(b)** the quasi-stable structure upon de-excitation

manifestations of the photoinduced structural disordering, while because the photodarkening arises from local atomic changes (such as bond twisting) and the expansion appears through successive macroscopic atomic flows [19.338], thermal recovery of the latter needs much longer times. Finally, it should be mentioned that, instead of the structural disordering, some researchers propose Coulombic forces [19.320,321] and thermal effects [19.339,340] as expansion stimuli. However, such ideas face to difficulties in interpreting the fact that these photoinduced changes become greater at lower temperatures [19.6, 216, 302].

### 19.6.3 Photo-crystallization

Photo-crystallization, its mechanism being comprehensively studied by *Dresner* and *Stringfellow* [19.247], has attracted considerable interest due to its peculiar features. For instance, the crystallization of a-Se to t-Se causes conspicuous morphological and electrical changes. However, it is still difficult to draw a whole picture of the photo-structural process, due to its complicated nature involving crystallite nucleation and successive growth [19.5, 6].

Pioneering researchers inspected the phenomenon mainly using optical microscopes, which revealed several unique features [19.247, 325, 341, 342]. A growth

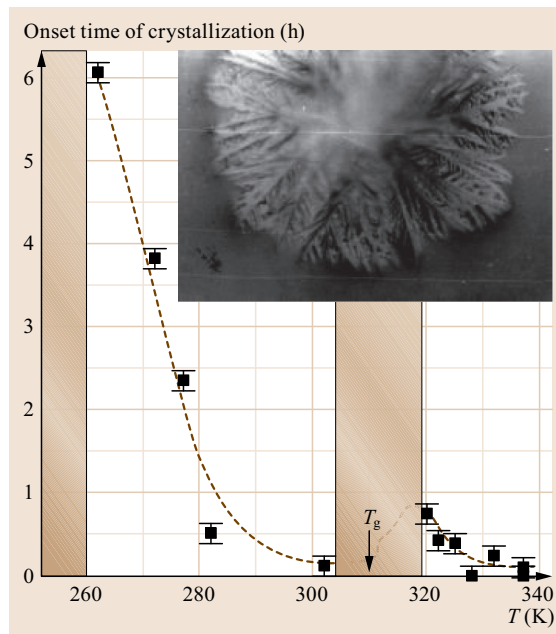


**Fig. 19.21** Exposure (incubation) times until photocrystallization is detected as a function of the sample temperature  $T$  (after [19.303]). Excitation light is 633 nm in wavelength and  $17 \text{ W/cm}^2$  in intensity. The inset shows a Se spherulite, the diameter being  $\approx 0.1 \text{ mm}$ , grown with a rate of  $\approx 0.1 \mu\text{m/min}$  on the free surface of an a-Se( $2 \mu\text{m-thick}$ )/Au/mica sample at 325 K under illumination of  $\approx 20 \text{ mW/cm}^2$  from an Hg lamp

rate of crystals in a-Se films just the crystallization temperature  $T_c$  ( $\approx 100^\circ\text{C}$ ) is markedly enhanced by light illumination, or specifically by photo-generated holes [19.247]. In this context, the photocrystallization may be related with the (photo-)electric phase change (Sect. 19.5.3). t-Se crystals emerge, depending upon conditions, on the free surface as spherulites and also at the boundary with substrates. On the other hand, suppressions of the crystallization by electron beams [19.341] and red light [19.343], the phenomena resembling infrared quenching in photoconductivity [19.208, 246], have been demonstrated. Also, the photocrystallization can be suppressed by alloying with other atoms such as Ge [19.344], Te [19.90, 92], etc. It is also known that the crystal growth is thermally activated, which exhibits vector behaviors (Sect. 19.6.4).

Raman measurements [19.31, 92, 134, 303, 337, 345] seem to have higher sensitivity in crystallite detection. And recently, a Canadian group has demonstrated that the photocrystallization occurs at two temperature regions, as shown in Fig. 19.21, lower and higher than  $T_g$  ( $\approx 310 \text{ K}$ ), the latter having been known as written above. By contrast, at the lower

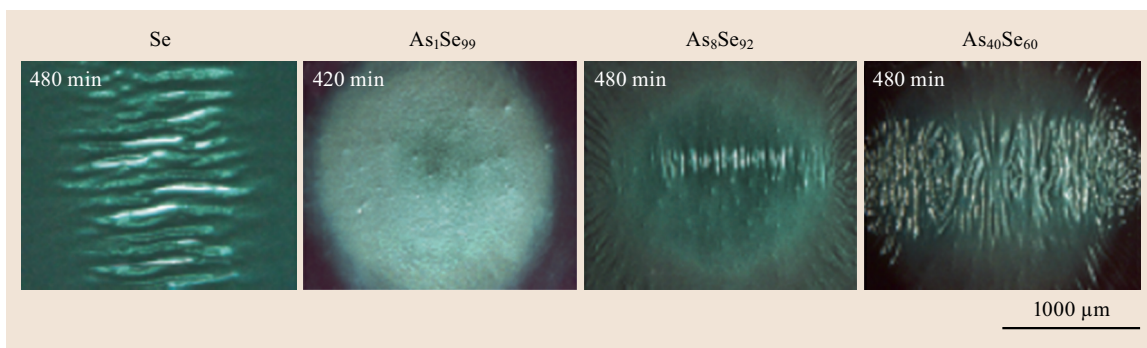


**Fig. 19.22** Vector deformations in As-Se films deposited upon silicone grease, induced by linearly (vertically) polarized bandgap light (exposure times given). Note that only a-Se produces vertical wrinkling pattern, with a transition at  $\text{As}_1\text{Se}_{99}$  to the horizontal (after [19.106]) (Copyright WILEY-VCH Verlag GmbH & Co. KGaA, Reproduced with permission)

temperatures, the incubation time of light-induced t-Se growth appears to become longer infinitely, with the variation curve resembling that of the viscosity (Fig. 19.8). The group proposes [19.31, 303, 337], following a Stephen's idea [19.347], that the crystallization at 260–300 K is driven by local strain. Note that they evaluate the sample temperature from Stokes and anti-Stokes Raman peak intensities, which assures that the sample temperature is accurately determined. Incidentally, several researchers have also reported photocrystallizations at  $T < T_g$  using intense or super-bandgap laser-beams; 676 nm light with intensity of  $\approx 250 \text{ W/cm}^2$  at 100 K [19.134] or 488 nm light with  $\approx 0.5 \text{ W/cm}^2$  at room temperature [19.346], while the crystallization could be enhanced by light-induced temperature rises.

These observations manifest that relations between the optical phase change (heat mode) and the photo-enhanced crystallization (photon mode) remain to be studied. For instance, more detailed experiments, which separately monitor crystallite nucleation and growth, are valuable. The insight will shed light also upon *photo-effects* in other materials such as amorphous ice [19.348] and proteins [19.349].

#### 19.6.4 Vector Effects

Zhdanov and Malinovskii [19.350] discovered optical vector effects (anisotropic changes appearing upon illumination of linearly-polarized light or sideward illumination of unpolarized light [19.6]) in  $\text{As}_2\text{S}_3$ , and we naturally envisage similar phenomena in a-Se. Actually, optical and structural vector effects have been demonstrated; dichroism [19.351], birefringence ( $\leq 0.008$ ) [19.352], transitory opto-mechanical deformation [19.338], M-shaped deformation [19.338], macroscopic elongation parallel to the light electric field by  $\approx 10\%$  (Fig. 19.22) [19.106], and oriented

photocrystallization at  $\approx 350 \text{ K}$  [19.353–357], which accompanies birefringence reaching to  $\approx 0.1$ .

For the vector effects, we may point out three interesting observations. First, as shown in Fig. 19.22 the vector deformation in the  $\text{As}_x\text{Se}_{100-x}$  system exhibit anomalous composition dependence; i.e., the deformation direction abruptly changes at the composition  $x \approx 1 \text{ at.}\%$ . Second, different from the photodarkening (Sect. 19.6.2), which becomes greater at lower temperatures, the dichroism and birefringence become maximal at  $\approx 200 \text{ K}$  [19.352], which implies that wider-scale structural changes are involved. Lastly, Kikineshi's group demonstrated that, not single, but two-beam interference patterns can produce clear sinusoidal deformations [19.314], and Trunov et al. have reported that the amplitude depends on the polarization directions of the two beams [19.358] and also on plasmonic enhancements [19.359].

These phenomena have been understood through extending Fritzsche's idea [19.6, 360]. We here assume that anisotropic photo-electronic excitation under illumination of linearly-polarized light makes Se segments tend to align normal to the polarization direction, which leads to the optical and shape changes [19.352]. That is, polarized illumination induces rotation and directional flow of atomic units. For the oriented photocrystallization, resultant atomic configurations have actually been detected by structural measurements [19.353, 355–357].

#### 19.6.5 Simulations

Photoinduced phenomena have been simulated using empirical [19.142, 143, 361] and ab-initio molecular dynamics [19.137, 302, 362, 363] and also analyzed with a quantum-chemical method [19.243]. In a pioneering work by Zhang and Drabold [19.137], initially, an Se cluster with 216 atoms is produced by cook and quench



procedures, and afterwards an electron is transferred from a HOMO to a LUMO level, which is followed by free structure evolution for a while (400 fs), and then the electron is deexcited and quenched. The process yields valence alternation pairs ( $C_{1-}$ ,  $C_{3+}$ ), which they assert as an origin of the photodarkening. Hegedüs et al. [19.361] have demonstrated that the volume of Se clusters consisting of 162 atoms expands and shrinks, respectively, *during* electrons and holes being excited.

These results illustrate plausible photo-structural changes that may occur under some restrictions, and

hence, further developments are promising. For instance, is it still difficult to trace slow phenomena such as the photocrystallization using molecular-dynamics simulations? For the photodarkening, the reversible behavior by annealing has not been demonstrated, and accordingly, we wonder if the simulated, photoinduced structures are really quasi-stable. In addition, to the author's knowledge, no simulations have been performed for the vector effect so far, which require quantal formulation of polarization-dependent photo-electro-structural processes.

## 19.7 Applications

### 19.7.1 Vidicon

TV cameras employing photoconducting chalcogenide films had been utilized [19.86], which has now been developed to HARP vidicons [19.258]. It operates with photo-triggered avalanche breakdown in a-Se films, giving rise to ultrahigh sensitivities, higher by  $\approx 10^2$  times than that of crystalline Si photo-detectors (CCD). However, the vacuum-tube structure having an electron gun and beam-scanning assembly cannot be compact, longer than  $\approx 10$  cm, and accordingly, challenging work is being devoted to reduce its size by replacing the scanning part to field-emitter arrays (FEA) with a thickness of  $\approx 1$  cm [19.364], shown in Fig. 19.23. Otherwise, charge images are scanned by

thin-film-transistors [19.365]. In addition, intense studies are now focused on suppressing thermal and optical un-stabilities of a-Se films [19.366] and on enhancing red-sensitivity [19.367, 368]. On the other hand, Imura et al. [19.268] have recently demonstrated photo-multiplication of electrons injected through metal/c-Se (not a-Se) interfaces, which may promote further developments of vidicons.

### 19.7.2 X-ray Imager

X-ray imaging plates of direct- and indirect-conversion types using a-Se films have been developed for medical [19.255, 369, 370] and scientific [19.371–373] purposes. The direct type has a simpler structure, an

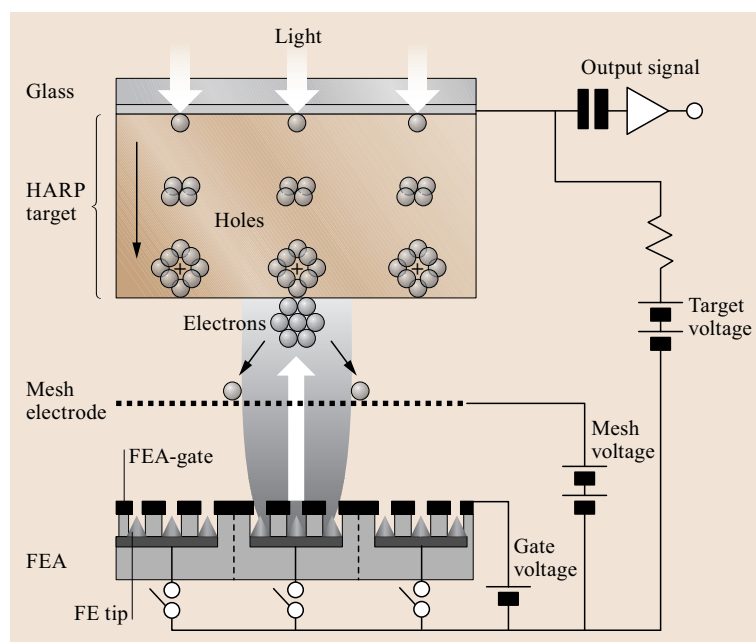


**Fig. 19.23** Schematic cross-sectional view of FEA-HARP vidicons. An image incident upon the top surface excites photo-holes, which are avalanche-amplified in the HARP film, and are read by electron beams emitted by a  $640 \times 480$ -pixel field emitter array (after [19.364], with permission from American Vacuum Society)

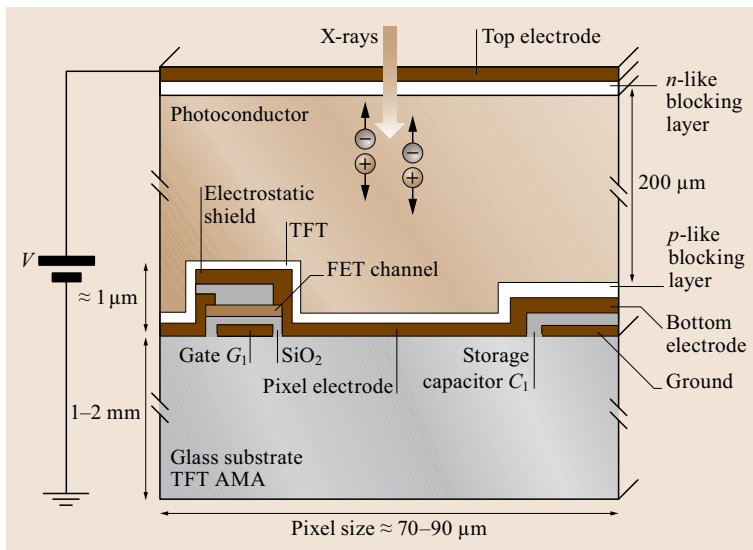


**Fig. 19.24** Schematic cross-sectional view of a pixel of a direct-type a-Se x-ray imager (after [19.255])

example being shown in Fig. 19.24, which is composed of a wide-area (typically,  $40\text{ cm} \times 40\text{ cm}$  for medical imaging) thick a-Se film sandwiched in between a positively-biased top electrode and back capacitors. The a-Se film converts x-ray photons into electrons and holes, which charge the pixel ( $\approx 80\text{ }\mu\text{m} \times 80\text{ }\mu\text{m}$ ) capacitors, from which signals are gated by thin-film transistors (TFT). X-ray detectors employing avalanche multiplication, with HARP [19.370] or similar structures [19.255, 371] to Fig. 19.23, have also been devised. On the other hand, in the indirect type, an a-Se film works as a photoconductor [19.374], which detects visible images emitted from a stacked x-ray fluorescent screen made from a material such as Tl-CsI. In this system, the a-Se film can be as thin as a few micrometers [19.374], and accordingly, it can operate in an avalanche-multiplication mode under moderate applied voltages. Needless to say, there exist other, competitive materials such as CdTe in the direct type and Si photodiodes in the indirect [19.375]. We summarize below some performances of the direct type.

The first concern would undoubtedly be x-ray sensitivity [19.102, 255, 376]. It is determined by several successive processes including x-ray absorption, electron-hole generation with recombination, and carrier transport to electrodes. As known, the x-ray absorption coefficient  $\alpha$  is proportional to  $\rho\lambda^3Z^3$ , where  $\rho$  is the density,  $\lambda$  the x-ray wavelength, and  $Z$  ( $= 34$ ) the atomic number of an absorber, which makes Se a potential material for x-ray detectors. However, for pertinent x-ray absorption, the a-Se films must be thicker than  $\approx 0.2\text{ mm}$ , which requires feasible and economic preparation techniques. An absorbed x-ray

photon then creates a primary electron-hole with energies  $E_X$  of a few tens of keV (x-ray photon energy), which produces  $n$  carriers through impact ionization cascades and instantaneous recombination. The number of resultantly generated carriers can be written as  $n = E_X/W_i$ , where  $W_i$  is an electron-hole pair creation energy, or an ionization threshold, which should be low as possible for obtaining high sensitivity. However, it is still difficult to theoretical predict  $W_i$  for a-Se [19.189, 190, 377, 378], and instead, we follow an empirical formula,  $W_i \approx W^0 + B/F$ , where  $W^0 \approx 7\text{ eV}$ , which may be related with the energy separation between the DOS peaks of the valence and the conduction band (Fig. 19.12),  $F$  an applied electric field, and  $B \approx 4.4 \times 10^6\text{ eV V/cm}$  [19.102]. Provided that all generated carriers being transported without recombination [19.379, 380], this relation suggests that a 50 keV x-ray photon is able to charge a capacitor by  $10^4$  electrons.

In addition to the sensitivity, several specifications should be satisfied. The dark current must be as low ( $\leq 10\text{ pA/mm}^2$  [19.260]) as possible under applied high voltages of, e.g.,  $2\text{ kV}$  ( $\approx 10\text{ V}/\mu\text{m}$ ). However, it is known that the dark current is affected by carrier injection from electrodes [19.293, 379] and bulk thermal generation. The latter increases with decreasing  $E_g$ , while we may assume  $W^0 \propto E_g$ , and accordingly, it is not straightforward to compromise high sensitivity and low dark current. Other performances concern image resolution [19.381], response times [19.382, 383], device degradation under x-ray exposures [19.384], thermal stability, etc. [19.255, 385]. Smooth amorphous structures, not containing polycrystalline grain boundaries, may be preferred in these measures.

### 19.7.3 Other Devices

As known, the usage of a-Se films in xerography and xero-radiography has now been mostly discarded. The xerographic use was replaced by organic photoconductors [19.15], probably because of cost and toxic problems. On the other hand, the xero-radiographic technique [19.376] has been transferred to the digital x-ray imagers (Sect. 19.7.2), in which x-ray detectability of a-Se remains an inherent advantage [19.102].

In contrast to such established usages, new applications to electrical, photoconductive, and photonic devices of crystalline, amorphous, and liquid

Se are now being explored. Those include Al/a-Se/Au diodes [19.288,386], ITO/TiO<sub>2</sub>/Se/Au solar cells with an efficiency of  $\approx 5\%$  [19.387], a supercapacitor of porous Se films [19.59], and a radioisotope I-Se battery generating 16 nW [19.388]. Besides, reported are several photo- and x-ray detectors having lateral configurations [19.389–392], fiber forms [19.393], and diamond cold cathodes [19.262]. Sharma et al. [19.318] have fabricated a-Se photo-optical switches having ps response times, which may be based upon a defect-absorption principle commonly appearing in other amorphous semiconductors [19.237, 394].

## 19.8 Nano-Structures and Single Molecules

The fact that Se forms ring and chain molecules (Fig. 19.1) makes preparations and characterizations of nano- and molecular-structures fascinating subjects. Such studies might start near the end of 20th century, while it should be noted that the smallest cluster, Se dimer, has been utilized as a precious dye in ultramarine-type solids over centuries [19.395] and still arouses renewed interest [19.396].

### 19.8.1 Nano-Selenium

Nanoscale Se structures with different shapes have been prepared through various procedures, as comprehensively reviewed by Chaudhary et al [19.397]. Those include spherical [19.398–405] and polygonal [19.406–408] free nano-particles of a-, m- and t-Se in gases and solutions. T-Se can also take a variety of shapes; needles [19.401,404,408–410], wires [19.391–416], belts [19.417], and tubes [19.414,418], the example being shown in Fig. 19.25. Nano-particles have

been produced also in transparent insulators such as polymers [19.237,419], silica [19.420,421], and opal [19.422]. Se nano-crystals can also be prepared through annealing g-Se [19.423].

These nano-Se exhibit several marked features [19.187,424], such as photoconduction [19.411, 415,425], irradiation effects [19.413,426], Li-conduction [19.427], and peculiar optical nonlinearities [19.421,428]. Deng et al. have fabricated filamental photo-detectors using cm-long t-Se wires with diameters of  $\approx 200$  nm [19.429]. In fundamental aspects, scale- and confined-effects on thermal and mechanical properties have provided interesting subjects such as how the glass-transition temperature varies in smaller and/or thinner flakes [19.187,424,430].

### 19.8.2 Isolated Molecules

Se can form isolated atomic clusters in vacuum and gases [19.2,431–434]. Se clusters have also been laid

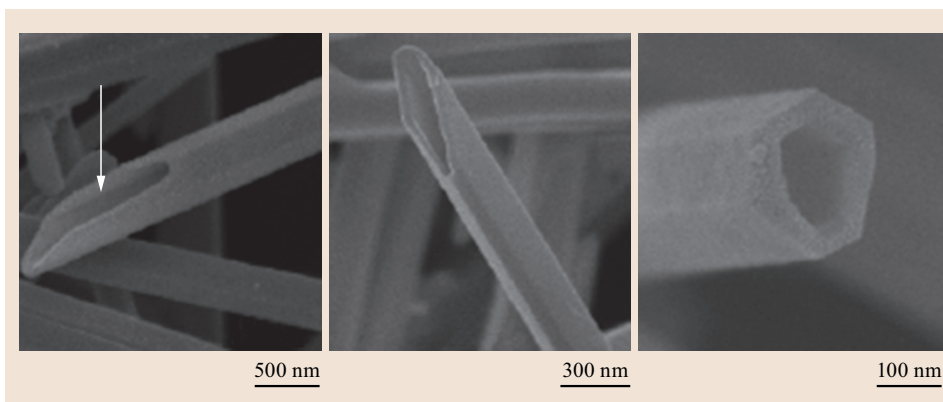


**Fig. 19.25** Se nanotubes. (Reprinted with permission [19.418]. Copyright 2006 American Chemical Society.)



**Fig. 19.26a–c** An illustration of ZSM-5 zeolite with magnified pore arrangements (a), and photographs of the zeolite (b) and a Se-loaded one (c), the dimension being  $\approx 40\ \mu\text{m} \times 40\ \mu\text{m} \times 200\ \mu\text{m}$ . ZSM-5 is a fairly non-polar zeolite with a composition of  $\text{Si}_{94}\text{Al}_2\text{O}_{192}$ , containing channels with diameters of  $\approx 0.7\ \text{nm}$  (Reprinted from [19.446] with the permission of AIP Publishing)

on graphite surfaces [19.435] and introduced into carbon nanotubes [19.436]. Among those, the gaseous Se would behave as free substances, while only limited properties such as cluster stability have been inspected.

On the other hand, after a pioneering work by Bogomorov et al. [19.437], substantial studies have been carried out for Se clusters incorporated into pores in zeolites [19.11] of various kinds [19.238, 239, 396, 437–448]. *Terasaki et al.* [19.438] evinced, by taking electron-microscopy photographs, single Se chains in a zeolite, mordenite ( $\text{Na}_8\text{Al}_5\text{Si}_{40}\text{O}_{96} \cdot 24\text{H}_2\text{O}$ ). Atomic structures of incorporated Se clusters have been investigated also using x-ray diffraction and Raman scattering [19.239, 396, 442–445, 447, 448]. Such zeolite-Se structures may manifest intrinsic properties to single Se clusters, while we should be careful to possible guest-host interaction, existing between Se clusters and

atoms (such as Na) forming inner walls of pores in zeolites [19.220].

The zeolite-Se system exhibits several characteristic properties, such as blue-shifting absorption edges [19.238, 239, 441, 443, 444, 447], rises of the glass-transition temperature [19.440, 444], and unique photoinduced phenomena [19.238, 239]. Specifically promising may be the optical nonlinearity of Se in ZSM-5 zeolites (Fig. 19.26) [19.446], higher by three orders of magnitude than that of g-Se, which may originate from confined excitons. Since there exist many kinds of zeolites, the zeolite-Se system will exhibit more diverse properties. Or, provided that single Se clusters could be arranged as photonic crystals, optical properties might be resonantly enhanced. It would also be challenging to explore the electrical conduction of single Se chains.

## 19.9 Summary

We have seen that the study of a-Se is promising toward two directions, fundamentals and applications, which may be related as shown in Fig. 19.27. The final goal will be to grasp all physical properties as the emergence from atomic structures on the basis of theoretical formulations. If a property would be useful to some purpose, the structure could then be tuned toward the target.

In the fundamental, the elemental structure (no chemical disorder) with dualistic atomic bonds (covalent and van der Waals) gives a simple stage for exploring the nature of disordered materials, amorphous semiconductors, and chalcogenide glasses. Currently, we have mostly understood the short-range structure, the band structure, and related properties such as gross optical absorption spectra (Sect. 19.4.1). However, other

atomic structures, including wider-scale conformations and defects, and associated properties cannot yet be correlated. Studies on light-induced phenomena, avalanche breakdown, responses to x-rays, and nano-structures are in progress.

Among the chalcogenide glass, a-Se exhibits common and uncommon features to those in compounds such as As(Ge)-S(Se). The common includes the two-fold coordinated chalcogen atoms with the valence band consisting of lone-pair states (Fig. 19.10), the Urbach edge with a steepness parameter  $E_U$  greater than  $\approx 50\ \text{meV}$  (Fig. 19.13), no dark ESR signals, and many photoinduced phenomena such as the photodarkening (Sect. 19.6.2). On the other hand, characteristic of a-Se are the power of  $n = 1$  in the Tauc's curve (19.3),

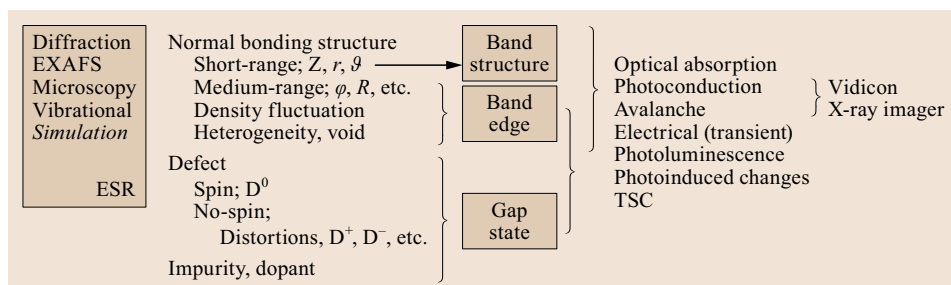


**Fig. 19.27** Relations between structure-analyzing methods (left), atomic structural components, related electronic states, macroscopic properties, and applications (right)

no clear weak absorption tail (Fig. 19.13), smaller spin density ( $\approx 10^{16} \text{ cm}^{-1}$ ) under moderate illumination, high photoconductivity, the highest hole drift mobility (Table 19.1), avalanche breakdown (Fig. 19.17), peculiar vector deformation (Fig. 19.22), and so forth. How can we understand such native facets? The photocrystallization is more-or-less unique to a-Se, probably because of its elemental structure.

In applications, the most valuable property of a-Se remains undoubtedly the visible and x-ray photoconduction. The HARP vidicon utilizing avalanche breakdown has been commercialized, and now being reduced in size to more compact devices (Fig. 19.23). Thick a-Se layers are employed as direct x-ray imag-

ing plates (Fig. 19.24), which are useful for medical inspections and probably for scientific purposes as well. In addition, indirect-type x-ray imagers in combination with the avalanche multiplication are also being developed. Finally, studies on nano-Se structures appear to be promising for future functional devices.

**Acknowledgments.** The author would like to thank Professor K. Nagata in Fukuoka University for showing several kinds of Se single crystals and supplying unpublished data. He is also grateful to A. Odajima and Y. Abe, emeritus professors of Hokkaido University, who introduced him to the physics of polymers and semiconductors.

## References

- 19.1 J. Tauc (ed.): *Amorphous and Liquid Semiconductors* (Plenum Press, London, 1974)
- 19.2 R.A. Zingaro, W.C. Cooper: *Selenium* (Van Nostrand Reinhold Company, New York, 1974)
- 19.3 E. Gerlach and P. Grosse (eds.): *The Physics of Selenium and Tellurium* (Springer-Verlag, Berlin, 1979)
- 19.4 N.F. Mott, E.A. Davis: *Electronic Processes in Non-Crystalline Materials* 2nd Ed. (Clarendon Press, Oxford, 1979)
- 19.5 M.A. Popescu: *Non-Crystalline Chalcogenides* (Kluwer Academic Pub., Dordrecht, 2001)
- 19.6 K. Tanaka, K. Shimakawa: *Amorphous Chalcogenide Semiconductors and Related Materials* (Springer, New York, 2011)
- 19.7 A. von Hippel: Structure and conductivity in the VIb group of the periodic system, *J. Chem Phys.* **16**, 372–380 (1948)
- 19.8 K. Nagata, Y. Miyamoto: Raman spectroscopic and X-ray diffraction study of selenium under high pressure, in: M. Senoo, K. Suito, T. Kobayashi, H. Kubota (eds.): *High Pressure Research on Solids* (Elsevier Sci. B. V., Amsterdam, 1995) pp. 19–38.
- 19.9 V.S. Minaev, S.P. Timoshenko, V.V. Kalugin: Structural and phase transformations in condensed selenium, *J. Optoelectronic. Adv. Mater.* **7**, 1717–1741 (2005)
- 19.10 G. Briegleb: Die dynamisch, allotropen Zustände des Selen, *Naturwissenschaften* **17**, 51 (1929)
- 19.11 G.N. Greaves, S. Sen: Inorganic glasses, glass-forming liquids and amorphizing solids, *Adv. Phys.* **56**, 1–166 (2007)
- 19.12 M.J. Williams, M. Bachmann: Stabilization of helical macromolecular phases by confined bending, *Phys. Rev. Lett.* **115**, 048301 (2015)
- 19.13 M.A. Kastner: Bonding bands, lone-pair bands, and impurity states in chalcogenide semiconductors, *Phys. Rev. Lett.* **28**, 355–357 (1972)
- 19.14 W. Smith: Effect of light on selenium during the passage of an electric current, *Nature* **7**, 303 (1873)
- 19.15 D.M. Pai, B.E. Springett: Physics of electrophotography, *Rev. Mod. Phys.* **65**, 163–212 (1993)
- 19.16 W.W. Warren, Jr., R. Dupree: Structural and electronic transformation of liquid selenium at high temperature and pressure: A  $^{77}\text{Se}$  NMR study, *Phys. Rev. B* **22**, 2257–2275 (1980)
- 19.17 S. Hosokawa, K. Tamura: Optical absorption spectra of fluid selenium near the nonmetal-metal transition region, *J. Non-Cryst. Solids* **117/118**, 489–492 (1990)
- 19.18 A. Pal, S. Gohil, S. Sengupta, H.K. Poswal, S.M. Sharma, S. Ghosh, P. Ayyub: Structural phase transitions in trigonal selenium induce the formation of a disordered phase, *J. Phys.: Condens. Matter* **27**, 415404 (2015)
- 19.19 Y. Akahama, M. Kobayashi, H. Kawamura: Pressure-induced metallization and structural



- transition of  $\alpha$ -monoclinic and amorphous Se, Phys. Rev. B **56**, 5027–5031 (1997)
- 19.20 W.A. Phillips, U. Buchenau, N. Nücker, A.-J. Dianoux, W. Petry: Dynamics of glassy and liquid selenium, Phys. Rev. Lett. **63**, 2381–2384 (1989)
- 19.21 L. Judovits, B. Wunderlich: On the entropies of glassy and monoclinic selenium at 0 K, J. Therm. Analysis **30**, 895–899 (1985)
- 19.22 Yu.P. Kirillov, V.A. Shaposhnikov, L.A. Kuznetsov, V.S. Shiryaev, M.F. Churbanov: Modeling of the evaporation of liquids and condensation of their vapor during distillation, Inorg. Mater. **52**, 1183–1188 (2016)
- 19.23 J.M. Marshall, A.E. Owen: The hole drift mobility of vitreous selenium, Phys. Stat. Sol. (a) **12**, 181–191 (1972)
- 19.24 P. Andonov: Studies of non-crystalline forms of selenium, J. Non-Cryst. Solids **47**, 297–339 (1982)
- 19.25 M.C. Assunção, Effect of halogen impurities on transport properties of selenium glasses, J. Non-Cryst. Solids **136**, 81–90 (1991)
- 19.26 D. Mortensen, G. Belev, K. Koughia, R.E. Johanson, S.O. Kasap: Thickness dependence of electron transport in pure a-Se photoconductive films, Can. J. Phys. **92**, 629–633 (2014)
- 19.27 J.P. Audiere, C. Mazieres, J.C. Carballes: Non-crystalline Se thin films deposited from controlled vapor – preparation, crystallization and optical properties, J. Non-Cryst. Solids **27**, 411–419 (1978)
- 19.28 K. Suzuki, K. Matsumoto, H. Hayata, N. Nakamura, N. Minari: Mass spectrometric study of evaporated Se films and melt-quenched Se glasses, J. Non-Cryst. Solids **95&96**, 555–562 (1987)
- 19.29 A.H. Goldan, C. Li, S.J. Pennycook, J. Schneider, A. Blom, W. Zhao: Molecular structure of vapor-deposited amorphous selenium, J. Appl. Phys. **120**, 135101 (2016)
- 19.30 F. Jansen: Effects of oxygen and chlorine on the interfacial crystallization of amorphous selenium films, J. Vac. Sci. Technol. **18**, 215–218 (1981)
- 19.31 G.P. Lindberg, T. O'Loughlin, N. Gross, A. Mishchenko, A. Reznik, S. Abbaszadeh, K.S. Karim, G. Belev, B.A. Weinstein: Photo-crystallization in a-Se layer structures: Effects of film-substrate interface-rigidity, J. Appl. Phys. **116**, 193511 (2014)
- 19.32 P.H. Keck: Photoconductivity in vacuum coated selenium films, J. Opt. Soc. Am. **42**, 221–225 (1952)
- 19.33 R. Kaplow, T.W. Rowe, B.L. Averbach: Atomic arrangement in vitreous selenium, Phys. Rev. **168**, 1068–1079 (1968)
- 19.34 E. Montrimas, B. Petrétis: The relation between deep trapping levels and the structure of Se layers, J. Non-Cryst. Solids **15**, 96–106 (1974)
- 19.35 N. Ohta, W. Scheuerman, K. Nakamoto: Resonance Raman spectrum of selenium thin films, Solid State Commun. **27**, 1325–1327 (1978)
- 19.36 T. Takahashi, K. Ohno, Y. Harada: Highly disordered amorphous selenium studied by ultraviolet photoemission spectroscopy, Phys. Rev. B **21**, 3399–3404 (1980)
- 19.37 P.J. Carroll, J.S. Lannin: Raman scattering of amorphous selenium films, Solid State Commun. **40**, 81–84 (1981)
- 19.38 V. Kriščiūnas, BR. Petrétis, R. Rinkūnas: Anisotropic properties and structure of amorphous films of selenium, Thin Solid Films **102**, 111–116 (1983)
- 19.39 L. Song, P. Galarneau, M. Cote, R.A. Lessard: Influence of the substrate temperature on the holographic properties of Se and SeGe thin films, Appl. Opt. **28**, 4613–4615 (1989)
- 19.40 H. Witte, H. Freistedt, J. Bläsing, H. Giesler: Correlation between structural and optical properties of a-Se films, Phys. Stat. Sol. (a) **145**, 363–368 (1994)
- 19.41 C. Juhasz, V. Gembala, S.O. Kasap: Growth characteristics of vacuum coated thick a-Se films for device applications, J. Vac. Sci. Technol. A **18**, 665–679 (2000)
- 19.42 G. Belev, S.O. Kasap: Reduction of the dark current in stabilized a-Se based X-ray detectors, J. Non-Cryst. Solids **352**, 1616–1620 (2006)
- 19.43 W.C. Tan, G. Belev, K. Koughia, R. Johanson, S.K. O'Leary, S. Kasap: Optical properties in vacuum deposited and chlorine doped a-Se thin films: aging effects. J. Mater. Sci.: Mater. Electron. **18**, S429–S433 (2007)
- 19.44 G. Belev, S.O. Kasap: The influence of the substrate temperature on charge transport in vacuum deposited amorphous selenium films, J. Optoelectron. Adv. Mater. **11**, 1053–1059 (2009)
- 19.45 V.I. Mikla, V.V. Mikla: Xerographic spectroscopy of gap states in Se-rich amorphous semiconductor review, J. Non-Cryst. Solids **357**, 3675–3688 (2011)
- 19.46 T. Hristova-Vasileva, I. Bineva, A. Dinescu, D. Arsova, D. Nesheva: "Cymatics" of selenium and tellurium films deposited in vacuum on vibrating substrates, Surf. Coating Technol. **307**, 542–546 (2016)
- 19.47 H.P.D. Lanyon: Electrical and optical properties of vitreous selenium, Phys. Rev. **130**, 134–143 (1963)
- 19.48 M. Shiojiri, Y. Saito, H. Okada, H. Sasaki: Densities of amorphous thin films, Jpn. J. Appl. Phys. **18**, 1931–1936 (1979)
- 19.49 S. Chaudhuri, S.K. Biswas, A. Choudhury, K. Goswami: Amorphous to crystalline transition of selenium thin films of different thicknesses, J. Non-Cryst. Solids **46**, 171–179 (1981)
- 19.50 A. Solieman, A.A. Abu-Sehly: Modelling of optical properties of amorphous selenium thin films, Physica B **405**, 1101–1107 (2010)
- 19.51 M.K. El-Mously, M.M. El-Zaidia: The effect of addition of 5 at% sulphur or tellurium to selenium on its electrical properties and on its rate of crystallization, J. Non-Cryst. Solids **11**, 519–525 (1973)
- 19.52 R. Brüning, E. Irving, G. LeBlanc: Reverse Monte Carlo study of structural relaxation in vitreous selenium, J. Appl. Phys. **89**, 3215–3222 (2001)
- 19.53 M. Abkowitz, S.S. Badesha, F.E. Knier: Reversible chemical modification of the electrical behavior of a-Se, Solid State Commun. **57**, 579–582 (1986)
- 19.54 G. Belev, D. Tonchev, B. Fogal, C. Allen, S.O. Kasap: Effects of oxygen and chlorine on charge transport in vacuum deposited pure a-Se films, J. Phys. Chem. Solids **68**, 972–977 (2007)



- 19.55 M.D. Reichtin, B.L. Averbach: Atomic arrangements and fast electron energy losses in sputtered thin films of vitreous Se-As alloys with 0–24 As, *J. Non-Cryst. Solids* **12**, 391–421 (1973)
- 19.56 P. Nagels, E. Sleetx, R. Callaerts, E. Márquez, J.M. González, A.M. Bernal-Oliva: Optical properties of amorphous Se films prepared by PECVD, *Solid State Commun.* **102**, 539–543 (1997)
- 19.57 T. Scopigno, W. Steurer, S.N. Yannopoulos, A. Chrissanthopoulos, M. Krisch, G. Ruocco, T. Wagner: Vibrational dynamics and surface structure of amorphous selenium, *Nature Commun.* **2**, 195 (2011).
- 19.58 H. Sun, X. Zhu, D. Yang, P. Wangyang, X. Gao, H. Tian: An economical method for amorphous selenium thick films preparation: e-beam evaporation, *Mater. Lett.* **183**, 94–96 (2016)
- 19.59 A.M. Patil, A.C. Lokhande, N.R. Chodanker, J.H. Kim, C.D. Lokhande: Electrochemical supercapacitor properties of highly porous sponge-like selenium thin films, *Int. J. Hydrogen Energy*, **41**, 17453–17461 (2016)
- 19.60 A. Peled, A.A. Friesem, K. Vinokur: Continuous-wave laser photodeposition of amorphous selenium films, *Thin Solid Films* **218**, 201–208 (1992)
- 19.61 A.P. Caricato, M. Martino, F. Romano, N. Mirchin, A. Peled: Pulsed laser photodeposition of a-Se nanofilms by ArF laser, *Appl. Surf. Sci.* **253**, 6517–6521 (2007)
- 19.62 H. Koseki, T. Ueno, A. Odajima: Thermal and photo effects on the textural change of red amorphous selenium, *Jpn. J. Appl. Phys.* **17**, 1143–1144 (1978)
- 19.63 F. Gompf: The phonon densities of states of trigonal, vitreous and red amorphous selenium, *J. Phys. Chem. Solids* **42**, 539–544 (1981)
- 19.64 B. Pejova, I. Grozdanov: Solution growth and characterization of amorphous selenium thin films: Heat transforms to nanocrystalline gray selenium thin films, *Appl. Surf. Sci.* **177**, 152–157 (2001)
- 19.65 T. Fukunaga, M. Utsumi, H. Akatsuka, M. Misawa, U. Mizutani: Structure of amorphous Se prepared by milling, *J. Non-Cryst. Solids* **205–207**, 531–535 (1996).
- 19.66 P. Jónvári, R.G. Delaplane, L. Pusztai: Structural models of amorphous selenium, *Phys. Rev. B* **67**, 172201 (2003)
- 19.67 Y.H. Zhao, K. Lu, T. Liu: EXAFS study of mechanical-milling induced solid-state amorphization of Se, *J. Non-Cryst. Solids* **333**, 246–251 (2004)
- 19.68 A.A. Joraid, S.N. Alamri, A.A. Abu-Sehly, M. Benganem: Nonisothermal crystallization kinetics of amorphous selenium prepared by high-energy ball milling: A comparison with the melt-quenching and thin-film techniques, *J. Non-Cryst. Solids* **358**, 1268–1273 (2012)
- 19.69 K. Tanaka: Gap states in non-crystalline selenium: roles of defective structures and impurities, *J. Optoelectron. Adv. Mater.* **17**, 1716–1727 (2015)
- 19.70 J.D. MacKenzie: Electronic conduction in non-crystalline solids, *J. Non-Cryst. Solids* **2**, 16–26 (1970)
- 19.71 S.G. Bishop, U. Strom, E.J. Friebele, P.C. Taylor: The effects of impurities upon photoluminescence and optically induced paramagnetic states in chalcogenide glasses, *J. Non-Cryst. Solids* **32**, 359–372 (1979)
- 19.72 B.T. Kolomiets, T.N. Mamontova, A.V. Chernyshov, G.Z. Vinogradova, N.V. Demokritova: The effect of low oxygen concentrations on the photoluminescence of vitreous selenium, *Phys. Stat. Sol. (a)* **79**, K89–K92 (1983)
- 19.73 A. Feltz, H. Aust: Glass formation and structure of chalcogenide systems XXV: Permittivity of vitreous Se, *J. Non-Cryst. Solids* **51**, 395–398 (1982)
- 19.74 N. Toyosawa, K. Tanaka: Photocurrent enhancement in light-soaked chalcogenide glasses, *Phys. Rev. B* **56**, 7416–7421 (1997)
- 19.75 M.M. Abdul-Gader, M.A. Al-Basha, K.A. Wishah: Temperature dependence of DC conductivity of as-deposited and annealed selenium films, *Int. J. Electron.* **85**, 21–41 (1998)
- 19.76 O. Oda, A. Onozuka, I. Tsuboya: Effect of oxygen on electrophotographic properties of selenium, *J. Non-Cryst. Solids* **83**, 49–62 (1986)
- 19.77 J. Schottmiller, M. Tabak, G. Lucovsky, A. Ward: The effects of valency on transport properties in vitreous binary alloys of selenium, *J. Non-Cryst. Solids* **4**, 80–96 (1970)
- 19.78 M. Abkowitz, F. Jansen, A.R. Melnyk: Electrical behavior of chemically modified amorphous Se studied by xerographic depletion discharge, *Philos. Mag. B* **51**, 405–420 (1985)
- 19.79 Y. Wang, C.H. Champness: Xerographic effects of small chlorine additions to amorphous selenium, *J. Appl. Phys.* **77**, 722–730 (1995)
- 19.80 S. Chand, G.D. Sharma, R.C. Bhatheja, S. Chandra: Effect of chloride doping on photostructural defect states in amorphous selenium films, *Appl. Phys. Lett.* **59**, 3514–3515 (1991)
- 19.81 D. Tonchev, S.O. Kasap: Influence of Cl doping on the thermal properties of amorphous Se, *Phys. Chem. Glasses* **43**, 66–71 (2002)
- 19.82 K. Koughia, Z. Shakoor, S.O. Kasap, J.M. Marshall: Density of localized electronic states in a-Se from electron time-of-flight photocurrent measurements, *J. Appl. Phys.* **97**, 033706 (2005)
- 19.83 I. Saito, W. Miyazaki, M. Onishi, Y. Kudo, T. Matsuzawa, T. Yamada, A. Koh, D. Chua, K. Soga, M. Overend, M. Aono, G.A.J. Amaratinga, K. Okano: A transparent ultraviolet triggered amorphous selenium p-n junction, *Appl. Phys. Lett.* **98**, 152102 (2011)
- 19.84 C. Allen, G. Belev, R. Johanson, S. Kasap: Relaxation of the electrical properties of vacuum-deposited a-Se<sub>1-x</sub>As<sub>x</sub> photoconductive films: Charge-carrier lifetimes and drift mobilities, *J. Vac. Sci. Technol. A* **28**, 1145–1156 (2010)
- 19.85 S. Fukuda, T. Shiosaki, A. Kawabata: Acoustic and acousto-optic properties of amorphous Se, *Jpn. J. Appl. Phys.* **19**, 2075–2083 (1980)
- 19.86 E. Maruyama: Amorphous built-in-field effect photoreceptors, *Jpn. J. Appl. Phys.* **21**, 213–223 (1982)

- 19.87 F. Serdouk, M.L. Benkhedir: Density of states in pure and As doped amorphous selenium determined from transient photoconductivity using Laplace-transform method, *Physica B* **459**, 122–128 (2015)
- 19.88 R.M. Mehra, R. Shyam, P.C. Mathur: Electrical transport in bulk amorphous Se, Se-Te, Se-Sb, and Se-Te-Ge, *Phys. Rev. B* **19**, 6525–6531 (1979)
- 19.89 G. Parthasarathy, E.S.R. Gopal: Effect of high pressure on chalcogenide glasses, *Bull. Mater. Sci.* **7**, 271–302 (1985)
- 19.90 R. Misra, S.K. Tripathi, A.K. Agnihotri, A. Kumar: Photocrystallization in amorphous thin films of  $\text{Se}_{100-x}\text{Te}_x$ , *Solid State Commun.* **77**, 797–800 (1991)
- 19.91 M. A. Abkowitz: Light-induced changes in the DOS of chalcogenide glasses studied by xerographic techniques, *J. Non-Cryst. Solids* **141**, 188–199 (1992)
- 19.92 D. Nesheva, I.P. Kotsalas, C. Raptis, E. D. Arsova: Stability of amorphous Se/ $\text{Se}_{100-x}\text{Te}_x$  multilayers: A Raman study, *J. Appl. Phys.* **86**, 4964–4970 (1999)
- 19.93 R. Svoboda, J. Málek: Crystallization mechanisms occurring in the Se-Te glassy system, *J. Therm. Anal. Calorim.* **119**, 155–166 (2015)
- 19.94 T.W. Kang, C. Tong, G.S. Eom, J.Y. Lee, T.W. Kim: Thermally stimulated current of  $\text{Li}^+$ -ion implanted amorphous selenium, *J. Appl. Phys.* **69**, 3119–3123 (1991)
- 19.95 S.G. Bishop, P.C. Taylor: Photoluminescence and optically induced ESR in pure and K-doped glassy Se, *J. Non-Cryst. Solids* **35 & 36**, 909–913 (1980)
- 19.96 E. Mytilineou, T. Petkova, M. Skaperda: The effect of the additive of Ag and AgI on the density of defect states in a-Se, *J. Optoelectron. Adv. Mater.* **4**, 711–715 (2002)
- 19.97 F. Mollot, J. Cernogora, C. Benoit á la Guillaume: Spectral analysis of the fatigue of the photoluminescence and of the creation of paramagnetic centres in amorphous  $\text{Ge}_x\text{Se}_{1-x}$ , *Philos. Mag. B* **42**, 643–670 (1980)
- 19.98 W.D. Gill, G.B. Street: Drift mobility in amorphous selenium-sulfur alloys, *J. Non-Cryst. Solids* **13**, 120–130 (1973/74)
- 19.99 M.M. El-Nahass, M.A.M. Seyam, H.E.A. El-Sayed, A.M. Abd El-Barry: Structural and electrical characterization of  $\text{S}_x\text{Se}_{100-x}$  thin films, *Appl. Surf. Sci.* **252**, 6218–6227 (2006)
- 19.100 Y. Takasaki, E. Maruyama, T. Uda, T. Hirai: Molecular doping in amorphous selenium, *J. Non-Cryst. Solids* **59&60**, 949–952 (1983)
- 19.101 B. Polischuk, S.O. Kasap, V. Aiyah, A. Bailie, M.A. Abkowitz: Measurement of mobility-lifetime products in amorphous semiconductors, *Can. J. Phys.* **69**, 361–369 (1991)
- 19.102 S.O. Kasap, J.A. Rowlands: Review: X-ray photoconductors and stabilized a-Se for direct conversion digital flat-panel X-ray image-detector, *J. Mater. Sci.: Mater. Electron.* **11**, 179–198 (2000)
- 19.103 B. Fogal, S. Kasap: Temperature dependence of charge carrier ranges in stabilized a-Se photoconductors, *Can. J. Phys.* **92**, 634–640 (2014)
- 19.104 K. Tanaka: Doping mechanisms in stabilized amorphous Se films, *J. Optoelectron. Adv. Mater.* **19**, 27–32 (2017)
- 19.105 P.S. Vincett, W.A. Barlow, G.G. Roberts: Quality of vacuum-deposited films, *Nature* **255**, 542–544 (1975)
- 19.106 K. Tanaka, M. Mikami: Photoinduced vector deformations of semi-freely fixed glassy As-S(Se), *Phys. Stat. Solidi C* **8**, 2756–2760 (2011)
- 19.107 E.W. Fischer, M. Dettenmaier: Structure of polymeric glasses and melts, *J. Non-Cryst. Solids* **31**, 181–205 (1978)
- 19.108 D. Caprion, J. Matsui, H.R. Schober: Dynamic heterogeneity of relaxation in glasses and liquids, *Phys. Rev. Lett.* **85**, 4293–4296 (2000)
- 19.109 S. Cazzato, T. Scopigno, S.N. Yannopoulos, G. Ruocco: Slow dynamics of liquid Se studied by infrared photon correlation spectroscopy, *J. Non-Cryst. Solids* **355**, 1797–1800 (2009)
- 19.110 M. Inui, S. Takeda, K. Maruyama, Y. Kawakita, S. Tamaki, M. Imai: SANS measurements of liquid and amorphous selenium, *Physica B* **213&214**, 552–554 (1995)
- 19.111 N.J. Schevchik, W. Paul: Voids in amorphous semiconductors, *J. Non-Cryst. Solids* **16**, 55–71 (1974)
- 19.112 F. Itoh, M. Matsuura, K. Suzuki, Y. Miyata, S. Noguchi: Positron annihilation in amorphous, trigonal, and  $\alpha$ -monoclinic selenium, *J. Phys. Soc. Jpn.* **45**, 1622–1625 (1978)
- 19.113 J. Bartoš, O. Šauša, P. Pusková, J. Šhánělová, J. Křištiak, J. Málek: Dilatometric and positron annihilation lifetime spectroscopic studies on amorphous and polycrystalline selenium, *J. Non-Cryst. Solids* **351**, 1082–1088 (2005)
- 19.114 R. Parthasarathy, P.R. Sarode, K.J. Rao: An EXAFS study of amorphous selenium, *J. Mater. Sci.* **16**, 3222–3225 (1981)
- 19.115 W. Wei, B.W. Corb, B.L. Averbach: A correlation model of amorphous selenium, *J. Non-Cryst. Solids* **53**, 19–28 (1982)
- 19.116 H. Hasegawa, M. Imaoka, I. Yasui: X-ray diffraction study of glasses in the system As-Se, *J. Non-Cryst. Solids* **56**, 291–296 (1983)
- 19.117 M. Inui, K. Maruyama, S. Takeda, S. Tamaki, Y. Waseda: Electron charge distribution in amorphous Se, *J. Phys. Soc. Jpn.* **63**, 1378–1385 (1994)
- 19.118 Y. Kobashi, S. Kodera: Structure of amorphous selenium, *Jpn. J. Appl. Phys.* **37**, 2590–2592 (1998)
- 19.119 A.V. Kolobov, H. Oyanagi, K. Tanaka: In situ x-ray absorption fine structure detection of reversible photoinduced anisotropy in amorphous selenium, *Phys. Rev. Lett.* **87**, 145502 (2001)
- 19.120 B.W. Corb, W. Wei, B.L. Averbach: Atomic models of amorphous selenium, *J. Non-Cryst. Solids* **53**, 29–42 (1982)
- 19.121 W.G. Wyckoff: *Crystal Structures Vol. 1*, 2<sup>nd</sup> ed. (Interscience, New York, 1963) pp. 36–42.
- 19.122 G. Lucovsky, R.M. White: Effects of resonance bonding on the properties of crystalline and amorphous semiconductors, *Phys. Rev. B* **8**, 660–667 (1973)
- 19.123 Y. Waseda, K. Yokoyama, K. Suzuki: Structure of molten selenium by x-ray diffraction, *Phys. Cond. Matter* **18**, 293–299 (1974)

- 19.124 G. Lucovsky: *ibid.* Ref. 3, pp. 178–192.
- 19.125 F. Kirchhoff, G. Kresse, M.J. Gillan: Structure and dynamics of liquid selenium, *Phys. Rev. B* **57**, 10482–10495 (1998)
- 19.126 Y.B. Wang, W.S. Dong, G. Zhao, J.X. Ding, S.H. Li, Y.J. Ge: Chain structure of liquid Se at high temperature and pressure investigated by *ab initio* molecular dynamics simulations, *J. Non-Cryst. Solids* **358**, 873–879 (2012)
- 19.127 P.J. Carroll and J.S. Lannin: Vibrational properties of crystalline group-VI solids: Te, Se, S, *Phys. Rev. B* **27**, 1028–1036 (1983)
- 19.128 K. Nakamura, A. Ikawa: Medium-range order in amorphous selenium: Molecular dynamics simulations, *Phys. Rev. B* **67**, 104203 (2003)
- 19.129 S.N. Yannopoulos, K.S. Andrikopoulos: Raman scattering study on structural and dynamical features of noncrystalline selenium, *J. Chem. Phys.* **121**, 4747–4758 (2004)
- 19.130 J.H. Wendorff: The structure of amorphous polymers, *Polymer* **23**, 543–557 (1982)
- 19.131 A.J. Leadbetter, A.J. Apling: Diffraction studies of glass structure (V). The structure of some arsenic chalcogenide glasses, *J. Non-Cryst. Solids* **15**, 250–268 (1974)
- 19.132 F. J. Bermejo, M. García-Hernández, F.J. Mompeán, D. MacMorrow, J.L. Martinez: Nature of the first diffraction peak in glassy selenium, *Phys. Rev. B* **51**, 11932 (1995)
- 19.133 D. Caprion, H.R. Schber: Structure and relaxation in liquid and amorphous selenium, *Phys. Rev. B* **62**, 3709–3716 (2000)
- 19.134 A.A. Baganich, V.I. Mikla, D.G. Semak, A.P. Sokolov, A.P. Shebanin: Raman-scattering in amorphous selenium – molecular structure and photoinduced crystallization, *Phys. Stat. Sol. B* **166**, 297–302 (1991)
- 19.135 D. Hohl, R.O. Jones: First-principles molecular-dynamics simulation of liquid and amorphous selenium, *Phys. Rev. B* **43**, (1991) 3856–3870
- 19.136 S. Balasubramanian, K.V. Damodaran, K.J. Rao: A molecular dynamics study of amorphous selenium, *Chem. Phys.* **166**, 131–137 (1992)
- 19.137 X. Zhang, D.A. Drabold, Direct molecular dynamic simulation of light-induced structural change in amorphous selenium, *Phys. Rev. Lett.* **83**, 5042–5045 (1999)
- 19.138 G. Kahl: Tight-binding model of selenium disordered phases, *Phys. Rev. B* **60**, 6372–6382 (1999)
- 19.139 E. Lomba, D. Molina, M. Alvarez: Hubbard corrections in a tight-binding Hamiltonian for Se: Effects on the band structure, local order, and dynamics, *Phys. Rev. B* **61**, 9314–9321 (2000)
- 19.140 J. Hegedüs, K. Kohary, S. Kugler: Comparative analysis of different preparation methods of chalcogenide glasses: molecular dynamics structure simulations, *J. Non-Cryst. Solids* **338–340**, 283–286 (2004)
- 19.141 J. Hegedüs, S. Kugler, Growth of amorphous selenium films: classical versus quantum mechanical molecular dynamics simulation, *J. Phys.: Condens. Matter* **17**, 6459–6468 (2005)
- 19.142 R. Lukács, J. Hegedüs, S. Kugler, Structure and photoinduced volume changes of obliquely deposited amorphous selenium, *J. Appl. Phys.* **104**, 103512 (2008)
- 19.143 R. Lukács, J. Hegedüs, S. Kugler: Microscopic and macroscopic models of photo-induced volume changes in amorphous selenium, *J. Mater. Sci.: Mater. Electron.* **20**, S33–S37 (2009)
- 19.144 J.A. Reyes-Retana, A.A. Valladares: Structural properties of amorphous selenium: An *ab initio* molecular-dynamics simulation, *Comp. Mater. Sci.* **47**, 934–939 (2010)
- 19.145 C. Oligschleger, C. Facius, H. Kutz, C. Langen, M. Thumm, S. von Brühl, S. Wang, L. Weber, J. Zischler: Molecular dynamics simulation of structural and dynamic properties of selenium structures with different degrees of amorphization, *J. Phys.: Condens. Matter* **21**, 405402 (2009)
- 19.146 S. Hunklinger: The universality of the density of states of low-energy excitations in glasses, *Philos. Mag. B* **56**, 199–211 (1987)
- 19.147 K.A. Topp, D.G. Cahill: Elastic properties of several amorphous solids and disordered crystals below 100 K, *Z. Phys. B* **101**, 235–245 (1996).
- 19.148 M. Inui, S. Hosokawa, K. Matsuda, S. Tsutsui, A.Q.R. Baron: Collective dynamics and de Gennes narrowing in polymeric liquid Se: High-resolution inelastic x-ray scattering, *Phys. Rev. B* **77**, 224201 (2008)
- 19.149 A. Chiba, Y. Ohmasa, S.M. Bennington, J.W. Taylor, M. Yao: Analysis of the optic-type collective mode in liquid selenium to determine the local structure, *Phys. Rev. B* **77**, 132202 (2008)
- 19.150 J.R. Lewandowski, M.E. Halse, M. Blackledge, L. Emsley: Direct observation of hierarchical protein dynamics, *Science* **348**, 578–581 (2015)
- 19.151 P. Chaudhari, P. Beardmore, M.B. Bever: On the thermodynamic properties of amorphous and hexagonal selenium, *Phys. Chem. Glass* **7**, 157–158 (1966)
- 19.152 J. Grenet, E. Bouthegourd, A. Esposito, A. Saiter, J.M. Saiter: Is the configurational entropic model able to predict the final equilibrium state reached by Se glasses after very long ageing durations?, *Philos. Mag.* **93**, 2932–2946 (2013).
- 19.153 S. Yannopoulos, S.O. Kasap: Glass transformation phenomena in bulk and film amorphous selenium via DSC heating and cooling scans, *J. Mater. Res.* **5**, 789–794 (1990)
- 19.154 R. Svoboda, P. Pusková, J. Málek: Relaxation behaviors of glassy selenium, *J. Phys. Chem. Solids* **68**, 850–854 (2007)
- 19.155 K. Vedam, D.L. Miller, R. Roy: Elastic constants of selenium in the hexagonal and glassy phases, *J. Appl. Phys.* **37**, 3432–3434 (1966)
- 19.156 R. Böhmer, C.A. Angell: Elastic and viscoelastic properties of amorphous selenium and identification of the phase transition between ring and chain structures, *Phys. Rev. B* **48**, 5857–5864 (1993)
- 19.157 V.F. Kozhevnikov, W.B. Payne, J.K. Olson, A. Allen, P.C. Taylor: Sound velocity in liquid and glassy selenium, *J. Non-Cryst. Solids* **353**, 3254–3259 (2007)

- 19.158 F. Yang, J.C.M. Li: Viscosity of selenium measured by impression test, *J. Non-Cryst. Solids* **212**, 136–142 (1997)
- 19.159 S.V. Nemilov: Interrelation between shear modulus and the molecular parameters of viscous flow for glass forming liquids, *J. Non-Cryst. Solids* **352**, 2715–2725 (2006)
- 19.160 C.M. Roland, P.G. Santangelo, D.J. Plazek, K.M. Bernaltz: Creep of selenium near the glass temperature, *J. Chem. Phys.* **111**, 9337–9342 (1999)
- 19.161 J.C. Mauro, D.C. Allan, M. Potuzak: Nonequilibrium viscosity in glass, *Phys. Rev. B* **80**, 094204 (2009)
- 19.162 P. Košťál, J. Málek: Viscosity of selenium melt, *J. Non-Cryst. Solids* **356**, 2803–2806 (2010)
- 19.163 S.O. Kasap, S. Yannacopoulos, P. Gundappa: Mechanical properties of the semiconducting glass a-Se, *J. Non-Cryst. Solids* **111**, 82–90 (1989)
- 19.164 W.H. Poisl, W.C. Oliver, B.D. Fabes: The relationship between indentation and uniaxial creep in amorphous selenium, *J. Mater. Res.* **10**, 2024–2032 (1995)
- 19.165 R.B. Stephens: Viscosity and structural relaxation rate of evaporated amorphous selenium, *J. Appl. Phys.* **49**, 5855–5864 (1978)
- 19.166 R.B. Stephens: Structural changes in a-Se near the glass transition by thermal relaxation kinetics, *Phys. Rev. B* **30**, 5195–5202 (1984)
- 19.167 I. Echeverría, P.L. Kolek, D.J. Plazek, S.L. Simon: Enthalpy recovery, creep and creep-recovery measurements during physical aging of amorphous selenium, *J. Non-Cryst. Solids* **324**, 242–255 (2003)
- 19.168 K. Tanaka: Structural studies of amorphous Se under pressure, *Phys. Rev. B* **42**, 11245–11251 (1990)
- 19.169 A. Drozd-Rzoska, S.J. Rzoska, A.R. Imre: On the pressure evolution of the melting temperature and the glass transition temperature, *J. Non-Cryst. Solids* **353**, 3915–3923 (2007)
- 19.170 Z. He, X. Liu, D. Zhang, L. Zhang, S. Hong: Pressure effect on thermal-induced crystallization of amorphous selenium up to 5.5 GPa, *Solid State Commun.* **197**, 30–33 (2014)
- 19.171 D. Caprion, H.R. Schober: Computer simulation of liquid and amorphous selenium, *J. Non-Cryst. Solids* **326&327**, 369–373 (2003)
- 19.172 H.Y. Zhang, Z.Q. Hu, K. Lu: Transformation from the amorphous to the nanocrystalline state in pure selenium, *Nanostructured Mater.* **5**, 41–52 (1995)
- 19.173 J. Málek, J. Barták, J. Štěpánková: Spherulitic crystal growth velocity in selenium supercooled liquid, *Cryst. Growth Des.* **16**, 5811–5821 (2016)
- 19.174 A.K. Bandyopadhyay, L.C. Ming: Pressure-induced phase transformations in amorphous selenium by x-ray diffraction and Raman spectroscopy, *Phys. Rev. B* **54**, 12049–12056 (1996)
- 19.175 H. Liu, L. Wang, X. Xiao, F. De Carlo, J. Feng, H. Mao, R.J. Hemley: Anomalous high-pressure behavior of amorphous selenium from synchrotron x-ray diffraction and microtomography, *PNAS* **105**, 13229–13234 (2008)
- 19.176 P.R. Couchman: Glass transition of materials with various degrees of covalent bonding, *Solid State Commun.* **77**, 553–554 (1991)
- 19.177 R.J. Freitas, K. Shimakawa, S. Kugler: Some remarks on the glass-transition temperature in chalcogenide glasses: A correlation with the microhardness, *Chalcogenide Lett.* **10**, 39–43 (2013)
- 19.178 K. Tanaka: Pressure-induced structural transformation in amorphous semiconductors, *J. Non-Cryst. Solids* **150**, 44–48 (1992)
- 19.179 J.D. Hoffman, R.L. Miller: Kinetics of crystallization from the melt and chain folding in polyethylene fractions revisited: theory and experiment, *Polymer* **38**, 3151–3212 (1997)
- 19.180 A.A. Abu-Sehly, S.N. Alamri, A.A. Joraid: Measurements of DSC isothermal crystallization kinetics in amorphous selenium bulk samples, *J. Alloys Compounds* **476**, 348–351 (2009)
- 19.181 W.R. Salaneck, C.B. Duke, A. Paton, C. Griffiths, R.C. Keezer: Electronic structure of monoclinic selenium (Se<sub>8</sub>): Comparison with S<sub>8</sub> and trigonal selenium, *Phys. Rev. B* **15**, 1100–1109 (1977)
- 19.182 B.R. Orton, J.C. Rivière: X-ray photoelectron spectroscopy of bulk glassy Se under Ar ion bombardment, *J. Non-Cryst. Solids* **37**, 401–406 (1980)
- 19.183 T. Takahashi: Comparative x-ray-photoemission study of monoclinic, trigonal, and amorphous selenium, *Phys. Rev. B* **26**, 5963–5964 (1982)
- 19.184 I. Ono, P.C. Grekos, T. Kouchi, M. Nakatake, M. Tamura, S. Hosokawa, H. Namatame, M. Taniguchi: A study of electronic states of trigonal and amorphous Se using ultraviolet photoemission and inverse-photoemission spectroscopies, *J. Phys.: Condens. Matter* **8**, 7249–7261 (1996)
- 19.185 J. Robertson: A new model for the structure of amorphous selenium, *Philos. Mag. B* **34**, 12–31 (1976)
- 19.186 J.D. Joannopoulos, M. Schlüter, M.L. Cohen: Electronic structure of trigonal and amorphous Se and Te, *Phys. Rev. B* **11**, 2186–2199 (1975)
- 19.187 M.U. Kahaly, P. Ghosh, S. Narasimhan, U.V. Waghmare: Size dependence of structural, electronic, elastic, and optical properties of selenium nanowires: a first-principles study, *J. Chem. Phys.* **128**, 044718 (2008)
- 19.188 O. Rubel, D. Laughton: Lone-pair states as a key to understanding impact ionization in chalcogenide semiconductors, *J. Phys.: Condens. Matter* **22**, 355803 (2010)
- 19.189 A. Darbandi, É. Devoire, O. Di Matteo, O. Rubel: Modeling the radiation ionization energy and energy resolution of trigonal and amorphous selenium from first principles, *J. Phys.: Condens. Matter* **24**, 455502 (2012)
- 19.190 A. Darbandi, O. Rubel: Impact ionization threshold energy of trigonal selenium: An ab initio study, *Can. J. Phys.* **91**, 483–485 (2013)
- 19.191 M. Matsui: Role of interchain interaction in determining the band gap of trigonal selenium: A density functional theory study with a linear combination of Bloch orbitals, *J. Phys. Chem.* **118**, 19294–19307 (2014)
- 19.192 M. Hirayama, R. Okugawa, S. Ishibashi, S. Murakami, T. Miyake: Weyl node and spin texture in trigonal tellurium and selenium, *Phys. Rev. Lett.*

- 114, 206401 (2015)
- 19.193 J. Mort, A.I. Lakatos: Steady state and transient photoemission into amorphous insulators, *J. Non-Cryst. Solids* **4**, 117-131 (1970)
- 19.194 P. Nielsen: Energy gap states and interfacial barriers in amorphous Se and  $\text{As}_2\text{Se}_3$ , *Solid St. Commun.* **9**, 1745-1748 (1971)
- 19.195 T. Innami, T. Miyazaki, S. Adachi: Optical constants of amorphous Se, *J. Appl. Phys.* **86**, 1382-1387 (1999)
- 19.196 L. Tichý, H. Tichá, P. Nagels, E. Sileckx, R. Callaert: Optical gap and Urbach edge slope in a-Se, *Mater. Lett.* **26**, 279-283 (1996)
- 19.197 M.A. Jafar, M.H. Saleh, M.J. Ahmad, B. Bulos, T. Al-Daraghme: Retrieval of optical constants of undoped amorphous selenium films from an analysis of their normal-incidence transmittance spectra using numeric PUMA method, *J. Mater. Sci.: Mater. Electron.* **27**, 3281-3291 (2016)
- 19.198 K. Tanaka: Have we understood the optical absorption edge in chalcogenide glasses?, *J. Non-Cryst. Solids* **431**, 21-24 (2016)
- 19.199 K. Tanaka: Minimal Urbach energy in non-crystalline materials, *J. Non-Cryst. Solids* **389**, 35-37 (2014)
- 19.200 G.P. Ceasar, M. Abkowitz, J.W.-P. Lin: Photoacoustic and xerographic investigation of the gap-state structure of a-Se: Comparison with a-Si:H, *Phys. Rev. B* **29**, 2353-2355 (1984)
- 19.201 K. Tanaka, T. Gotoh, N. Yoshida, S. Nonomura: Photothermal deflection spectroscopy of chalcogenide glasses, *J. Appl. Phys.* **91**, 125-128 (2002)
- 19.202 K. Tanaka, S. Nakayama: Band-tail characteristics in amorphous semiconductors studied by the constant-photocurrent method, *Jpn. J. Appl. Phys.* **38**, 3986-3992 (1999)
- 19.203 J.C. Knights, E.A. Davis: Photogeneration of charge carriers in amorphous selenium, *J. Phys. Chem. Solids* **35**, 543-554 (1974)
- 19.204 K. Tanaka: Photoconducting Urbach edge in amorphous Se, *J. Non-Cryst. Solids* **426**, 32-34 (2015)
- 19.205 J. Rabit and J.C. Perron: Photoconductivity in liquid selenium, *J. Phys. C* **42**, 1047-1050 (1981)
- 19.206 D.M. Pai, R.C. Enck: Onsager mechanism of photogeneration in amorphous selenium, *Phys. Rev. B* **11**, 5163-5174 (1975)
- 19.207 H. Scher, E.W. Montroll: Anomalous transit-time distribution in amorphous solids, *Phys. Rev. B* **12**, 2455-2477 (1975)
- 19.208 S. Imamura, Y. Kanemitsu, T. Hayano, T. Kitamura: Characterization of deep defect levels in amorphous selenium by optical methods, *J. Non-Cryst. Solids* **97&98**, 663-666 (1987)
- 19.209 P.K. Weimer: Photo-conductivity in amorphous selenium, *Phys. Rev.* **79**, 171 (1950)
- 19.210 A. Reznik, K. Jandieri, F. Gebhard, S. D. Baranovskii: Non-Onsager mechanism of long-wave photogeneration in amorphous selenium at high electric fields, *Appl. Phys. Lett.* **100**, 132101 (2012)
- 19.211 N. Hijazi, M.Z. Kabir: Mechanisms of charge photogeneration in amorphous selenium under high electric fields, *J. Mater. Sci.: Mater. Electron.* **27**, 7534-7539 (2016)
- 19.212 K. Nagata, Y. Miyamoto, H. Nishimura, H. Suzuki, and S. Yamasaki: Photoconductivity and photoacoustic spectra of trigonal, rhombohedral, orthorhombic, and  $\alpha$ -,  $\beta$ -, and  $\gamma$ -monoclinic selenium, *Jpn. J. Appl. Phys. Pt.2* **24**, L858-L860 (1985)
- 19.213 R.A. Street, N.F. Mott: States in the gap in glassy semiconductors, *Phys. Rev. Lett.* **35**, 1293-1296 (1975)
- 19.214 M. Kastner, D. Adler, H. Fritzsche: Valence-alternation model for localized gap states in lone-pair semiconductors, *Phys. Rev. Lett.* **37**, 1504-1507 (1976)
- 19.215 S.G. Bishop, U. Strom, P.C. Taylor: Optically induced metastable paramagnetic states in amorphous semiconductors, *Phys. Rev. B* **15**, 2278-2294 (1977)
- 19.216 K. Shimakawa, A. Kolobov, S.R. Elliott: Photoinduced effects and metastability in amorphous semiconductors and insulators, *Adv. Phys.* **44**, 475-588 (1995)
- 19.217 R.A. Street: Luminescence in amorphous semiconductors, *Adv. Phys.* **25**, 397-454 (1976)
- 19.218 D. Vanderbilt, J.D. Joannopoulos: Total energies in Se. III. Defects in the glass, *Phys. Rev. B* **27**, 6311-6321 (1983)
- 19.219 S. Itoh, K. Nakao: Electronic states in allotropes of sulphur and selenium - localized orbital approach, *J. Phys. C: Solid State Phys.* **17**, 3373-3389 (1984)
- 19.220 A. Ikawa, H. Fukutome: Electronic and lattice structures of isolated Se chains and defects in them. II, *J. Phys. Soc. Jpn.* **59**, 1002-1016 (1990)
- 19.221 G. Kresse, F. Kirchhoff, M.J. Gillan: Defects in liquid selenium, *Phys. Rev. B* **59**, 3501-3513 (1999)
- 19.222 T. Koslowski, M. Koblichke, A. Blumen: Modified small-world networks as models of liquid and amorphous selenium, *Phys. Rev. B* **66**, 064205 (2002)
- 19.223 S.A. Dembovsky: New sight into the structure of selenium: Four-valence Se in glass, *J. Non-Cryst. Solids* **353**, 2944-2948 (2007)
- 19.224 F.V. Grigor'ev: Stabilization of charged and neutral defects and formation of centers with negative correlation energy in a-Se, *Russ. J. Inorg. Chem.* **54**, 295-299 (2009)
- 19.225 C.K. Wong, G. Lucovsky, J. Bernholc: Intrinsic localized defect states in a-Se associated with dihedral angle distortions, *J. Non-Cryst. Solids* **97&98**, 1171-1174 (1987)
- 19.226 M. Springborg, R.O. Jones: Sulfur and selenium helices: Structure and electronic properties, *J. Chem. Phys.* **88**, 2652-2658 (1988)
- 19.227 A. Ikawa, H. Fukutome: Electronic and lattice structures of isolated Se chains and defects in them. I. A semi-empirical model and properties of regular Se helix, *J. Phys. Soc. Jpn.* **58**, 4517-4529 (1989)
- 19.228 M. Kumeda, Y. Nakagaki, M. Suzuki, T. Shimizu: The reversible photostructural change studied by ESR of  $\text{Mn}^{2+}$  in  $\text{As}_2\text{Se}_3$  films, *Solid State Commun.*



- 21, 717 (1977)
- 19.229 S.R. Ovshinsky, D. Adler: Local structure, bonding, and electronic properties of covalent amorphous semiconductors, *Contemp. Phys.* **19**, 109–126 (1978)
- 19.230 S.C. Agarwal: Nature of localized states in amorphous semiconductors—A study by electron spin resonance, *Phys. Rev. B* **7**, 685–691 (1973)
- 19.231 A.V. Kolobov, M. Kondo, H. Oyanagi, A. Matsuda, K. Tanaka: Negative correlation energy and valence alternation in amorphous selenium: An in situ optically induced ESR study, *Phys. Rev. B* **58**, 12004–12010 (1998)
- 19.232 K. Tanaka: Photoluminescence in chalcogenide glasses: revisited, *J. Optoelectron. Adv. Mater.* **15**, 1165–1178 (2013)
- 19.233 H. Lundt, G. Weiser: Defect luminescence and its excitation spectra in As-doped Se single crystals, *Philos. Mag. B* **51**, 367–380 (1985)
- 19.234 T. Aoki, S. Komodoori, S. Kobayashi, T. Shimizu, A. Ganjoo, K. Shimakawa: Photoluminescence lifetime distributions of chalcogenide glasses obtained by wide-band frequency resolved spectroscopy, *J. Non-Cryst. Solids* **326&327**, 273–278 (2003)
- 19.235 C.Y. Chen, M.A. Kastner: Transient photoinduced optical absorption in trigonal single-crystal selenium, *Phys. Rev. B* **33**, 1073–1075 (1986)
- 19.236 Y. Sakaguchi, K. Tamura: A large photoinduced change in liquid selenium: transient dc conductivity and transient absorption measurements, *J. Non-Cryst. Solids* **250–252**, 441–446 (1999)
- 19.237 K.V. Yumashev, V.P. Mikhailov, P.V. Prokoshin, M.V. Artermeyev, V.S. Gurin: Optical transient induced absorption in ultrasmall particles of a selenium, *Opt. Commun.* **125**, 59–64 (1996)
- 19.238 Y. Katayama, M. Yao, Y. Ajiro, M. Inui, H. Endo: Photo-induced phenomena in isolated selenium chains, *J. Phys. Soc. Jpn.* **58**, 1811–1822 (1989)
- 19.239 A. Saitoh, H. Takebe, K. Tanaka: Selenium chains in ZSM-5 zeolite: Atomic structure and optical properties, *J. Optoelectron. Adv. Mater.* **13**, 1524–1530 (2011)
- 19.240 T.E. Orlowski, M. Abkowitz: Microstripline transient photocurrents in a-Se: Structure resolved in shallow band-tail states, *Solid State Commun.* **59**, 665–668 (1986)
- 19.241 G.J. Adriaenssen, M.L. Benkhedir: Energy levels and charge state of intrinsic defects in amorphous selenium, *J. Non-Cryst. Solids* **354**, 2687–2690 (2008)
- 19.242 S. Kasap, C. Koughia, J. Berashevich, R. Johanson, A. Reznik: Charge transport in pure and stabilized amorphous selenium: re-examination of the density of states distribution in the mobility gap and role of defects, *J. Mater. Sci.: Mater. Electron.* **26**, 4644–4658 (2015)
- 19.243 J. Berashevich, A. Mishchenko, A. Reznik: Two-step photoexcitation mechanism in amorphous Se, *Phys. Rev. Appl.* **1**, 034008 (2014)
- 19.244 C. Koughia, A. Reznik, C. Allen, R. Johanson, S. Kasap: Density of localized state distribution near the valence band in stabilized a-Se using interrupted field time of flight measurements with long interruption times. *Phys. Status Solidi A* **213**, 1856–1863 (2016)
- 19.245 V.I. Mikla, V.V. Mikla: Trap level spectroscopy in amorphous selenium-based semiconductors. *J. Mater. Sci.: Mater. Electron.* **20**, 1059–1067 (2009)
- 19.246 J. Dresner: Quenching effects and negative photoconductivity in amorphous selenium, *J. Chem. Phys.* **35**, 1628–1635 (1961)
- 19.247 J. Dresner, G.B. Stringfellow: Electronic processes in the photo-crystallization of vitreous selenium, *J. Phys. Chem. Solid* **29**, 303–311 (1968)
- 19.248 Y. Hoshino, H. Miyata: Thermally stimulated currents in amorphous selenium: Relationship to trapping levels and the noncrystalline state, *J. Appl. Phys.* **52**, 6214–6217 (1981)
- 19.249 S. Chand, G.D. Sharma, S. Dwivedi: Effect of polyvinylcarbazole barrier layer on charge storage in amorphous selenium films, *Appl. Phys. Lett.* **75**, 621–622 (1999)
- 19.250 J. Mort: Transient photoconductivity in trigonal selenium single crystals, *J. Appl. Phys.* **39**, 3543–3549 (1968)
- 19.251 R.J.F. Dalrymple, W.E. Spear: A comparison of the electronic structure and properties of orthorhombic sulphur and monoclinic selenium, *J. Phys. Chem. Solids* **33**, 1071–1078 (1972)
- 19.252 M. Yao, S. Hosokawa, H. Endo: The effect of charged additives on the conductivity and the thermopower in liquid selenium, *J. Non-Cryst. Solids* **59 & 60**, 1083–1086 (1983)
- 19.253 M. Itoh, K. Tanaka: Time-of-flight photocurrents in  $As_2Se_3$  and Se under bias illumination, *J. Non-Cryst. Solids* **164–166**, 1235–1238 (1993)
- 19.254 J. Kaladé, E. Montrimas, V. Jankauskas: Investigation of charge carrier lifetime in high-resistivity semiconductor layers by the method of small charge photocurrent, *J. Non-Cryst. Solids* **243**, 158–167 (1999)
- 19.255 S. Kasap, J.F. Frey, G. Belev, O. Tousignant, H. Mani, J. Greenspan, L. Laperriere, O. Bubon, A. Reznik, G. DeCrescenzo, K.S. Karim, J.A. Rowlands: Amorphous and polycrystalline photoconductors for direct conversion flat panel x-ray image sensors, *Sensors* **11**, 5112–5157 (2011)
- 19.256 G. Juška, K. Arlauskas: Impact ionization and mobilities of charge carriers at high electric fields in amorphous selenium, *Phys. Stat. Sol. (a)* **59**, 389–393 (1980)
- 19.257 G. Juška, K. Arlauskas: Features of hot carriers in amorphous selenium, *Phys. Stat. Sol. (a)* **77**, 387–391 (1983)
- 19.258 K. Tanioka, J. Yamazaki, K. Shidara, K. Take-toshi, T. Kawamura, S. Ishioka, Y. Takasaki: An avalanche-mode amorphous selenium photoconductive layer for use as a camera tube target, *IEEE EDL* **8**, 392–394 (1987)
- 19.259 K. Tsuji, Y. Takasaki, T. Hirai, J. Yamazaki, K. Tanioka: Avalanche phenomena in amorphous selenium, *OPTOELECTRONICS* **9**, 367–378 (1994)
- 19.260 A. Reznik, K. Jandieri, F. Gebhard, S.D. Baranovskii: Non-Onsager mechanism of long-wave

- photogeneration in amorphous selenium at high electric fields, *Appl. Phys. Lett.* **100**, 132101 (2012)
- 19.261 O. Bubon, G. DeCrescenzo, W. Zhao, Y. Ohkawa, K. Miyakawa, T. Matsubara, K. Kikuchi, K. Tanioka, M. Kubota, J.A. Rowlands, A. Reznik: Electroded avalanche amorphous selenium (a-Se) photosensor, *Curr. Appl. Phys.* **12**, 983–988 (2012)
- 19.262 T. Masuzawa, I. Saito, T. Yamada, M. Onishi, H. Yamaguchi, Y. Suzuki, K. Oonuki, N. Kato, S. Ogawa, Y. Takakuwa, A.T.T. Koh, D.H.C. Chua, Y. Mori, T. Shimosawa, K. Onano: Development of an amorphous selenium-based photodetector driven by a diamond cold cathode, *Sensors* **13**, 13744–13778 (2013)
- 19.263 W.-D. Park, K. Tanioka: Avalanche multiplication and impact ionization in amorphous selenium photoconductive target, *Jpn. J. Appl. Phys.* **53**, 031401 (2014)
- 19.264 V. Mortet, A. Soltani: Impurity impact ionization avalanche in p-type diamond, *Appl. Phys. Lett.* **99**, 202105 (2011)
- 19.265 G. Juska: Properties of free-carrier transport in a-Se and a-Si:H, *J. Non-Cryst. Solids* **137&138**, 401–406 (1991)
- 19.266 M. Akiyama, M. Hanada, K. Sawada, M. Ishida: Multiplication characteristics of a-Si:H p-i-n photodiode film in high electric field, *Jpn. J. Appl. Phys.* **42**, 2345–2348 (2003)
- 19.267 H.P.D. Lanyon, R.E. Richardson, Jr.: Ionization coefficient for holes in polycrystalline selenium, *Phys. Stat. Sol. (a)* **7**, 421–425 (1971)
- 19.268 S. Imura, K. Kikuchi, K. Miyakawa, M. Kubota: Optical properties of photoconductor using crystalline selenium, *Can. J. Phys.* **92**, 645–647 (2014)
- 19.269 V.I. Arkhipov, S.O. Kasap: Is there avalanche multiplication in amorphous semiconductors?, *J. Non-Cryst. Solids* **266–269**, 959–963 (2000)
- 19.270 S. Kasap, J.A. Rowlands, S.D. Baranovskii, K. Tanioka: Lucky drift impact ionization in amorphous semiconductors, *J. Appl. Phys.* **96**, 2037–2048 (2004)
- 19.271 A. Reznik, S.D. Baranovskii, O. Rubel, G. Juska, Y. Ohkawa, K. Tanioka, J.A. Rowlands: Avalanche multiplication phenomenon in amorphous semiconductors: Amorphous selenium versus hydrogenated amorphous silicon, *J. Appl. Phys.* **102**, 053711 (2007)
- 19.272 O. Rubel, A. Potvin, D. Laughton: Generalized lucky-drift model for impact ionization in semiconductors with disorder, *J. Phys.: Condens. Matter* **23**, 055802 (2011)
- 19.273 M.Z. Kabir, N. Hijazi: Temperature and field dependent effective hole mobility and impact ionization at extremely high fields in amorphous selenium, *Appl. Phys. Lett.* **104**, 192103 (2014)
- 19.274 E. Bringuier: High-field transport statics and impact excitation in semiconductors, *Phys. Rev. B* **49**, 7974–7989 (1994)
- 19.275 K. Tanaka: Avalanche breakdown in amorphous selenium (a-Se) and related materials: Brief review, critique, and proposal, *J. Optoelectron. Adv. Mater.* **16**, 243–251 (2014)
- 19.276 S.R. Ovshinsky, H. Fritzsche: Amorphous semiconductors for switching, memory, and imaging applications, *IEEE Trans.* **ED-20**, 91–105 (1973)
- 19.277 S. Hudgens: Progress in understanding the Ovshinsky effect: Threshold switching in chalcogenide amorphous semiconductors, *Phys. Stat. Sol. B* **246**, 1951–1955 (2012)
- 19.278 D. Armitage, C.H. Champness: Switching in amorphous selenium, *J. Non-Cryst. Solids* **7**, 410–416 (1972)
- 19.279 T. Matsushita, T. Yamagami, M. Okuda: Polarized memory effect observed on Se-SnO<sub>2</sub> system, *Jpn. J. Appl. Phys.* **11**, 1657–1662 (1972)
- 19.280 T. Hayashi, Y. Ono, M. Fukaya, H. Kan: Polarized memory switching in amorphous Se film, *Jpn. J. Appl. Phys.* **13**, 1163–1164 (1974)
- 19.281 B. Petretis, K. Bacevičiūtė, E. Montrimas, S. Tamošiūnas: Structure investigation of conductive breakdown filaments in electrophotography, *J. Non-Cryst. Solids* **16**, 418–426 (1974)
- 19.282 I.E. Bolotov, L.I. Komarova: Effect of an electric field on the texture of selenium crystals formed in amorphous films, *Sov. Phys. Solid State* **17**, 478–480 (1975)
- 19.283 A.I. Popov, I.Kh. Geller, V.K. Shemetova: Memory and threshold switching effects in amorphous selenium, *Phys. Stat. Sol. (a)* **44**, K71–K73 (1977)
- 19.284 G. Jones, R.A. Collins: Threshold and memory switching in amorphous selenium thin-films, *Phys. Stat. Sol. A* **53**, 339–350 (1979)
- 19.285 J.C. Bernede, A. Conan, E. Fouesnant, B. El Bouchairi, G. Goureaux: Polarized memory switching in As<sub>2</sub>Se/Se/M thin film sandwiches, *Thin Solid Films* **97**, 165–171 (1982)
- 19.286 M. Okuda, T. Matsushita, T. Yamaguchi, K. Yamamoto: Highly sensitive light-induced memory effect with amorphous Se-SnO<sub>2</sub> heterojunction, *Appl. Opt.* **13**, 799–802 (1974)
- 19.287 H.W. Pinsler, W.E. Brower: Se crystallization induced by corotron charging, *J. Phys. Chem. Solids* **38**, 393–396 (1977)
- 19.288 Y. Ema, T. Hayashi: Aging effect of capacitance and related effects in Au/a-Se/Al structure, *Jpn. J. Appl. Phys.* **21**, 1665–1670 (1982)
- 19.289 J.R. Scheuermann, Y. Miranda, H. Liu, W. Zhao: Charge transport model in solid-state avalanche amorphous selenium and defect suppression design, *J. Appl. Phys.* **119**, 024508 (2016)
- 19.290 M.Z. Kabir, S.-Al Imam: Transient and steady-state dark current mechanisms in amorphous selenium avalanche radiation detectors, *Appl. Phys. Lett.* **102**, 153515 (2013)
- 19.291 T.-Y. Yu, F.-M. Pan, C.-Y. Chang, T. Hu, J.-F. Chen, J.-F. Wang, C.-L. Lin, T.-H. Chen, T.-M. Chen: Dark current suppression of amorphous selenium based photosensors by the ZnO hole blocking layer, *Curr. Appl. Phys.* **14**, 659–664 (2014)
- 19.292 S. Abbaszadeh, N. Allec, S. Ghanbarzadeh, U. Shafique, K.S. Karim: Investigation of hole-blocking contacts for high-conversion-gain amorphous selenium detector for x-ray imaging, *IEEE Trans. Electron Devices* **59**, 2403–2409 (2012)

- 19.293 S. Ghaffari, S. Abbaszadeh, S. Gahnbarzadeh, K.S. Karim: Characterization of optically sensitive a-Se photodetector at high electric fields, *IEEE Trans. Electron Devices* **62**, 2364–2366 (2015)
- 19.294 V.G. Uss, I.B. Sidaravichyus: Transient photoconductivity of poly-n-vinyl carbazole amorphous selenium double-layer electrophotographic systems, *Sov. Phys. Semicond.* **9**, 1091–1094 (1975)
- 19.295 C. Juhasz, M. Vaezi-Nejad, S.O. Kasap: Interface hole traps in double-layer amorphous semiconductor  $\text{Se}_{1-x}\text{Te}_x$  photoreceptor devices, *Semicond. Sci. Technol.* **1**, 302–304 (1986)
- 19.296 I.H. Campbell: Improving the spectral response of amorphous Se photodetectors using organic semiconductors, *Appl. Phys. Lett.* **99**, 063303 (2011)
- 19.297 T. -Y. Yu, F.-M. Pan, C.-Y. Chang, J.-S. Lin, W.-H. Huang: Thermal stability and photoconductive properties of photosensors with an alternating multilayer structure of amorphous Se and  $\text{As}_x\text{Se}_{1-x}$ , *J. Appl. Phys.* **118**, 044509 (2015)
- 19.298 D. Nesheva, I.P. Kotsalas, C. Raptis, E. Vateva: On the structural stability of amorphous Se/CdSe multilayers: a Raman study, *J. Non-Cryst. Solids* **224**, 283–290 (1998)
- 19.299 K. Tanaka, Y. Ichimura, M. Komazaki: Photoinduced effect in glassy chalcogenide heterojunctions, *Thin Solid Films* **189**, 51–58 (1990)
- 19.300 M. Malyovanik, A. Kikineshi, S.H. Messaddeq, Y. Messaddeq, I. Ivan, S.J.L. Ribeiro: Photo-induced transformations in chalcogenide composite layers, *J. Non-Cryst. Solids* **348**, 144–148 (2004)
- 19.301 O.U. Vonwiller: Notes on the elastic properties of Se, *Nature* **104**, 347–347 (1919)
- 19.302 A.V. Kolobov (ed.): *Photo-Induced Metastability in Amorphous Semiconductors* (Wiley-VCH, Weinheim, 2003)
- 19.303 R.E. Tallman, B.A. Weinstein, A. Reznik, M. Kubota, K. Tanioka, J.A. Rowlands: Photocrystallization in a-Se imaging targets: Raman studies of competing effects, *J. Non-Cryst. Solids* **354**, 4577–4581 (2008)
- 19.304 P. Yu, W.H. Wang, R.J. Wang, S.X. Lin, X.R. Liu, S.M. Hong, H.Y. Bai: Understanding exceptional thermodynamic and kinetic stability of amorphous sulfur obtained by rapid compression, *Appl. Phys. Lett.* **94**, 011910 (2009)
- 19.305 J. Akola, R.O. Jones: Structure and dynamics in amorphous tellurium and  $\text{Te}_n$  clusters: A density functional study, *Phys. Rev. B* **85**, 134103 (2012)
- 19.306 A. Roy, A.V. Kolobov, H. Oyanagi, K. Tanaka: Photo-induced ring-to-chain conversion in as-evaporated films of amorphous selenium, *Philos. Mag. B* **78**, 87–94 (1998)
- 19.307 M. Shiojiri: Crystallization of amorphous selenium films prepared by vacuum-evaporation, *Jpn. J. Appl. Phys.* **6**, 163–172 (1967)
- 19.308 S.R. Herd, P. Chaudhari: Electron-beam-induced reversible transformations from glass to crystalline, liquid, and vapor phases in Se thin films, *J. Appl. Phys.* **44**, 4102–4107 (1973)
- 19.309 R. Calemczuk, E. Bonjour: Gamma-ray induced relaxation in selenium glass, *J. Non-Cryst. Solids* **43**, 427–432 (1981)
- 19.310 J.P. Larmagnac, J. Grenet, P. Michon: Photo-dependence of sub- $T_g$  relaxation in a-Se thin films, *Philos. Mag. B* **45**, 627–638 (1982)
- 19.311 H. Koseki, A. Odajima: Photo-induced stress relaxation in amorphous selenium films, *Jpn. J. Appl. Phys.* **21**, 424–428 (1982)
- 19.312 J. Grenet, D. Carles, G. Lefrancois, J.P. Larmagnac: Evidence for a diffusion of photo-induced defect in a-Se, *J. Non-Cryst. Solids* **56**, 285–290 (1983)
- 19.313 V.V. Poborchii, A.V. Kolobov, K. Tanaka: Photomelting of selenium at low temperature, *Appl. Phys. Lett.* **74**, 215–217 (1999)
- 19.314 V. Palyok, I.A. Szabó, D.L. Beke, A. Kikineshi: Surface grating formation and erasing on a-Se films, *Appl. Phys. A* **74**, 683–687 (2002)
- 19.315 M. Repka, M. Frumar, M. Hrdlicka: Photo-induced changes of viscosity of glassy selenium below its glass transition temperature, *J. Phys. Chem. Solids* **68**, 940–942 (2007)
- 19.316 B.V. Deryagin, Yu.P. Toporov, K.I. Merzhanov, N.M. Gal'vidis, I.N. Aleinikova, L.N. Burta-Gapanovich: Photomechanical effect in amorphous semiconductors, *Sov. Phys. Solid State* **16**, 1155–1156 (1974)
- 19.317 E. Montrimas, R. Rinkūnas, S. Kuskevičius, R. Purlys: Influence of light on structure of amorphous selenium layers, *Lithuanian J. Phys.* **48**, 249–258 (2008)
- 19.318 R. Sharma, D. Kumar, V. Srinivasan, H. Jain, K.V. Adarsh: Engineering the optical response of a-Se thin films by employing morphological disorder, *Opt. Express* **23**, 14085–14094 (2015)
- 19.319 H. Koseki, A. Odajima: Photo-illumination effect on the glass transition of annealed amorphous selenium, *Jpn. J. Appl. Phys.* **22**, 542–542 (1983)
- 19.320 Y. Ikeda, K. Shimakawa: Real-time in situ measurements of photoinduced volume changes in chalcogenide glasses, *J. Non-Cryst. Solids* **338–340**, 539–542 (2004)
- 19.321 M. Popescu, F. Sava, K. Shimakawa, Y. Ikeda, V. Babin: Thickness oscillation effect in photoexpansion and photocontraction of amorphous selenium, *J. Optoelectron. Adv. Mater.* **9**, 3558–3562 (2007)
- 19.322 A. Reznik, M. Klebanov, V. Lyubin: Transient photorefractive effect in a-Se films, *J. Appl. Phys.* **105**, 013518 (2009)
- 19.323 A. Mishchenko, G.P. Lindberg, B.A. Weinstein, A. Reznik: Comparative study of the photodarkening relaxation-kinetics in amorphous selenium for above-bandgap and sub-gap illumination, *Appl. Phys. Lett.* **105**, 051912 (2014)
- 19.324 K. Tanaka, A. Odajima: Photodarkening in amorphous selenium, *Solid State Commun.* **43**, (1982) 961–964
- 19.325 I.A. Paribok-Aleksandrovich: Photocrystallization of amorphous selenium, *Sov. Phys. – Solid State* **11**, 1631(1970)
- 19.326 A.V. Kolobov, H. Oyanagi, Ka. Tanaka, Ke. Tanaka: Structural study of amorphous selenium by *in situ* EXAFS: Observation of photoinduced bond alteration, *Phys. Rev. B* **55**, 726–734 (1997)

- 19.327 R. Chang, Changes in the electronic states of vitreous selenium upon light radiation and plastic deformation, *Mat. Res. Bull.* **2**, 145–153 (1967)
- 19.328 K. Tanaka: Relation between photodarkening and photoexpansion in  $As_2S_3$  glass, *Phys. Stat. Sol. B* **249**, 2019–2023 (2012)
- 19.329 R.T. Phillips: Photodarkening of amorphous selenium, *J. Non-Cryst. Solids* **70**, 359–366 (1985)
- 19.330 L. Tichy, H. Ticha, P. Nagels, R. Callaerts: Photoinduced optical changes in amorphous Se and Ge–Se films, *J. Non-Cryst. Solids* **240**, 177–181 (1998)
- 19.331 K. Tanaka: Photodarkening in amorphous  $As_2S_3$  and Se under hydrostatic pressure, *Phys. Rev. B* **30**, 4549–4554 (1984)
- 19.332 K. Tanaka: Configurational and structural models for photodarkening in glassy chalcogenides, *Jpn. J. Appl. Phys.* **25**, 779–786 (1986)
- 19.333 H. Ikemoto, T. Tsuzuki, M. Inui, M. Yao, H. Endo: Photodarkening of amorphous selenium under high pressure, *Z. Phys. Chem.* **216**, 1107–1121 (2002)
- 19.334 V.L. Averianov, A.V. Kolobov, B.T. Kolomiets, V.M. Lyubin: Thermal and optical bleaching in darkened films of chalcogenide vitreous semiconductors, *Phys. Stat. Sol. (a)* **57**, 81–88 (1980)
- 19.335 A. Reznik, B.J.M. Lui, J.A. Rowland, S.D. Baranovskii, O. Ruble, V. Lyubin, M. Klebanov, S.O. Kasap, Y. Ohkawa, T. Matsubara, K. Miyakawa, M. Kubota, K. Tanioka, T. Kawai: Kinetics of the photostructural changes in a-Se films, *J. Appl. Phys.* **100**, 113506 (2006)
- 19.336 R.E. Tallman, A. Reznik, B.A. Weinstein, S.D. Baranovskii, J.A. Rowlands: Similarities in the kinetics of photocrystallization and photodarkening in a-Se, *Appl. Phys. Lett.* **93**, 212103 (2008)
- 19.337 A. Mischenko, G.P. Lindberg, B.A. Weinstein, A. Reznik: Comparative study of the photodarkening relaxation–kinetics in amorphous selenium for above- and sub-bandgap illumination, *Appl. Phys. Lett.* **105**, 051912 (2014)
- 19.338 H. Asao, K. Tanaka: Polarization-dependent photoinduced mechanical deformations in covalent chalcogenide glasses, *J. Appl. Phys.* **102**, 043508 (2007)
- 19.339 D. Zhao, J. Jain, L. Malacarne, P.R.B. Pedreira: Role of photothermal effect in photoexpansion of chalcogenide glasses, *Phys. Stat. Sol. B* **250**, 983–987 (2013)
- 19.340 R. Bohdan, S. Molnar, I. Csarnovics, M. Veres, A. Csik, S. Kökenyesi: Optical recording of surface relief on amorphous selenium, *J. Non-Cryst. Solids* **408**, 57–61 (2015)
- 19.341 R. Clement, J.C. Carballes, B. de Cremoux: The photo-crystallization of amorphous selenium thin films, *J. Non-Cryst. Solids* **15**, 505–516 (1974)
- 19.342 G. Gross, R.B. Stephens, D. Turnbull: On the crystallization of amorphous selenium films: Thermal effects and photoeffects, *J. Appl. Phys.* **48**, 1139–1148 (1977)
- 19.343 A. Roy, A.V. Kolobov, K. Tanaka: Laser-induced suppression of photo-crystallization rate in amorphous selenium films, *J. Appl. Phys.* **83**, 4951–4956 (1998)
- 19.344 T. Matsushita, A. Suzuki, M. Okuda, T.T. Nang: Photocrystallization of amorphous  $Ge_xSe_{1-x}$  thin films, *Thin Solid Films* **58**, 413–417 (1979)
- 19.345 K. Okano, I. Saito, T. Mine, Y. Suzuki, T. Yamada, N. Rupesinghe, G.A.J. Amaratunga, E.I. Milne, D.R.T. Zahn: Characterization of a-Se based photodetectors using X-ray photoelectron spectroscopy and Raman spectroscopy, *J. Non-Cryst. Solids* **353**, 308–312 (2007)
- 19.346 L. Song, P. Galarneau, R.A. Lessard: Optical recording characteristics of SeGe films at  $\lambda = 488$  nm, *Opt. Engn.* **28**, 290–296 (1989)
- 19.347 R.B. Stephens: Stress-enhanced crystallization in amorphous selenium films, *J. Appl. Phys.* **51**, 6197–6201 (1989).
- 19.348 D. Chakarov, B. Kasemo: Photoinduced crystallization of amorphous ice films on graphite, *Phys. Rev. Lett.* **81**, 5181–5184 (1998)
- 19.349 H. Adachi, K. Takano, Y. Hosokawa, T. Inoue, Y. Mori, H. Matsumura, M. Yoshimura, Y. Tsunaka, M. Morikawa, S. Kanaya, H. Masuhara, Y. Kai, T. Sasaki: Laser irradiated growth of protein crystal, *Jpn. J. Appl. Phys.* **42**, L798–L800 (2003)
- 19.350 V.G. Zhdanov, V.K. Malinovskii: Photoinduced birefringence and dichroism in  $As_2S_3$  films, *Sov. Tech. Phys. Lett.* **3**, 387–388 (1977)
- 19.351 V.K. Tikhomirov, G.J. Adriaenssens, S.R. Elliott: Temperature dependence of the photoinduced anisotropy in chalcogenide glasses: Activation energies and their interpretation, *Phys. Rev. B* **55**, R660–R663 (1997)
- 19.352 K. Tanaka, K. Ishida, N. Yoshida: Mechanism of photoinduced anisotropy in chalcogenide glasses, *Phys. Rev. B* **54**, 9190–9195 (1996)
- 19.353 K. Ishida and K. Tanaka: Photoinduced anisotropic crystallization of amorphous Se, *Phys. Rev. B* **56**, 206–209 (1997)
- 19.354 V. Lyubin, M. Klebanov, M. Mitkova, T. Petkova: Polarization-dependent, laser-induced anisotropic photocrystallization of some amorphous chalcogenide films, *Appl. Phys. Lett.* **71**, 2118–2120 (1997)
- 19.355 V.V. Poborchii, A.V. Kolobov, K. Tanaka: An in situ Raman study of polarization-dependent photocrystallization in amorphous selenium films, *Appl. Phys. Lett.* **72**, 1167–1169 (1998)
- 19.356 V.K. Tikhomirov, P. Hertogen, G.J. Adriaenssens, C. Glorieux, R. Ottenburgs: Anisotropic laser crystallization of a-Se, *J. Non-Cryst. Solids* **227–230**, 732–738 (1998)
- 19.357 T. Innami, S. Adachi: Structural and optical properties of photocrystallized Se films, *Phys. Rev. B* **60**, 8284–8289 (1999)
- 19.358 M.L. Trunov, P.M. Lytvyn, S.N. Yannopoulos, I.A. Szabo, S. Kökenyesi: Photoinduced mass-transport based holographic recording of surface relief gratings in amorphous selenium films, *Appl. Phys. Lett.* **99**, 051906 (2011)
- 19.359 M.L. Trunov, P.M. Lytvyn, P.M. Nagy, A. Csik, V.M. Rubish, S. Kökenyesi: Light-induced mass transport in amorphous chalcogenides: Toward surface plasmon-assisted nanolithography and



- near-field nanoimaging, *Phys. Stat. Sol. B* **251**, 1354–1362 (2014)
- 19.360 H. Fritzsche: Critical discussion of models proposed to explain photo-induced anisotropies in chalcogenide glasses, *Phys. Stat. Sol. B* **246**, 1768–1772 (2009)
- 19.361 J. Hegedüs, K. Kohary, D.G. Pettifor, K. Shimakawa, S. Kugler: Photoinduced volume changes in amorphous selenium, *Phys. Rev. Lett.* **95**, 206803 (2005)
- 19.362 K. Hoshino, F. Shimojo, T. Nishida: The photo-induced structural change in a Se chain and a Se<sub>8</sub> ring: an ab initio molecular-dynamics simulation, *J. Phys. Soc. Jpn.* **68**, 1907–1911 (1999)
- 19.363 K. Prasai, P. Biswas, D.A. Drabod: Electrons and phonons in amorphous semiconductors, *Semicond. Sci. Technol.* **31**, 073002 (2016)
- 19.364 M. Nanba, Y. Takiguchi, Y. Honda, Y. Hirano, T. Watanabe, N. Egami, K. Miya, K. Nakamura, M. Taniguchi, S. Itoh, A. Kobayashi: 640×480 pixel active-matrix Spindt-type field emitter array image sensor with high-gain avalanche rushing amorphous photoconductor target, *J. Vac. Sci. Technol. B* **28**, 96–103 (2010)
- 19.365 J.R. Scheuermann, A.H. Goldan, O. Tousignant, S. Léveillé, W. Zhao, Development of solid-state avalanche amorphous selenium for medical imaging, *Med. Phys.* **42**, 1223–1226 (2015)
- 19.366 A. Reznik, B.J.M. Lui, V. Lyubin, M. Klebanov, Y. Ohkawa, T. Matsubara, K. Miyakawa, M. Kubota, T. Kawai, J.A. Rowlands: The effect of temperature on photoinduced metastability in avalanche a-Se layers, *J. Non-Cryst. Solids* **352**, 1595–1598 (2006)
- 19.367 Y. Ohkawa, K. Miyakawa, T. Matsubara, K. Kikuchi, S. Suzuki, K. Tanioka, M. Kubota, N. Egami, A. Kobayashi: Heat treatment to suppress image defect occurrence in amorphous selenium avalanche multiplication photoconductive film with improved red-light sensitivity, *IEICE Electron. Express* **6**, 1118–1124 (2009)
- 19.368 W.-D. Park, K. Tanioka: Tellurium doping effect in avalanche-mode amorphous selenium photoconductive film, *Appl. Phys. Lett.* **105**, 192106 (2014)
- 19.369 S. Adachi, N. Hori, K. Sato, S. Tokuda, T. Sato, K. Uehara, Y. Izumi, H. Nagata, Y. Yoshimura, S. Yamada: Experimental evaluation of a-Se and CdTe flat-panel x-ray detectors for digital radiography and fluoroscopy, *Proc SPIE* **3977**, 38–47 (2000)
- 19.370 D.C. Hunt, S.S. Kirby, J.A. Rowlands: X-ray imaging with amorphous selenium: X-ray to charge conversion gain and avalanche multiplication gain, *Med. Phys.* **29**, 2464–2471 (2002)
- 19.371 T. Miyoshi, N. Igarashi, N. Matsugaki, Y. Yamada, K. Hirano, K. Hyodo, K. Tanioka, N. Egami, M. Namba, M. Kubota, T. Kawai, S. Wakatsuki: Development of an X-ray HARP-FEA detector system for high-throughput protein crystallography, *J. Synchrotron Rad.* **15**, 281–284 (2008)
- 19.372 A. Sultana, A. Reznik, K.S. Karim, J.A. Rowlands: Design and feasibility of active matrix flat panel detector using avalanche amorphous selenium for protein crystallography, *Med. Phys.* **35**, 4324–4332 (2008)
- 19.373 T.-T. Kuo, C.-M. Wu, H.-H. Lu, I. Chan, K. Wang, K.-C. Leou: Flexible x-ray imaging detector on direct conversion in amorphous selenium, *J. Vac. Sci. Technol. A* **32**, 041507 (2014)
- 19.374 A. Sultana, M.W. Wronski, K.S. Karim, J.A. Rowlands: Digital x-ray imaging using avalanche a-Se photoconductor, *IEEE Sensors J.* **10**, 347–352 (2010)
- 19.375 M. Spahn: X-ray detectors in medical imaging, *Nuclear Instrum. Methods Phys. Research A* **731**, 57–63 (2013)
- 19.376 J.W. Boag: Xeroradiography, *Phys. Med. Biol.* **18**, 3–37 (1973)
- 19.377 M. Lachaine, B.G. Fallone: Calculation of inelastic cross-sections for the interaction of electrons with amorphous selenium, *J. Phys. D-Appl. Phys.* **33**, 551–555 (2000)
- 19.378 E. Fourkal, M. Lachaine, B.G. Fallone: Signal formation in amorphous-Se-based x-ray detectors, *Phys. Rev. B* **63**, 195204 (2001)
- 19.379 M.Z. Kabir, E.V. Emelianova, V.I. Arkhipov, M. Yunus, S.O. Kasap, G. Adriaenssens: The effect of large signals on charge collection in radiation detectors: Application to amorphous selenium detectors, *J. Appl. Phys.* **99**, 124501 (2006)
- 19.380 O. Bubon, K. Jandieri, S.D. Baranovskii, S.O. Kasap, A. Reznik: Columnar recombination for x-ray generated electron-holes in amorphous selenium and its significance in a-Se x-ray detectors, *J. Appl. Phys.* **119**, 124511 (2016)
- 19.381 D.M. Hunter, G. Belev, S. Kasap, M.J. Yaffe: Measured and calculated K-fluorescence effects on the MTF of an amorphous-selenium based CCD x-ray detector, *Med. Phys.* **39**, 608–622 (2012)
- 19.382 A.H. Goldan, O. Tousignant, L. Laperrière, K.S. Karim: Reduced photocurrent lag using unipolar solid-state photoconductive detector structures: Application to stabilized *n-i-p* amorphous selenium, *Appl. Phys. Lett.* **96**, 053507 (2010)
- 19.383 S. Abbaszadeh, S. Ghaffari, S. Siddiquee, M.Z. Kabir, K.S. Karim: Characterization of lag signal in amorphous selenium detectors, *IEEE Trans. Electron Devices* **63**, 704–709 (2016)
- 19.384 M. Walornyj, S.O. Kasap: X-ray irradiation induced changes in electron transport in stabilized a-Se photoconductors, *J. Appl. Phys.* **114**, 214505 (2013)
- 19.385 N. Allec, S. Abbaszadeh, A. Fleck, O. Tousignant, K.S. Karim: K-edge imaging using dual-layer and single-layer large area flat panel imagers, *IEEE Trans. Nuclear Sci.* **59**, 1856–1861 (2012)
- 19.386 J.C. Bernède, S. Touihri, G. Safoula: Electrical characteristics of an aluminum/amorphous selenium rectifying contact, *Solid-State Electron.* **42**, 1775–1778 (1998)
- 19.387 T. Nakada, A. Kunioka: Polycrystalline thin-film TiO<sub>2</sub>/Se solar cells, *Jpn. J. Appl. Phys.* **24**, L536–L538 (1985)
- 19.388 T. Wacharasindhu, J.W. Kwon, D.E. Meier, J.D. Robertson: Radioisotope microbattery based on liquid semiconductor, *Appl. Phys. Lett.* **95**, 014103 (2009)



- 19.389 K. Wang, F. Cheng, G. Belev, S. Kasap, K.S. Karim: Lateral metal-semiconductor-metal photodetectors based on amorphous selenium, *Appl. Phys. Lett.* **95**, 013505 (2009)
- 19.390 S. Abbaszadeh, N. Allec, K.S. Karim: Characterization of low dark-current lateral amorphous-selenium metal-semiconductor-metal photodetectors, *IEEE Sensors J.* **13**, 1452–1458 (2013)
- 19.391 F. Chen, K. Wang, Y. Fang, N. Allec, G. Belev, S. Kasap, K.S. Karim: Direct-conversion x-ray detector using lateral amorphous selenium structure, *IEEE Sensors J.* **11**, 505–509 (2011)
- 19.392 C.-Y. Chang, F.-M. Pan, J. -S. Lin, T.-Y. Yu, Yi-M. Li, C.-Y. Chen: Lateral amorphous selenium metal-insulator-semiconductor-insulator-metal photodetectors using ultrathin dielectric layers for dark current suppression, *J. Appl. Phys.* **120**, 234501 (2016)
- 19.393 G.W. Tang, Q. Qian, K.L. Peng, X. Wen, G.X. Zhou, M. Sun, X.D. Chen, Z.M. Yang: Selenium semiconductor core optical fibers, *AIP Adv.* **5**, 027113 (2015)
- 19.394 J. Tauc: Band tails in amorphous semiconductors, *J. Non-Cryst. Solids* **97&98**, 149–154 (1987)
- 19.395 D. Reinen, G.-G. Lindner: The nature of the chalcogen colour centres in ultramarine-type solids, *Chem. Soc. Rev.* **28**, 75–84 (1999)
- 19.396 V.V. Poborchii, G.-G. Lindner, M. Sato: Selenium dimers and linear chains in one-dimensional cancrinite nanochannels: Structure, dynamics, and optical properties, *J. Chem. Phys.* **116**, 2609–2617 (2002)
- 19.397 S. Chaudhary, A. Umar, S.K. Mehta: Selenium nanomaterials: An overview of recent developments in synthesis, properties and potential applications, *Prog. Mater. Sci.* **83**, 270–329 (2016)
- 19.398 N.M. Dimitri, P.V. Kamat: Photoelectrochemistry in particulate systems. 8. Photochemistry of colloidal selenium, *Langmuir* **4**, 782–784 (1988)
- 19.399 U. Jeong, Y. Xia: Synthesis and crystallization of monodispersed spherical colloids of amorphous selenium, *Adv. Mater.* **17**, 102–106 (2005)
- 19.400 Z.-H. Lin, C.R. Chris Wang: Evidence of the size-dependent absorption spectral evolution of selenium nanoparticles, *Mater. Chem. Phys.* **92**, 591–594 (2005)
- 19.401 G. Kaur, M. Iqbal, M.S. Bakshi: Biomineralization of fine selenium crystalline rods and amorphous spheres, *J. Phys. Chem. C* **113**, 13670–13676 (2009)
- 19.402 Q. Li, T. Chen, F. Yang, J. Liu, W. Zheng: Facile and controllable one-step fabrication of selenium nanoparticle assisted by L-cysteine, *Mater. Lett.* **64**, 614–617 (2010)
- 19.403 S. Sinha, S.K. Chatterjee, J. Ghosh, A.K. Meikap: Semiconducting selenium nanoparticles: Structural, electrical characterization, and formation of a back-to-back Schottky diode device, *J. Appl. Phys.* **113**, 123704 (2013)
- 19.404 A. Kumar, I. Sevonkaev, D.V. Goia: Synthesis of selenium particles with various morphologies, *J. Colloid Interface Sci.* **416**, 119–123 (2014)
- 19.405 O. Van Overschelde, G. Guisbiers: Photo-fragmentation of selenium powder by excimer laser ablation in liquids, *Opt. Laser Technol.* **73**, 156–161 (2015)
- 19.406 C. Kaito, K. Fujita: Growth of crystalline selenium particles by gas evaporation method, *Jpn. J. Appl. Phys.* **25**, 496–497 (1986)
- 19.407 J.A. Johnson, M.-L. Saboungi, P. Thiyagarajan, R. Csencsits, D. Meisel: Selenium nanoparticles: A small-angle neutron scattering study, *J. Phys. Chem.* **103**, 59–63 (1999)
- 19.408 T. Ohtani, N. Takayama, K. Ikeda, M. Araki: Unusual crystallization behavior of selenium in the presence of organic molecules at room temperature, *Chem. Lett.* **33**, 100–101 (2004)
- 19.409 S. Xiong, B. Xi, W. Wang, C. Wang, L. Fei, H. Zhou, Y. Qian: The fabrication and characterization of single-crystalline selenium nanoneedles, *Cryst. Growth Design* **6**, 1711–1716 (2006)
- 19.410 R. Zhang, X. Tian, L. Ma, C. Yang, Z. Zhou, Y. Wang, S. Wang: Visible-light-responsive t-Se nanorod photocatalysts: synthesis, properties, and mechanism, *RSC Adv.* **5**, 45165–45171 (2015)
- 19.411 B. Gates, B. Mayers, B. Cattle, Y. Xia: Synthesis and characterization of uniform nanowires of trigonal selenium, *Adv. Funct. Mater.* **12**, 219–227 (2002)
- 19.412 U.K. Gautam, M. Hath, C.N.R. Rao: New strategies for the synthesis of t-selenium nanorods and nanowires, *J. Mater. Chem.* **13**, 2845–2847 (2003)
- 19.413 B. Zhang, W. Dai, X. Ye, F. Zuo, Y. Xie: Photothermally assisted solution-phase synthesis of microscale tubes, rods, shuttles, and urchin-like assembly of single-crystalline trigonal selenium, *Angew. Chem. Int. Ed.* **45**, 2571–2574 (2006)
- 19.414 H. Chen, D.-W. Shin, J.-G. Nam, K.-W. Kwon, J.-B. Yoo: Selenium nanowires and nanotubes synthesized via a facile template-free solution method, *Mater. Res. Bull.* **45**, 699–704 (2010)
- 19.415 Z.-M. Liao, C. Hou, L.-P. Liu: Temperature dependence of photoelectrical properties of single selenium nanowires, *Nanoscale Res. Lett.* **5**, 926–929 (2010)
- 19.416 K. Mondal, S.K. Srivastava: A new hydrothermal route to nano- and microstructures of trigonal selenium exhibiting diverse morphologies, *Mater. Chem. Phys.* **124** (2010) 535–540.
- 19.417 Q. Xie, Z. Dai, W. Huang, W. Zhang, D. Ma, X. Hu, Y. Qian: Large-scale synthesis and growth mechanism of single-crystal Se nanobelts, *Cryst. Growth Design* **6**, 1514–1517 (2006)
- 19.418 G. Xi, K. Xiong, Q. Zhao, R. Zhang, H. Zhang, Y. Qian: Nucleation-dissolution-recrystallization: A new growth mechanism for t-selenium nanotubes, *Cryst. Growth Design* **6**, 577–582 (2006)
- 19.419 M. Rajalakshmi, A.K. Arora: Optical properties of selenium nanoparticles dispersed in polymer, *Solid State Commun.* **110**, 75–80 (1999)
- 19.420 A. Ueda, M. Wu, R. Aga, A. Meldrum, C.W. White, W.E. Collins, R. Mu: Temperature dependence and annealing effects of absorption edges for selenium quantum dots by ion implantation in silica glass, *Surf. Coating Technol.* **201**, 8542–8546 (2007)

- 19.421 K.A. Ann Mary, N.V. Unnikrishnan, R. Phillip: Cubic to amorphous transformation of Se in silica with improved ultrafast optical nonlinearity, *RSC Adv.* **5**, 14034–14041 (2015)
- 19.422 V.N. Bogomolov, N.F. Kartenko, L.S. Parfen'eva, A.V. Prokof'ev, I.A. Smirnov: Heat conductivity of three-dimensional regular structures of crystalline and amorphous selenium incorporated in voids of synthetic opal, *Phys. Solid State* **40**, 528–531 (1998)
- 19.423 Y.H. Zhao, K. Zhang, K. Lu: Structure characteristics of nanocrystalline element selenium with different grain sizes, *Phys. Rev. B* **56**, 14322–14329 (1997)
- 19.424 K. Tanaka, Nanostructured Chalcogenide Glasses, in *Encyclopedia of Nanoscience and Nanotechnology Vol 7*, H.S. Nalwa (ed.) (American Scientific Pub. 2004) pp. 629–640.
- 19.425 K. Hu, H. Chen, M. Jiang, F. Teng, L. Zheng, X. Fang: Broadband photoresponse enhancement of a high-performance t-Se microtube photodetector by plasmonic metallic nanoparticles. *Adv. Funct. Mater.* **26**, 6641–6648 (2016)
- 19.426 K.M. Chintala, S. Panchal, P. Rana, R.P. Chauhan: Structural, optical and electrical properties of gamma-rays exposed selenium nanowires, *J. Mater. Sci.: Mater. Electron.* **27**, 8087–8093 (2016)
- 19.427 X. Zhou, P. Gao, S. Sun, D. Bao, X. Li, T. Wu, Y. Chen, P. Yang: Amorphous, crystalline and crystalline/amorphous selenium nanowires and their different (de)lithiation mechanisms, *Chem. Mater.* **27**, 6730–6736 (2015)
- 19.428 C.R. Ma, J.H. Yan, Y.M. Wei, G.W. Yang: Second harmonic generation from an individual amorphous selenium nanosphere, *Nanotechnology* **27**, 425206 (2016)
- 19.429 D.S. Deng, N.D. Orf, S. Danto, A.F. Abouraddy, J.D. Joannopoulos, Y. Fink: Processing and properties of centimeter-long, in-fiber, crystalline-selenium filaments, *Appl. Phys. Lett.* **96**, 023102 (2010)
- 19.430 H. Yoon, G. McKenna: Dynamical and temperature dependent response of physical vapor deposited Se in freely standing nanometric thin films, *J. Chem. Phys.* **144**, 184501 (2016)
- 19.431 D.G. Streets, J. Berkowitz: Photoelectron spectroscopy of Se<sub>2</sub> and Te<sub>2</sub>, *J. Electron Spectro. Related Phenom.* **9**, 269–287 (1976)
- 19.432 K. Nagaya, T. Hayakawa, M. Yao, H. Endo: Photo-induced effects on chalcogen free-microclusters, *J. Non-Cryst. Solids* **205–207**, 807–810 (1996)
- 19.433 C. Bréchnignac, Ph. Cahuzac, N. Kébaïli, J. Leygnier: Photothermodissociation of selenium clusters, *J. Chem Phys.* **112**, 10197–10203 (2000)
- 19.434 K. Kooser, D.T. Ha, E. Itälä, J. Laksman, S. Urpelainen, E. Kukk: Size selective spectroscopy of Se microclusters, *J. Chem. Phys.* **137**, 044304 (2012)
- 19.435 Z.Q. Li, J.Z. Yu, K. Ohno, B.L. Gu, R. Czajka, A. Kasuya, Y. Nishina, Y. Kawazoe: Electronic states and stability of selenium clusters, *Phys. Rev. B* **52**, 1524–1527 (1995)
- 19.436 J. Chancelon, F. Archaimbault, S. Bonnamy, A. Tra-verse, L. Olivi, G. Vlaic: Confinement of selenium inside carbon nanotubes. Structural character-ization by X-ray diffraction and X-ray absorption spectroscopy, *J. Non-Cryst. Solids* **352**, 99–108 (2006)
- 19.437 V.N. Bogomolov, V.V. Poborchii, S.V. Kholodkevich: Absorption edge of a semiconductor NaX-Se super lattice, *JETP Lett.* **31**, 434–437 (1980).
- 19.438 O. Terasaki, K. Yamazaki, J.M. Thomas, T. Ohsuna, D. Watanabe, J.V. Sanders, J.C. Barry: Isolating individual chains of selenium by incorporation into the channels of a zeolite, *Nature* **330**, 58–60 (1987)
- 19.439 L. Khouchaf, M.-H. Tuilier, J.L. Guth, B. Elouadi: Atomic structure of selenium inserted in zeolites of the Na-mordenite type, *J. Phys. Chem. Solids* **57**, 251–258 (1996)
- 19.440 K. Matsuishi, K. Nogi, H. Ogura, S. Onari, T. Arai: Dynamics of glass transition of bulk a-Se and Se clusters incorporated into zeolites, *J. Non-Cryst. Solids* **227–230**, 799–803 (1998).
- 19.441 K. Matsuishi, T. Isome, J. Ohmori, S. Onari, T. Arai: Optical properties of selenium clusters/particles incorporated into porous materials, *Phys. Stat. Sol. (b)* **215**, 301–306 (1999)
- 19.442 P. Simoncic, T. Armbruster: Se incorporated into zeolite mordenite-Na: a single-crystal X-ray study, *Microporous Mesoporous Mater.* **71**, 185–198 (2004)
- 19.443 A. Goldbach, M.-L. Saboungi: Selenium/zeolite Y nanocomposites, *Acc. Chem. Rev.* **38**, 705–712 (2005)
- 19.444 I.L. Li, J.P. Zhai, P. Launois, S.C. Ruan, Z.K. Tang: Geometry, phase stability, and electronic properties of isolated selenium chains incorporated in a nanoporous matrix, *J. Am. Chem. Soc.* **127**, 16111–16119 (2005)
- 19.445 A.M.M. Abeykoon, J. Li, M. Castro-Colin, S.C. Moss, A.J. Jacobson: Structure of selenium clusters in the framework of zeolite Nd-Y, *Phys. Rev. B* **79**, 132104 (2009)
- 19.446 K. Tanaka, A. Saitoh: Optical nonlinearities of Se-loaded zeolite (ZSM-5): A molded nanowire system, *Appl. Phys. Lett.* **94**, 241905 (2009)
- 19.447 W. Ren, J.-T. Ye, W. Shi, Z.-K. Tang, C.T. Chan, P. Sheng: Negative compressibility of selenium change confined in the channels of AlPO<sub>4</sub>-5 single crystals, *New J. Phys.* **11**, 103014 (2009)
- 19.448 N. Togashi, K. Sugiyama, J. Yu, S. Qiu, O. Terasaki: Single crystal structure analysis of the Se-incorporated mordenite, coupled with the anomalous X-ray scattering, *Solid State Sci.* **13**, 684–690 (2011)
- 19.449 The Landolt-Börnstein Database 41C (Springer, 2014), n.a.: Selenium (Se) crystal structure, general; in Landolt-Börnstein – Group III Condensed Matter 41C(Non-Tetrahedrally Bonded Elements and Binary Compounds I) doi: 10.1007/10681727\_1230 (Springer-Verlag, Berlin Heidelberg 1998)
- 19.450 D.R. Lide (ed.): Handbook of Chemistry and Physics 74th Ed. (CRC Press, Boca Raton 1993),
- 19.451 V. Prosser: The optical constants of single crystals of hexagonal selenium, *Czech. J. Phys.* **B10**, 306–316 (1960).

- 19.452 J. M. Caywood, J.D. Tynai: Optical absorption of selenium in the  $\alpha$ -monoclinic crystal and some solvents, J. Phys. Chem. Solids 30, 1573–1577 (1969).
- 19.453 J. C. Knights, E.A. Davis: Optical properties of monoclinic selenium, Solid State Commun. 11, 543–546 (1972).

**Keiji Tanaka**

Hokkaido University  
Graduate School of Engineering  
Sapporo, Japan  
[keiji@eng.hokudai.ac.jp](mailto:keiji@eng.hokudai.ac.jp)

After graduating in Applied Physics at Hokkaido University in 1972, Keiji Tanaka worked on photoreceptors at Canon Co. Ltd. After his return to the university, he was promoted to Professor in 1991. He received the 1st Ovshinsky Award in 2001 for the excellence in chalcogenide glass research. Since 2011 he is an Emeritus Professor.

Springer Handbook of Glass

Musgraves, J.D.; Hu, J.; Calvez, L. (Eds.)

2019, XXXVI, 1841 p. 1400 illus. in color., Hardcover

ISBN: 978-3-319-93726-7